GLUTAMINE SENSING LICENSES CHOLESTEROL SYNTHESIS

Inaugural-Dissertation

zur

Erlangung des Doktorgrades

der Mathematisch-Naturwissenschaftlichen Fakultät

der Universität zu Köln

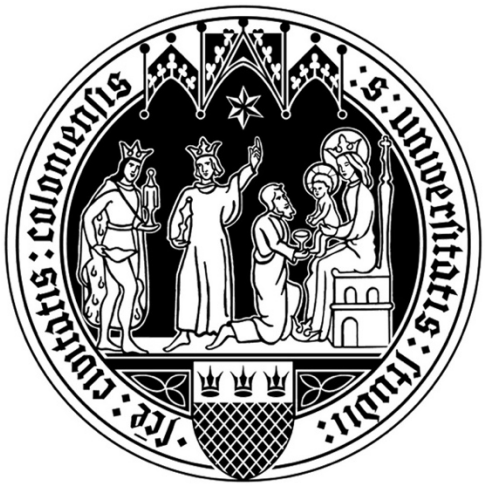

vorgelegt von

Bruna Martins Garcia

aus São Caetano do Sul, Brasilien

Köln, 2023

Berichterstatter: Dr. Lena Pernas

Prof. Dr. Jan Riemer

Prüfungsvorsitzender: Prof. Dr. Christian Frezza

Tag der Disputation: 20.10.2023

"While looking at the graph, I thought about how I now knew something for certain that only an hour ago had been an absolute unknown, and I slowly began to appreciate how my life had just changed. […] In a wide, wide world, full of unimaginable numbers of people, I was — in addition to being small and insufficient — special. I was not only a quirky bundle of genes, but I was also unique existentially, because of the tiny detail that I knew about Creation, because of what I had seen and then understood."

Hope Jahren in the book "Lab Girl" (2016)

Zusammenfassung

Cholesterol ist ein essentielles Lipid, das notwendig ist für die Funktion und das Überleben der Zelle. Der Cholesterinspiegel ist strikt reguliert und wird durch seine metabolischen Vorläufer inhibiert. Wie Metaboliten die Cholesterol Synthese aktivieren ist bislang jedoch unbekannt. Hier zeige ich, dass die nicht-essentielle Aminosäure Glutamin die Cholesterol Synthese anregen kann. Glutamin Mangel verringerte den Umsatz der Cholesterol Synthese durch verminderte Expression der Cholesterol Synthese Enzyme; unteranderem HMGCR, das geschwindigkeitsbestimmende Enzym der Synthese. Die Zugabe von Glutamin Derivaten nach Glutamin Mangel war ausreichend, um zelluläre und metabolische Stresswege zu retten, nicht aber den HMGCR-Spiegel. Ich habe diesen Glutamin-spezifischen Effekt der Cholesterol Synthese zu der Restriktion des ER-zu-Golgi Transports von SREBP2 zugeordnet, dem wichtigsten Transkriptionsregulator der Cholesterol Synthese. Während Glutamin Mangel findet eine Blockierung des ER-zu-Golgi Transports von SREBP2 statt, welche notwendig ist für die Aktivierung von SREBP2. Das Erzwingen von Golgi-zu-ER Retrotranslokation durch Brefeldin A oder durch Überexpression von aktivierten SREBP2, rettete SREBP2 Aktivierung und HMGCR-Spiegel in der Abwesenheit von Glutamin. In einem Krankheitsmodel, in dem ein mitochondrialer Defekt die Glutamin Aufnahme erhöht, waren SREPB2 Aktivierung und zelluläres Cholesterol erhöht. Zusammenfassend spürt der Cholesterol Synthese Weg Glutamin und wird durch dieses aktiviert. Die Anpassung der Glutamine Verfügbarkeit könnte in pathophysiologischen Konditionen eine Strategie sein, um den Cholesterinspiegel zu regulieren.

Abstract

Cholesterol is an essential lipid required for cell function and viability. The levels of cholesterol are tightly regulated and metabolic intermediates negatively regulate its synthesis. However, little is known about metabolites that positively regulate cholesterol synthesis. Here I found that the non-essential amino acid glutamine activates the cholesterol synthesis pathway. Glutamine starvation decreased the cholesterol synthesis rate by reducing the expression of the cholesterol synthesis enzymes, including HMGCR, the rate-limiting enzyme in the pathway. In the absence of glutamine, the addition of glutamine derivatives was sufficient to rescue metabolic and cellular stress pathways, but not HMGCR levels. I pinpointed this glutamine-specific effect on cholesterol synthesis to the licensing of ER-to-Golgi trafficking of SREBP2, the major transcriptional regulator of cholesterol synthesis. Under glutamine starvation, there is a block in the ER-to-Golgi trafficking of SREBP2 which is required for SREBP2 activation. Enforced Golgi-to-ER retrotranslocation using brefeldin A or activated SREBP2 overexpression rescued SREBP2 activation and HMGCR levels during glutamine starvation. In a mitochondrial disease model in which glutamine uptake is enhanced, SREBP2 activation and cellular cholesterol were increased. Thus, the cholesterol synthesis pathway senses and is activated by glutamine, and the modulation of glutamine availability may be a strategy to regulate cholesterol levels in pathophysiological conditions.

Acknowledgments

I would like to first thank Dr. Lena Pernas for the supervision. When I meet Lena for the first time, I could barely speak English and had few experiences in the methods required to perform my project. However, Lena saw something in me and gave me a unique life opportunity. She trusted in me and let me follow my curiosity and explore a field that was not our expertise. There are no words to express how I am glad for everything she has made for me professionally and personally. Lena, you will be my forever model and I hope you will never forget the potential that you have to impact the life of young scientists. Be sure I will always be sending you good energies doesn't matter where I go and how much time passes.

Thank you to the most important people in my life: my family. Obrigada pai e mãe (Alexandre Garcia e Rubinete Aparecida Martins Garcia) por todos os sacrifícios feitos por vocês que me fizeram chegar até aqui. Todas as minhas conquistas são suas também. O amor incondicional de vocês me sustentou até aqui, amo vocês com todo o meu ser. Thanks to my little sister (Larissa Martins Garcia) for always pushing me further to be a good model for her. My life is better knowing that I will never be alone while you are somewhere in this world. You are my person and my partner in this life. I love you, Lala. Obrigada vô Rebola, Tia Cris, Tia Deia e Dani por todo o suporte e inspiração. Vocês sempre estiveram comigo mesmo de tão longe e sempre me lembraram da onde eu vim e o quanto eu conquistei.

Thanks to the whole Pernas Lab for all the support and friendship. Thank you for the best friends I could ever wish for: Kavan Prabhu and Dr. Xianhe Li. You two were with me in the most difficult moments of my life in Germany. You two are responsible for huge personal growth and for opening my mind to so important things. You two made me happy daily. You will always be in my heart and I will always love you two. Thank you, Julian Straub, for being a sweet and loyal friend. I am glad for being part of your life. Thank you, Tim Bartsch, for being such a pretty person outside and inside. There is no chocolate enough in the world to show you as much I adore you. Thank you, Paddy (Patrick Julian Krüger) for being the biggest paradox in my life and never refusing to help me, doesn't matter when and how. Thank you, Phil (Philipp Melchinger) for being my favorite German! Thank you, Little C (Chahat Mehra) for all the support and warm hugs. Sharing life with you was a big pleasure. Thank you, Dr.

Tania Medeiros, for being such a special person. You were a changeling since day one but taught me so much about friendship, forgiveness, and acceptance. You made my journey lighter and I will forever be grateful to you. Obrigada, miga.

Thanks Steph (Dr. Stephanie de Alcantara Fernandes). You were my north reference even before I arrive at the MPI. You were the example that we can do it. That a Brazilian woman from a small city has the potential to be admired and make an impact in an important European institute. We are a good match, personally and professionally, and our friendship was nothing less than light, easy and happy. We shared the same struggles, dreams, and ambitions, and following your steps made my life so much easier. I am anxious already to move our friendship to another level, although not so close, but still in the exponential phase. Te amo.

Obrigada João Valente, por balancear minha vida e nunca duvidar do meu potencial. Por me apoiar nos piores e mais estressantes dias desse Ph.D. com paciência e amor. Por me trazer o leve da vida, a sorte de um amor quentinho. Dividir a vida com você é um privilegio.

I would also like to thank all the MPI core facilities, especially the metabolomics and bioinformatics facility. Dr. Patrick Giavalisco was one of the most important people for the completion of this thesis. His curiosity and scientific love are an inspiration. Thank you for all, Patrick.

Thanks, Dr. Noam Zelcer for opening your lab for me, and mentoring me as I was your student for a long time. This experience was of great value and I will always be grateful for what I have learned during this time. Thanks, Sebastian Hendrix, for all the help with the mice experiments. It was a pleasure to share science, thoughts, and iced white coffee with you.

I want to thank my thesis advisory committee, Prof. Dr. Thomas Langer and Prof. Dr. Aleksandra Trifunovic who provided feedback and support during my Ph.D. Special thanks to my thesis committee Prof. Dr. Jan Riemer and Prof. Dr. Christian Frezza. I also would like to thank Prof. Dr. Nuno Raimundo who kindly agreed to be my external reviewer.

A big thanks also to Dr. Daniela Morick who always has the best for the Ph.D. students in her heart. Never give up on us, we need you!

"Portanto dele, por Ele e para Ele são todas as coisas".

Erklärung zur Dissertation

gemäß der Promotionsordnung vom 12. März 2020

Hiermit versichere ich an Eides statt, dass ich die vorliegende Dissertation selbstständig und ohne die Benutzung anderer als der angegebenen Hilfsmittel und Literatur angefertigt habe. Alle Stellen, die wörtlich oder sinngemäß aus veröffentlichten und nicht veröffentlichten Werken dem Wortlaut oder dem Sinn nach entnommen wurden, sind als solche kenntlich gemacht. Ich versichere an Eides statt, dass diese Dissertation noch keiner anderen Fakultät oder Universität zur Prüfung vorgelegen hat; dass sie - abgesehen von unten angegebenen Teilpublikationen und eingebundenen Artikeln und Manuskripten - noch nicht veröffentlicht worden ist sowie, dass ich eine Veröffentlichung der Dissertation vor Abschluss der Promotion nicht ohne Genehmigung des Promotionsausschusses vornehmen werde. Die Bestimmungen dieser Ordnung sind mir bekannt. Darüber hinaus erkläre ich hiermit, dass ich die Ordnung zur Sicherung guter wissenschaftlicher Praxis und zum Umgang mit wissenschaftlichem Fehlverhalten der Universität zu Köln gelesen und sie bei der Durchführung der Dissertation zugrundeliegenden Arbeiten und der schriftlich verfassten Dissertation beachtet habe und verpflichte mich hiermit, die dort genannten Vorgaben bei allen wissenschaftlichen Tätigkeiten zu beachten und umzusetzen. Ich versichere, dass die eingereichte elektronische Fassung der eingereichten Druckfassung vollständig entspricht.

Teilpublikationen:

1- Garcia, B.M. et al., 2023. Glutamine sensing licenses cholesterol synthesis. Developmental Cell. *Under review.*

2- Melchinger, P., Garcia, B.M., 2023. Mitochondria are midfield players in steroid synthesis. Int J Biochem Cell Biology 160, 106431.

Köln, den 20 Oktober 2023

Bruna Martins Garcia

TABLE OF CONTENTS

LIST OF FIGURES AND TABLES

Chapter 1 - Introduction

Chapter 3 - Results

ABBREVIATIONS

General

CHO - Chinese hamster ovary cells

CM - Chylomicron

CRISPR - Clustered Regularly Interspaced Short Palindromic Repeats

ER - Endoplasmic reticulum

HeLa - Henrietta Lacks; human cervical cancer cell

HepG2 - Human hepatoblastoma cell line

HFFs - Human foreskin fibroblasts

ISR - Integrated Stress Response

KO - Knockout

LDL - Low-density lipoprotein

MEFs - Mouse embryonic fibroblasts

NASH - Nonalcoholic Steatohepatitis

OXPHOS - Oxidative phosphorylation

PM - Plasma Membrane

TCA - Tricarboxylic acid

U2OS - Human osteosarcoma cell

VLDL - Very low-density protein

Metabolites

25-HC - 25-hydroxycholesterol

27-HC - 27-hydroxycholesterol

AA - Amino acid

Acetyl-CoA - Acetyl coenzyme A

ADP - Adenosine diphosphate

aKG - Alpha-ketoglutarate

AMP - Adenosine monophosphate

ATP - Adenosine triphosphate

CA - Cholic Acid

CDCA - Chenodeoxycholic acid

CDP - Cytidine diphosphate

CMP - Cytidine monophosphate

CoQ10 - Coenzyme Q10

CTP - Cytidine triphosphate

DON- 6-Diazo-5-oxo-L-norleucina

GDP- Guanosine diphosphate

Glc - Glucose

Gln - Glutamine

GMP - Guanosine monophosphate

GSH - Reduced glutathione

GSSH - Oxidized glutathione

GTP- Guanosine triphosphate

NEAAs - Non-essential amino acids

NH_4 - Ammonia

PC - Phosphatidylcholines

ROS - Reactive oxygen species

TG - Triglyceride

UDP – Uridine diphosphate

UDP-GlnNac - Uridine diphosphate N-acetylglucosamine

UMP- Uridine monophosphate

UTP- Uridine triphosphate

Genes and proteins

ACAT - cholesterol acyltransferase

ASNS - Asparagine synthetase

ATF4 - Activating Transcription Factor 4

ATF6 - Activating Transcription Factor 6

ATP5 - ATP synthase subunit 5

c-MYC - MYC Proto-Oncogene

CH25H - Cholesterol 25-hydroxylase

COPII - Coatomer II

CS - Citrate synthase

CYP11A1 - Cytochrome P450 family 11 subfamily A member 1

CYP27A1 - Cholesterol 27-hydroxylase

CYP7A - 7-alpha-monooxygenase or cytochrome P450 7A1

eIF2a - Eukaryotic translation initiation factor 2A

ERLINs - ER Lipid Raft Associated proteins

FDFT1 - farnesyl-diphosphate farnesyltransferase 1

FDPS - Farnesyl pyrophosphate synthase

GCL - Glutamate-cysteine ligase

GDH - Glutamate dehydrogenase

GLUL - Glutamine synthase, also known as GS

GLS - Glutaminase

GP78 - Glycoprotein 78, also known as AMFR

GPR78 - Probable G-protein coupled receptor 78

GSS - Glutathione synthetase

HMGCR - 3-hydroxy-3-methyl-glutaryl-coenzyme A reductase

INSIG - Insulin-induced gene

LCAT - Lecithin–cholesterol acyltransferase

LDLR - LDL receptor

LMAN1 - Lectin, Mannose Binding 1

MAN2 - Alpha-Mannosidase 2

MARCH6 - Membrane Associated Ring-CH-Type Finger 6

MFN1 - Mitofusin 1

MFN2 - Mitofusin 2

OPA1 - Optic atrophy 1

PAQR3 - AdipoQ receptor 3

PDH - Pyruvate dehydrogenase

PFK1 - Phosphofructokinase 1

PFK2 - Phosphofructokinase 2

RNF145 - Ring Finger Protein 145

S1P - Site 1 protease)

S2P - Site 2 protease

S6K - Ribosomal protein S6 kinase

SCAP - Sterol Regulatory Element-Binding Protein Cleavage-Activating Protein

SDHA – Succinate dehydrogenase

SLC1A5 - Solute Carrier Family 1 Member, also known as ASCT2

SLC25A1 - Mitochondrial citrate transporter

SLC25A11 - Solute Carrier Family 25 Member 11

SLC25A18 - Solute Carrier Family 25 Member 18

SLC25A22 - Solute Carrier Family 25 Member 22

SLC38A1 - Solute Carrier Family 38 Member 1

SLC38A2 - Solute Carrier Family 38 Member 2

SM or SQLE - Squalene monooxygenase/squalene epoxidase

SURF4 - Surfeit locus protein 4

SREBP2 - Sterol regulatory element binding protein 2

TOM 20 - Translocase Of Outer Mitochondrial Membrane 20

TOM 40 - Translocase Of Outer Mitochondrial Membrane 40

TOM 70 - Translocase Of Outer Mitochondrial Membrane 70

TRC8 - Ring Finger Protein 139; also known as RNF139

UB - Ubiquitin

UBIAD1 - UbiA Prenyltransferase Domain Containing 1

VDAC1/2 - Voltage Dependent Anion Channel ½

Reagents and methods

BFA - Brefeldin A

BPTES - bis-2-(5-phenylacetamido-1,3,4-thiadiazol-2-yl)ethyl sulfide

DMEM – Dulbecco's Modified Eagle Medium

FBS - Fetal Bovine Serum

ISRIB - Integrated stress response (ISR) inhibitor

MSX - Methionine sulfoximine

RUSH - Retention Using Selective Hooks

CHAPTER 1

INTRODUCTION

1. The lipid cholesterol

1.1. Cholesterol is an essential metabolite

Cholesterol ($C_{27}H_{46}O$) was first isolated in 1789 from gallstones and since then, its essential uses and intricate regulation attracted the attention of diverse researchers including biologists, chemists, and biophysicists (Ikonen, 2008; Luo et al., 2019). The discoveries of Michael S. Brown and Joseph L. Goldstein elucidated much of the regulation of cholesterol metabolism and led to the Nobel Prize in 1985 (Nair, 2013). However, new mechanisms of cholesterol metabolic regulation have emerged since and several open questions remain.

1.1.1. Cholesterol is an essential precursor

Cholesterol is a precursor to several other metabolites (Figure 1.1) such as cholesterol esters, oxysterol, steroid hormones, and bile acids (reviewed in Melchinger and Garcia, 2023). Higher cholesterol levels are toxic to cells once it leads to membranes damages and inhibition of membrane proteins (Tabas, 1997). To avoid toxicity, cholesterol can be esterified by the endoplasmic reticulum (ER)-resident protein ACAT (Cholesterol Acyltransferase) which generates cholesterol esters (Chang et al., 2009). Cholesterol esters are formed by the addition of long fatty acid chains to the hydroxyl group of the cholesterol molecule. After, cholesterol esters are stored in lipid droplets together with other lipids. On the other hand, if intracellular cholesterol levels are low, cholesterol esters can undergo hydrolysis and be released from lipid droplets to increase free cholesterol levels (Brown et al., 1980).

Oxysterols are formed by the addition of a hydroxyl group in the cholesterol molecule through autoxidation or monooxygenases enzymes (such as the Cytochrome P-450 family) activity. As a result, oxysterols are more water-soluble and have distinct physicochemical properties. The exact carbon of the cholesterol molecule where the hydroxyl group is added dictates which oxysterol will be produced (Brown et al., 2021b). For example, the CYP27A1

(Cholesterol 27-hydroxylase) enzyme will add a hydroxyl group to the 27th carbon of cholesterol (Figure 1.2), generating 27-HC (27-hydroxycholesterol). On the other hand, CH25H (Cholesterol 25-hydroxylase) enzyme will add a hydroxyl group to the 25th carbon of cholesterol, generating 25-HC (25-hydroxycholesterol). Although oxysterols play diverse roles from inter-organ communication to immunology (Chen et al., 2022; Spann and Glass, 2013; Tomita et al., 2022) and the first studies with oxysterols are dated to 1895 (Brown et al., 2021b) — decades before the discovery of the cholesterol structure — the functions of these metabolites are still not fully understood.

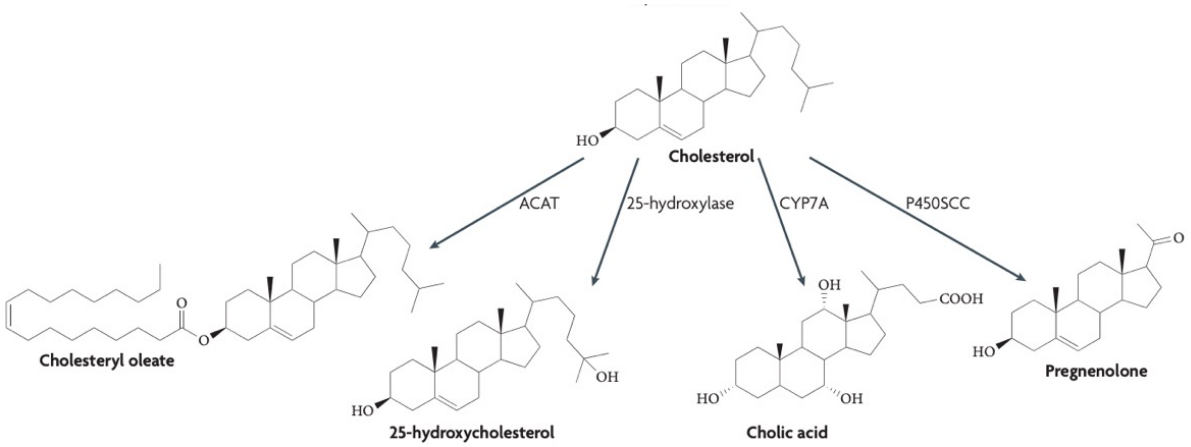

Figure 1.1. Cholesterol is a building block precursor. Cholesterol is the precursor to different metabolite families. Cholesterol is esterified by the addition of long fatty acids to its molecule (here represented by cholesteryl oleate) by the enzyme ACAT (cholesterol acyltransferase) inside the cells or LCAT (Lecithin–cholesterol acyltransferase) in the plasma. Cholesterol can be oxidized by autoxidation or mediated by enzymes (such as Cholesterol 25-hydroxylase) to produce oxysterols (here represented by 25-hydroxycholesterol). In hepatocytes, cholesterol can also be oxidized to bile acids (here represented by Cholic acid) by the enzyme CYP7A (7-alpha-monooxygenase or cytochrome P450 7A1). In steroidogenic tissues, cholesterol is oxidized to steroid hormones (here represented by Pregnenolone) by the enzyme P450SCC (cholesterol side-chain cleavage). Adapted from (Ikonen, 2008).

Bile acids (or bile salts) are another derivative of cholesterol that play an important role in facilitating digestion and absorption of nutrients. Bile acid synthesis involves hydroxylation, saturation, epimerization, and oxidation of cholesterol, requiring 17 enzymes residents of diverse intracellular compartments — cytosol, ER, mitochondria, and peroxisomes (Chiang, 2013; Fuchs, 2003). Cholic acid (CA) and chenodeoxycholic acid (CDCA) are the major primary bile acids and are synthesized in the human liver by the enzyme CYP7A (7-alpha-Monooxygenase or Cytochrome P450 7A1). Every day a healthy human liver produces

approximately 500 mg of bile acids which will all be excreted in the feces, making bile acid synthesis a daily task (Chiang, 2013).

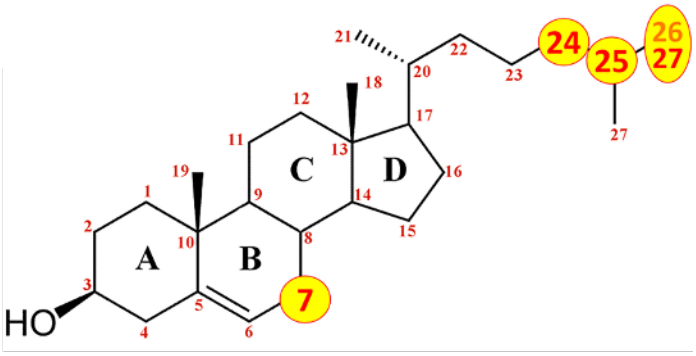

Figure 1.2. Cholesterol molecule with the indication of the most common oxidized carbons. The exact carbon of the cholesterol molecule where the hydroxyl group is added dictates which oxysterol will be produced. However, carbon 26 is more frequently referred to as 27 in the literature. Adapted from (Brown et al., 2021b).

All steroid hormones are produced from cholesterol. The main steroid hormones in vertebrates are androgens, estrogens, progesterone, glucocorticoids, and mineralocorticoids which participate not only in reproduction but also in the regulation of cell survival and death (Billig et al., 1993; Cohen and Duke, 1984; Frick et al., 2015; Larson, 2018; Rotello et al., 1992; Tenniswood et al., 1992). Interestingly, although the steroid hormone synthesis starts in the mitochondria with the conversion of cholesterol into pregnenolone — by the CYP11A1 (Cytochrome P450 family 11 subfamily A member 1) enzyme — subsequent steps in the pathway demand a crosstalk between ER and mitochondria (Melchinger and Garcia, 2023). Both, the synthesis of bile acids and steroid hormones illustrate the complexity of cholesterol metabolism.

1.1.2. Cholesterol as a membrane constituent

In higher eukaryotes, cholesterol is the major non-polar lipid constituent of membranes. However, its concentration deeply varies among organellar membranes (Figure 1.3) and even membrane regions in the same compartment (e.g., lipid rafts domains and organelles contact sites) (Fujimoto et al., 2012; Meer et al., 2008). 90% of intracellular cholesterol is found in the plasma membrane (PM), which has the highest concentration of cholesterol. Cholesterol represents ~45 mol% of total PM lipids and has a ratio of cholesterol/phospholipids of 10 (Lange et al., 1989; Meer et al., 2008; Ray et al., 1969). On the other hand, the lowest levels

are in the ER (1% of intracellular cholesterol) where cholesterol represents ~5 mol% of total ER membrane lipids (Sokolov and Radhakrishnan, 2010) and has a ratio of cholesterol/phospholipids of 0.15 (Meer et al., 2008) (Figure 1.3).

Membrane cholesterol creates a semi-permeable barrier, regulating membrane fluidity and affecting the diffusion of different ions, solutes, and membrane proteins. Moreover, cholesterol interacts with other membrane lipids and proteins to modulate several cellular processes, including the regulation of its synthesis and uptake regulation (Goldstein et al., 2002; Ikonen, 2008).

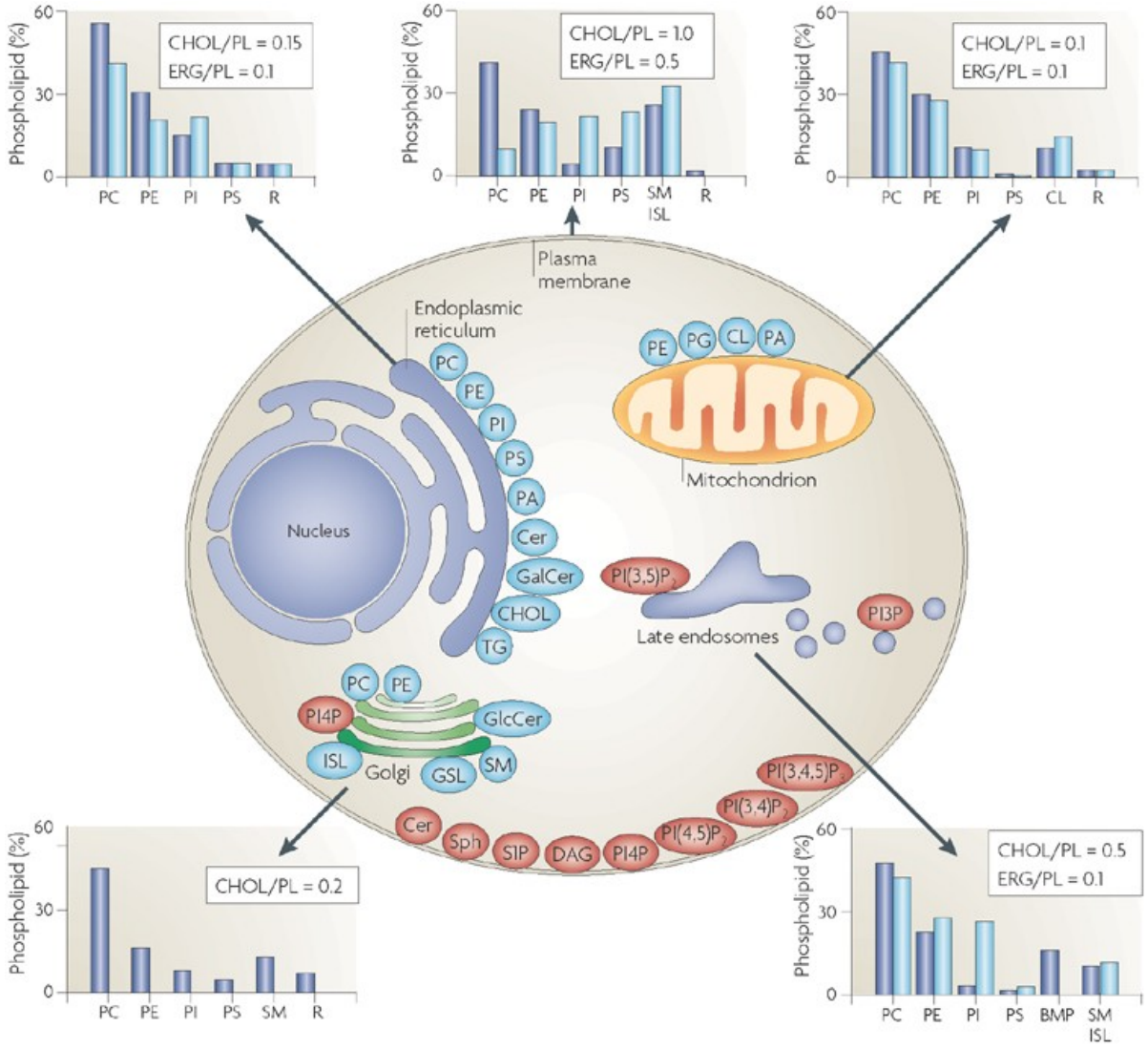

Figure 1.3. Cholesterol content in the different organellar membranes. The membrane lipid composition of organellar compartments varies inside cells. The graphs represent the lipid percentage (as indicated) of total phospholipid composition in mammals (dark blue) and yeast (light blue). In the corner of each square, there is the ratio of cholesterol (CHOL) and ergosterol (ERG — cholesterol in yeast cells) to the total PL. Abbreviations:

Ceramides (Cer), Phosphatidylcholine (PC), Phosphatidylethanolamine (PE), Phosphatidylinositol (PI), Phosphatidylserine (PS), Phosphatidic acid (PA), Phosphatidylglycerol (PG), Galactosylceramide (GalCer), triacylglycerol (TG), Sphingomyelin (SM), Complex glycosphingolipids (GSLs), Yeast inositol sphingolipid (ISL), Diacylglycerol (DAG), Cardiolipin (CL), Bis (monoacylglycerol) phosphate (BMP), Phosphatidylinositol-(3,5)-bisphosphate (PI(3,5)P2), Phosphatidylinositol-(4,5)-bisphosphate (PI(4,5)P2), Phosphatidylinositol-(3,4,5)-trisphosphate (PI(3,4,5)P3), Phosphatidylinositol-4-phosphate (PI4P), Remaining lipids (R), Sphingosine-1-phosphate (S1P), and Sphingosine (Sph). Figure from (Meer et al., 2008).

1.2. Cholesterol levels regulation

There are two major sources of intracellular cholesterol: synthesis and uptake. All mammalian cells are able to uptake and/or synthesize cholesterol and both processes are under tight regulation to avoid toxicity and unnecessary energy expense (over one hundred ATP per molecule of cholesterol) (Brown et al., 2021a). So far, this regulation has been shown to be mediated through transcriptional and post-translational mechanisms (Luo et al., 2019).

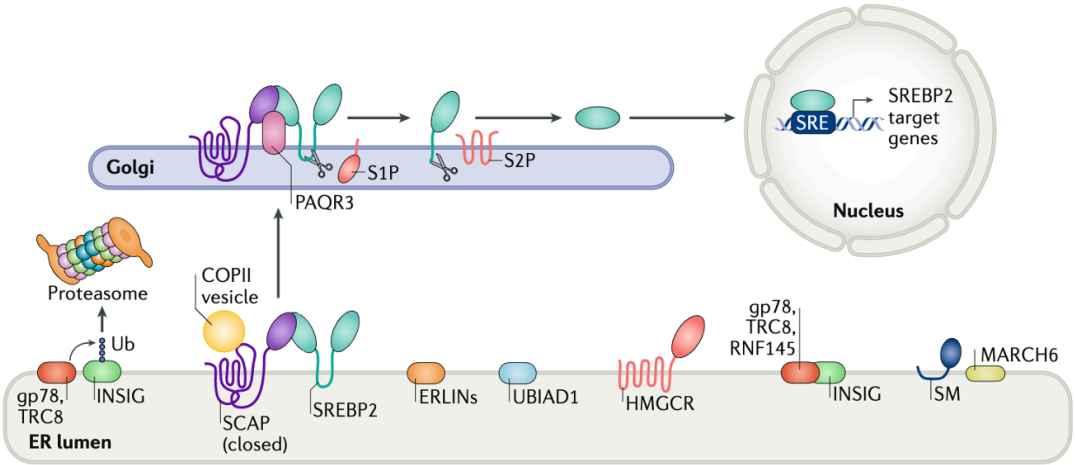

Figure 1.4. Positive regulation of cholesterol synthesis. The master regulator of cholesterol synthesis is the sterol regulatory element-binding protein 2 (SREBP2). Under cholesterol depletion conditions, SREBP2-SCAP (Sterol Regulatory Element-Binding Protein Cleavage-Activating Protein) complex travels from the endoplasmic reticulum (ER) to the Golgi in COPII (Coatomer II) vesicles for its activation. At the Golgi, SREBP2 will be anchored by Golgi proteins such as PAQR3 (AdipoQ Receptor 3) to further undergo two cleaves mediated by S1P (Site 1 Protease) and S2P (Site 2 Protease). After the cleavages, the N-terminal domain of SREBP2 traffics to the nucleus and binds the SRE (Regulatory Element) DNA regions to promote the transcription of the SREBP2 target genes: enzymes in the cholesterol synthesis pathway and the LDLR (Low-Density Lipoprotein Receptor). Simultaneously, INSIG (Insulin-Induced Gene) — which normally anchors the SREBP2-SCAP complex at the ER — is degraded by the proteasome machinery after ubiquitination by GP78 (Glycoprotein 78; also known as AMFR) and TRC8 (Ring Finger Protein 139; also known as RNF139). Adapted from (Luo et al., 2019).

The master regulator of cholesterol synthesis is the transcription factor SREBP2 (Sterol Regulatory Element Binding Protein 2), an ER-resident protein that forms a complex with

SCAP (Sterol Regulatory Element-Binding Protein Cleavage-Activating Protein) and INSIG (Insulin-Induced Gene) (Figure 1.4). When levels of cholesterol are <5 mol% of total ER membrane lipids, INSIG dissociates from the complex and is ubiquitinated by the E3 ubiquitin (Ub) ligase GP78 (Glycoprotein 78), resulting in INSIG degradation by the proteasome machinery. As a consequence, the SREBP2-SCAP complex traffics to the Golgi through COPII (coatomer II) vesicles. In the Golgi, SREBP2-SCAP is anchored by PAQR3 (AdipoQ Receptor 3) (Xu et al., 2015) and undergoes two cleavages by the proteases S1P (Site 1 Protease) and S2P (Site 2 Protease), respectively (Sakai et al., 1996). These cleavages release the N-terminal domain of SREBP2 from the Golgi, which will further traffic to the nucleus to promote the transcription of the genes required for cholesterol synthesis and uptake (e.g., *LDLR* — LDL Receptor).

Two of the SREBP2 target genes are the enzymes *HMGCR* (3-Hydroxy-3-Methylglutaryl-CoA Reductase) and *SM or SQLE* (Squalene Monooxygenase/Squalene Epoxidase). The reactions mediated by HMGCR and SM — also ER-resident proteins — are rate-limiting steps in the cholesterol synthesis pathway (Brown and Goldstein, 1980; Gill et al., 2011) and are tightly regulated at the protein level by the proteasome machinery at the ER (Figure 1.5 and 1.6). When levels of cholesterol at the ER membrane are low, HMGCR and SM are stable at the ER membrane and promote the conversion of HMG-CoA into mevalonate (Figure 1.5) and squalene to 2,3-epoxysqualene, respectively.

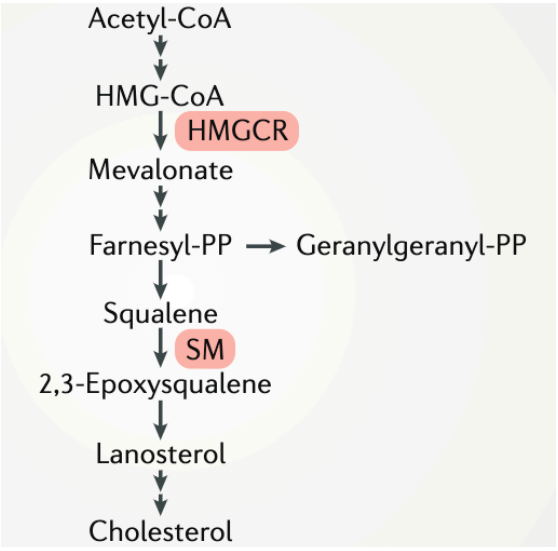

Figure 1.5. Simplified scheme of the cholesterol synthesis enzymes. Highlighted in pink are the endoplasmic reticulum-resident proteins HMGCR (3-Hydroxy-3-Methylglutaryl-CoA Reductase) and SM (squalene

monooxygenase; also known as SQLE — squalene epoxidase). Both enzymes are rate-limiting steps in the cholesterol synthesis pathway and their levels are transcriptional and post-translational regulated. Adapted from (Luo et al., 2019).

On the other hand, when cholesterol levels are >5 mol% of total ER membrane lipids, the INSIG-SREBP2-SCAP complex is stabilized at the ER membrane, preventing the trafficking of SREBP2-SCAP to the Golgi and nucleus (Figure 1.6). This stability is promoted by cholesterol-induced conformational changes in SCAP which promotes its interaction with INSIG. INSIG also senses oxysterol levels which promote INSIG binding to SCAP and anchor INSIG-SREBP2-SCAP at the ER — surprisingly exerting a stronger effect than cholesterol on SCAP (Adams et al., 2004). Moreover, other ER-resident proteins can also mediate INSIG-SREBP2-SCAP anchoring (Figure 1.6) such as ERLINs (ER Lipid Raft Associated proteins), TRC8 (Ring Finger Protein 139; also known as RNF139), UBIAD1 (UbiA Prenyltransferase Domain Containing 1), and RNF145 (Ring Finger Protein 145) (Huber et al., 2013; Irisawa et al., 2009; Jiang et al., 2019; Kuan et al., 2020).

HMGCR and SM are also degraded by the proteasome machinery triggered by high cholesterol levels (Huang and Chen, 2023; Tsai et al., 2012). Interestingly, INSIG, GP78 (Glycoprotein 78, also known as AMFR), TRC8, and RFN145 bind HMGCR to promote its degradation. Thus, these proteins negatively regulate cholesterol synthesis through two fronts: the anchor of SREBP2 and HMGCR degradation (Figure 1.6). In the same way, MARCH6 (Membrane Associated Ring-CH-Type Finger 6) — another E3 ubiquitin ligase — binds SM, resulting in its ubiquitination and further degradation by the proteasome machinery (Zelcer et al., 2014).

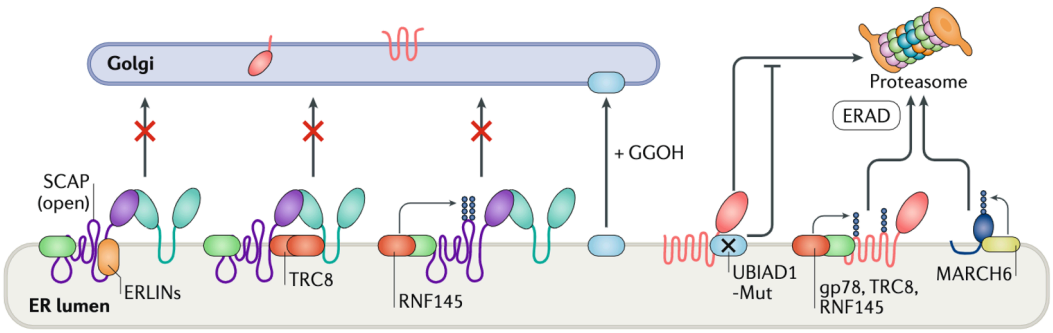

Figure 1.6. Negative regulation of cholesterol synthesis. Under cholesterol-repleted conditions, cholesterol synthesis and uptake are downregulated by negative feedback. The downregulation of cholesterol synthesis happens on two fronts: 1) retention of SREBP2 (Sterol Regulatory Element-Binding Protein) at the endoplasmic

reticulum (ER); and 2) degradation of the rate-limiting enzymes HMGCR (3-Hydroxy-3-Methylglutaryl-CoA Reductase) and SM (Squalene Monooxygenase) by the proteasomal machinery. In the first case, ER-resident proteins will mediate the anchoring of SCAP (Sterol Regulatory Element-Binding Protein Cleavage-Activating Protein)-SREBP2 complex in the ER membrane — such as the insulin-induced gene (INSIG), ERLINs (ER Lipid Raft Associated proteins), and the associated E3 ubiquitin ligases GP78 (Glycoprotein 78; also known as AMFR), TRC8 (Ring Finger Protein 139; also known as RNF139), and RNF145 (Ring Finger Protein 145). Meanwhile, INSIG also binds to HMGCR to promote its ubiquitination and degradation by the proteasomal machinery. In the same way, MARCH6 binds to SM to promote its ubiquitination and degradation by the proteasomal machinery. Moreover, in the presence of cholesterol and geranylgeraniol, UBIAD1 (UbiA prenyltransferase domain-containing protein 1) does not interact with HMGCR, promoting its degradation. Adapted from (Luo et al., 2019).

1.3. Cholesterol metabolism *in vivo*

Although the total amount of cholesterol synthesis in the human body was defined decades ago to be roughly 700-900 mg/day in humans, the specific contribution of each organ is unclear (Dietschy, 1984). On the other hand, in animal models, the liver was shown as the main site of cholesterol synthesis (Figures 1.7 and 1.8) together with the intestines (Spady and Dietschy, 1983).

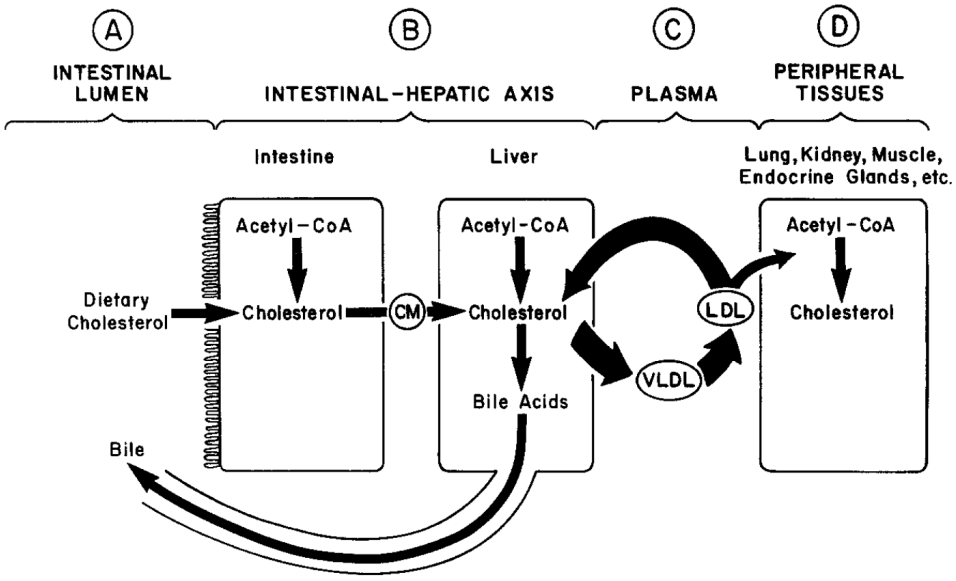

Figure 1.7. *In vivo* cholesterol homeostasis. To supplement the cholesterol synthesis in the tissues, cholesterol from the diet is uptake in the intestines, and together with the intestinal synthesized cholesterol, traffics to the liver in chylomicron (CM). In the liver — the main site of cholesterol synthesis *in vivo* — cholesterol from the diet and new synthesized will be incorporated in very low-density lipoproteins (VLDL) and secreted to the plasma. In the plasma, VLDL will be metabolized into low-density lipoproteins (LDL) and delivered to the other tissues, but the brain. The remaining, and the majority of, LDL will be taken up by the liver again. In all the tissues including the liver, LDL-derivated cholesterol will participate in the negative feedback to downregulate its synthesis. Adapted from (Dietschy, 1984).

Another source of body cholesterol is diet. Approximately 300-500 mg of cholesterol are absorbed daily (Spady and Dietschy, 1983). Cholesterol from the diet is absorbed in the intestines (Iqbal and Hussain, 2009) and together with the locally synthesized cholesterol is incorporated into the lipoprotein CM (chylomicron). CM containing cholesterol is further released into the plasma and is absorbed by the liver (Nervi et al., 1975; Sherrill and Dietschy, 1978) where it will contribute to local negative feedback of the cholesterol synthesis (Figure 1.7).

Very low-density proteins (VLDL) are next produced in the liver and are delivered to the peripheric tissues through the plasma to supply their demand for cholesterol to cell membrane production and its derivatives synthesis. In these tissues, the cholesterol delivered from the liver participates in the local regulation of cholesterol synthesis (Andersen and Dietschy, 1977) to avoid excess cholesterol load. Interestingly, the liver also uptakes LDL (Low-Density Lipoprotein) from the plasma and is responsible for 75% of the LDL turnover in hamsters (Spady et al., 1983) — pinpointing the liver as a major player in cholesterol homeostasis regulation (Figures 1.7 and 1.8).

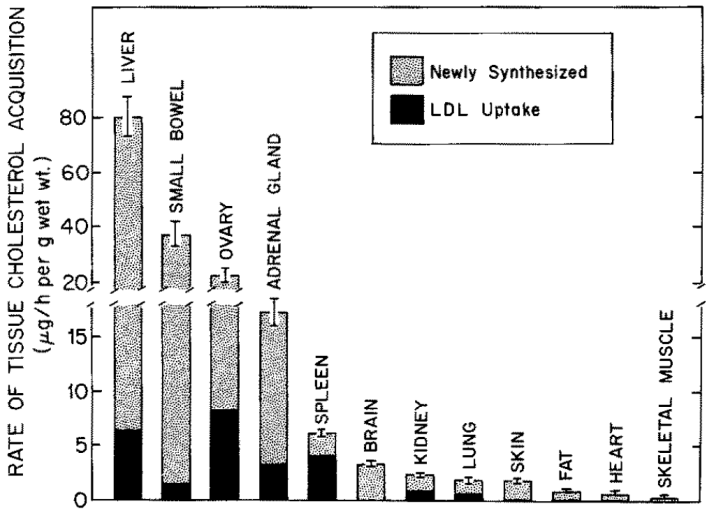

Figure 1.8. Cholesterol synthesis and uptake rates in rats. The data show the amount of cholesterol (μg) acquired in each organ through synthesis or uptake through low-density lipoproteins (LDL) per hour. The total amount of cholesterol in each organ can also be estimated by the sum of synthesis and LDL uptake. This data does not take into consideration cholesterol uptake from chylomicron (CM) or HLDL (High-Density Lipoproteins). Figure from (Dietschy, 1984).

Another interesting player in cholesterol homeostasis *in vivo* is the brain. Due to the blood-brain barrier (BBB), the brain cannot uptake cholesterol through plasmatic LDL (Jeske

and Dietschy, 1980), and thus relies exclusively on its own cholesterol synthesis (Figure 1.8). Moreover, even though the brain has a lower ratio of cholesterol synthesis when compared to the liver (Dietschy, 1984), it contains about 20% of the whole cholesterol content in the body (Bjo□rkhem and Meaney, 2004). It can be explained by the fact that the half-life of the brain's cholesterol is 6 months to 5 years, while the half-life in the plasma for example is only a few days (Andersson et al., 1990; Dietschy and Turley, 2004).

1.4. Cholesterol levels dysregulation and diseases

Mutations in the genes involved in cholesterol metabolism are the cause of congenital human diseases such as Niemann-Pick type C disease (Scriver et al., 2001), Schnyder corneal dystrophy (Weiss, 2009), Smith-Lemli-Opitz syndrome (Nowaczyk and Irons, 2012), Familial hypercholesterolemia (Henderson et al., 2016; Scriver et al., 2001), Tangier disease (Kolovou et al., 2006), and Sitosterolemia (Escolà-Gil et al., 2014). All these diseases have as common symptoms higher levels of cholesterol or its derivatives in a certain organelle, tissue, or plasma (Luo et al., 2019).

Moreover, there is increasing evidence that alterations in cholesterol or its derivatives levels are related to acquired diseases such as cardiovascular diseases, neurodegenerative diseases (e.g., Alzheimer, Parkinson, and Huntington's diseases), and cancer. Differently from congenital diseases, the levels of cholesterol and its derivatives are controversial in acquired diseases. A good example of this controversy is the contribution of cholesterol in Alzheimer's disease (Arenas et al., 2017). Higher levels of cholesterol or a cholesterol-rich diet were shown to promote or be a risk factor for Alzheimer's disease in rabbits (Sparks et al., 1994) and mice (Refolo et al., 2000; Shie et al., 2002; Thirumangalakudi et al., 2008) models as well as humans (Martins et al., 2009; Notkola et al., 1998; Wolozin et al., 2000). However, several other studies found decreased cholesterol levels and its derivatives in the brains of Alzheimer's disease patients (Arenas et al., 2017). This incongruence may be due to the difficulty of isolating the brain from other tissues' metabolic influence once the BBB is impaired in patients and animal models of Alzheimer's (UJIIE et al., 2009).

Cholesterols levels are also a predictor of metabolic disease development and progression, such as NASH (nonalcoholic steatohepatitis) to hepatocellular carcinoma. NASH

is the most common cause of chronic liver disease worldwide and is caused by the accumulation of lipids triggering liver fibrosis and inflammation. Polymorphisms in cholesterol metabolism-related genes were found in patients with NASH (Horn et al., 2021) who also have higher levels of serum cholesterol, however without negatively regulating SREBP2 activation in the liver — increasing, even more, the cholesterol levels through synthesis (Min et al., 2012; Zhao et al., 2011). Moreover, several studies showed a positive correlation between cholesterol intake and NASH (Ioannou et al., 2009; Liang et al., 2018; Noureddin et al., 2020) indicating that cholesterol lipotoxicity may play a role in the development of NASH.

Surprisingly, although NASH patients treated with statins had decreased steatosis and inflammation (Dongiovanni et al., 2015), the inhibition of cholesterol synthesis increased the levels of other lipids and led to other metabolic diseases, e.g., diabetes and insulin resistance (Margerie et al., 2019; Preiss et al., 2011; Sattar et al., 2010). Interestingly, mutations in HMGCR also increase the risk of diabetes (Swerdlow et al., 2015) and, on the other hand, patients with Familial hypercholesterolemia — higher levels of cholesterol in the plasma — have less risk of diabetes (Besseling et al., 2015). Although there is a clear association between cholesterol levels and the development of metabolic diseases, the mechanisms are not elucidated yet.

1.5. Cholesterol metabolism in mitochondrial dysfunction

Mitochondria are the main site for steroid and bile acid synthesis (Melchinger and Garcia, 2023) (see Chapter 1.1.1 and Figure 1.1). However, these organelles are considered cholesterol-poor organelles (Meer et al., 2008) (see Chapter 1.1.2 and Figure 1.3) and are very sensitive to changes in their cholesterol content (Garcia-Ruiz et al., 2008). Accumulation of mitochondrial cholesterol triggers mitochondrial dysfunction *in vitro* and *in vivo* (Garcia-Ruiz et al., 2008; Zhao et al., 2010) due to changes in the membrane's physical properties and consequently OXPHOS (Oxidative Phosphorylation) machinery assembly — causing energy and redox imbalance (Solsona-Vilarrasa et al., 2019). Higher levels of mitochondrial cholesterol were also found in neurodegenerations and myocardial ischemia injury animal models (Rouslin et al., 1982; Yu et al., 2005). However, it is not clear yet whether this accumulation is a cause or consequence of these diseases.

The opposite is also true: mitochondrial dysfunction affects cholesterol homeostasis by decreasing cholesterol and its derivatives levels (Quirós et al., 2017). Recently, the effect of acute mitochondrial dysfunction induced by 3 different inhibitors (Figure 1.9-A) on the transcriptome was assessed (Mick et al., 2020). Acute inhibition of complex 1 by piericidin, complex III by antimycin, or ATP synthase by oligomycin had a severe effect on the transcriptome (Figure 1.9-B), especially regarding the SREBP2 target genes (see Chapter 1.2). The decrease in the expression of the SREBP2 target genes expression was pinpointed to an SREBP2 activation impairment (Wall et al., 2022). Thus, acute OXPHOS impairment downregulates cholesterol synthesis by reducing SREBP2 activation. However, the mechanism is still unknown.

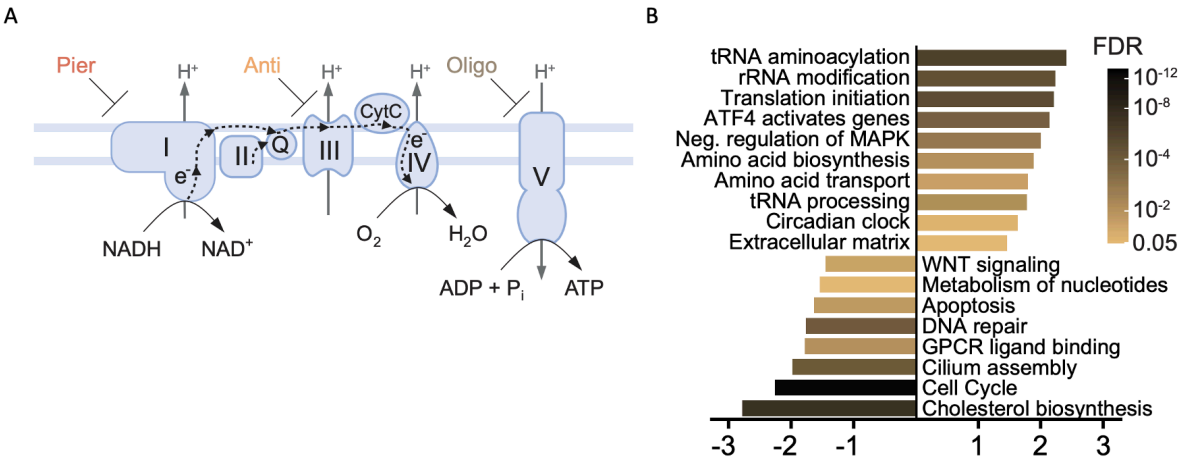

Figure 1.9. Acute mitochondrial dysfunction downregulates the cholesterol synthesis pathway. Acute mitochondrial dysfunction can be caused by drugs that inhibit the OXPHOS (Oxidative phosphorylation) complexes **(A)**. Acute mitochondrial dysfunction downregulates cholesterol synthesis by decreasing the expression of the enzymes in the pathway **(B)**. Interestingly, this effect is independent of which OXPHOS complex is inhibited. Abbreviations: Piericidin (Pier), Antimycin (Anti), and Oligomycin (Oligo). Adapted from (Mick et al., 2020).

Healthy mitochondria are constantly undergoing fission and fusion events (Pernas and Scorrano, 2015) making these organelles highly dynamic. Mitochondrial fusion is mediated by the proteins MFN1 (Mitofusin 1), MFN2 (Mitofusin 2), and OPA1 (Optic Atrophy 1). Mitochondrial dynamics impairment also impacts lipid homeostasis and *MFN1* and *MFN2* double knockout was shown to decrease cholesterol synthesis in human cells and Drosophila larvae (Chung et al., 2019; Sandoval et al., 2014). Surprisingly, although these two proteins have several distinct roles in cellular homeostasis (Carvalho et al., 2020; Casellas-Díaz et al., 2021; Chandhok et al., 2018; Chen et al., 2020; Ishihara et al., 2004; Pernas and Scorrano,

2015; Zaman and Shutt, 2022), the individual effect of them on cholesterol synthesis is not well understood. Currently, it is believed that while MFN1 is important for glucose metabolism (Ramírez et al., 2017; Zhang et al., 2020), MFN2 plays a stronger role in lipid metabolism (Boutant et al., 2017; Ma et al., 2021; Mancini et al., 2019; Mann et al., 2023; Zhang et al., 2013). In accordance, human patients with mutations in *MFN2* show severe lipodystrophy syndrome (Capel et al., 2018; Rocha et al., 2017) which causes loss and gain of fat in different parts of the body and organs (Mann et al., 2023).

2. Glutamine is a versatile metabolite

Glutamine (gln) is a conditional-essential amino acid (AA) that is highly abundant in the plasma (Barle et al., 1996; Newsholme et al., 2003) and muscle (Bergström et al., 1974). The levels of gln are regulated by a balance between synthesis/uptake and consumption/release, that sustains cellular homeostasis and proliferation. The importance of gln is pertinent to the versatility of this AA that feeds several important cellular pathways such as 1) AA synthesis; 2) TCA (Tricarboxylic Acid) cycle intermediates synthesis (Anaplerosis); 3) nucleotide synthesis; and 4) glycosylation substrate production (Figure 1.9).

2.1. Glutamine is a conditional non-essential AA (NEAA)

Although glucose is considered the main energetic substrate for cellular homeostasis, under catabolic conditions, cells utilize gln at similar or greater rates (Vinicius Fernandes Cruzat et al., 2014; Newsholme, 2001). In cell culture, glucose, and gln are present in high concentrations — up to 5-25 mM and 2-4 mM, respectively — being both required for cellular viability and growth.

In the human body, gln is the most abundant free AA and reaches its highest concentration in the muscle where gln concentration is 19.45 ± 1.52 mM while glutamate, the first hydrolysis product of gln (Figure 1.9), is 4.38 ± 0.615 mM (Bergström et al., 1974). Although no study has systematically quantified gln levels across all organs and tissues, it is estimated that other organs also require a robust supply of gln. For example, high levels of gln were found in the plasma at 0.7 mM (compared to glutamate concentration of 0.02 mM), liver at 2.06 ± 0.59 mMol/Kg wet weight (while glutamate 1.81 ± 0.53 mMol/Kg), and brain

at 4.3 ± 0.7 μMol/mL (while glutamate 9.1 ± 1.7 μMol/mL) (Barle et al., 1996; Gruetter et al., 1994; Newsholme et al., 2003; Rothman et al., 1992).

The total levels of gln in the body are the result of the synthesis, uptake, hydrolysis, and release by cells, organs, and tissues. Approximately 40 to 80 g/day of gln is synthesized in the human body (Boza et al., 2001; Wernerman, 2008), Therefore, gln is considered a non-essential AA (NEAA) in healthy conditions. However, under stress conditions, gln comes to light as an essential AA once its synthesis is not sufficient to supply its demand (Hankard et al., 1999; Lacey and Wilmore, 1990). For example, gln demand is increased in diseases such as cancer (Altman et al., 2016), during infections (Kao et al., 2013; Karinch et al., 2001), after surgeries and traumas (FLÄRING et al., 2003), or after intense physical exercise (Cruzat et al., 2010; Leite et al., 2016). In these cases, gln supplementation has been used as a possible therapeutic approach (Bakalar et al., 2006; Vinicius F. Cruzat et al., 2014; Ferreira et al., 2020; Gianotti et al., 1995).

2.2. Maintenance of glutamine levels

Gln levels are regulated by a balance between synthesis/uptake and consumption/release. Some tissues are able to synthesize large amounts of gln (such as the liver and brain), while others rely on its uptake from the plasma. Gln uptake is performed through membrane transporters (Pochini et al., 2014) such as SLC1A5 (Solute Carrier Family 1 Member, also known as ASCT2), SLC38A1 (Solute Carrier Family 38 Member 1), and SLC38A2 (Solute Carrier Family 38 Member 2). Once inside the cells, gln feeds several pathways (Figure 1.9).

Gln synthetase (GS or GLUL) is the enzyme that catalyzes the conversion of ammonium ions (NH_4^+) and glutamate into gln in the cytosol (Krebs, 1935). GLUL was first isolated in 1962 from sheep brains (Häberle et al., 2006; Pamiljans et al., 1962) and in Chinese hamsters remarkably represents ~1% of the total soluble proteins in the brain and liver (Tiemeier and Milman, 1972). In these tissues, GLUL not only provides gln — which is essential for brain and liver function — but also avoids NH_4^+ accumulation preventing hyperammonemia and its deleterious effects on cellular homeostasis (Kanamori et al., 1996; Tanigami et al., 2005; Tuchman et al., 1997).

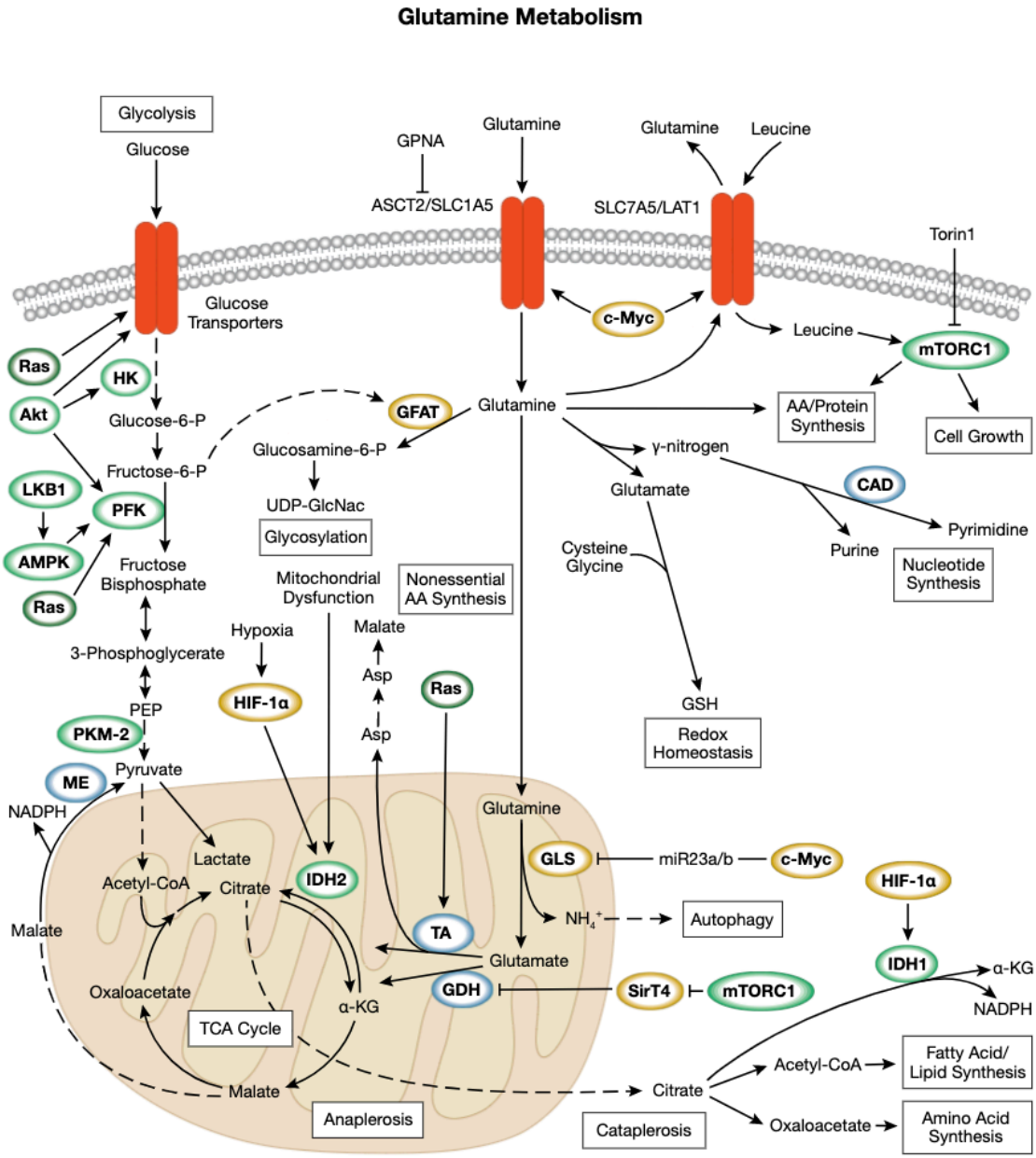

Figure 1.10. Glutamine fuels several cellular pathways. Glutamine (gln) feeds the production of several metabolites such as TCA cycle intermediates (Anaplerosis), ATP, reducing agents, nucleotides, amino acids, fatty acids, and glycosylation substrates. Gln enters the cells through plasma membrane transporters ASCT2/SLC1A5 (here shown) and SLCA38A1/2. On the other hand, gln can be exported through the SLC7A5/LAT1 transporter. Once inside the cells, gln can undergo reactions in the cytosol or be imported to the mitochondria through a variant form of ASCT2/SLC1A5. Inside mitochondria, gln can undergo hydrolysis by the glutaminase (GLS) enzyme, generating glutamate and ammonia. Glutamate can also undergo hydrolysis by the glutamate dehydrogenase (GDH) enzyme, generating alpha-ketoglutarate (aKG) and another ammonia molecule. aKG will further feed the TCA cycle for anaplerosis. Citrate is generated as a result of anaplerosis and fuels the cycle, or is exported to the cytosol to feed the fatty acid synthesis. aKG can also be generated in the cytosol and activates mTORC1 to promote cellular growth and proliferation. Illustration reproduced courtesy of Cell Signaling Technology, Inc. (www.cellsignal.com).

On the other hand, gln is hydrolyzed into glutamate and NH_4^+ (Krebs, 1935) by the enzyme glutaminase (GLS). Interestingly, GLS is found in the cytosol and mitochondria (Katt et al., 2017), where gln hydrolysis is an important step to generate gln-deviated metabolites for the TCA cycle (Ahn et al., 2017; Bowtell and Bruce, 2002; Le et al., 2012; Yang et al., 2014). The mitochondrial glutamate and NH_4^+ can be further exported to the cytosol (Figure 1.9) — through SLC25A18 (Solute Carrier Family 25 Member 18) and SLC25A22 (Solute Carrier Family 25 Member 22) transporters (Monné et al., 2019) — to also feed other pathways (Choi and Coloff, 2019; Yoo et al., 2020).

2.3. Glutamine is an amino and a carbon donor

As mentioned above, gln can be hydrolyzed to generate glutamate and NH_4^+ through GLS activity. The NH_4^+ generated by gln hydrolysis will feed the nucleotide synthesis and is a limiting metabolite in the de novo synthesis of pyrimidines and purines (J. Zhang et al., 2017). Moreover, the gln-derived nitrogen will also feed the hexosamine synthesis such as glucosamine and galactosamine (Altman et al., 2016). Interestingly, glutamate will also undergo further hydrolysis generating aKG (alpha-ketoglutarate) and another molecule of NH_4^+ which — differently from the first gln-derived nitrogen — feeds the NEAA synthesis (Figure 1.9) of alanine, aspartate, proline, and serine (Yoo et al., 2020; Zhu et al., 2017). These last are further used for the synthesis of asparagine, arginine, cysteine, and glycine.

In addition, gln hydrolysis is catalyzed by the aminotransferase ASNS (Asparagine synthetase) which also converts aspartate into asparagine in the same reaction (Lomelino et al., 2017). Thus, the products of ASNS are glutamate and asparagine at the same time. Interestingly, asparagine promotes the synthesis of gln by increasing GLUL levels, indicating that gln and asparagine synthesis are interconnected (Pavlova et al., 2018).

Beyond donating amino groups, gln can also be a carbon donor for the production of TCA cycle intermediates (Anaplerosis), and lipid and glutathione synthesis (Figure 1.9). To this end, mitochondrial gln-derived glutamate will undergo subsequent hydrolysis by the enzyme glutamate dehydrogenase (GDH) or other aminotransferases (Legendre et al., 2020), generating NH_4^+ and aKG — a TCA cycle intermediate. aKG feeds the TCA cycle and is the

building block for other TCA cycle intermediates (such as malate, oxaloacetate, and citrate) (Figure 1.9).

Citrate is generated inside mitochondria by the enzyme citrate synthase (CS) and can have two different outcomes: 1) feed the TCA cycle to supply the cellular energy demand and anaplerosis, or 2) be exported to the cytosol by the transporter SLC25A1 (Solute Carrier Family 25 Member 1). Cytosolic citrate is converted into Acetyl-CoA (acetyl coenzyme A) which promotes acetylation of histones and feeds fatty acid and cholesterol synthesis. Although citrate export may play an important role in the synthesis of lipids, whether CS and SLC25A1 play a regulatory role in this pathway is not known yet (Melchinger and Garcia, 2023; Zhao et al., 2016).

Gln also donates carbons to glutathione synthesis (Yoo et al., 2020) — an important antioxidant that deactivates peroxide-free radicals — through the ligation of gln-derived glutamate and cysteine by GCL (Glutamate-Cysteine Ligase). After, glycine is also added (Amores-Sánchez and Medina, 1999) by the enzyme GSS (Glutathione Synthetase) generating the tripeptide glutathione (Glutamate–Cysteine–Glycine). Gln is the major carbon source for glutathione synthesis, being a rate-limiting metabolite in the pathway (Amores-Sánchez and Medina, 1999; Sappington et al., 2016; Tompkins et al., 2019). Thus, glutamine may be a link between bioenergetic and redox states.

2.4. Glutamine and cellular stress

Due to its importance for cellular homeostasis and proliferation, gln starvation triggers stress response pathways (Yoo et al., 2020). Two major cellular homeostasis maintenance pathways respond to gln levels: 1) mTORC1 (Serine/threonine Kinase Mammalian Target of Rapamycin Complex 1); and 2) ISR (Integrated Stress Response).

mTORC1 regulates cellular growth and proliferation by sensing and integrating several metabolic statuses — such as nutrient availability, energy, and growth factors (Bodineau et al., 2021; González et al., 2020). Gln-derived aKG can feed anaplerosis (see section 1.2.3) or be exported from mitochondria (Stine and Dang, 2020) through the transporter SLC25A11 (Solute Carrier Family 25 Member 11). Once in the cytosol, aKG activates mTORC1 (Durán et

al., 2013, 2012; Durán and Hall, 2012) thereby promoting protein translation and cellular proliferation. Moreover, aKG-activation of mTORC1 suppresses autophagy and the DNA damage response (Sanli et al., 2014; Shen and Houghton, 2013). Under gln-depletion, and consequently gln-derived aKG depletion, mTORC1 is inactivated which suppresses cellular growth and proliferation.

Gln is also sensed by the ISR which is activated under gln depletion to adapt and maintain cellular homeostasis (Yoo et al., 2020). The activation of the ISR is mediated by the transcription factor ATF4 (Activating Transcription Factor 4) which is translated under gln depletion (Qing et al., 2012) — or gln hydrolysis impairment (Kim et al., 2019) — and promotes a metabolic adaption to gln depletion. ATF4 activation increases the expression of several genes including the c-MYC (MYC Proto-Oncogene) to promote gln uptake and metabolism (Tambay et al., 2021). Interestingly, there is evidence that gln suppresses ATF4 by feeding the NEAA synthesis and not by a direct effect (Pavlova et al., 2018; Zhang et al., 2014). Both mTORC1 and ATF4 activation are good examples of how gln levels can be sensed through gln derivatives and dictate cell fate. However, it is not known whether gln per se is sensed independently of its derivatives.

2.5. Glutamine associated diseases

Depletion of gln levels through congenital GLUL deficiency diseases is incompatible with life, and newborns with mutations in GLUL die after a few days (Häberle et al., 2005). Gln was depleted in these newborns while glutamate levels were unchanged, pinpointing the importance of gln beyond its derivatives. The newborns showed severe brain malformation, indicating that gln synthesis is important for brain development. However, further studies are required to understand whether the detrimental effects of GLUL deficiency are due to the loss of gln or the accumulation of NH_4^+ when the gln synthesis is impaired (Häberle et al., 2006).

Acquired GLUL deficiency in the brain and liver results in hyperammonemia and death (Robinson, 2000; Tuchman et al., 1997), reinforcing the detoxication role of the gln synthesis by decreasing NH_4^+ levels in these organs. Moreover, secondary GLUL deficiencies were also related to epilepsy (Eid et al., 2004; Hel et al., 2005; Zhou et al., 2019), schizophrenia

(Bruneau et al., 2005), Alzheimer's disease (Robinson, 2000), and seizures (Eid et al., 2008). In addition, gln synthesis promotes cancer proliferation and the progression of metabolic diseases, highlighting the importance of gln synthesis in organismal health (Kim et al., 2021; Spodenkiewicz et al., 2016).

Cancer cells rely on high levels of gln to supply fast growth and replication. Because the need for gln is so high, gln synthesis is not sufficient to supply cancer cell demand and it becomes an essential AA (J. Zhang et al., 2017). Consequently, cancer cells are addicted to exogenous gln that supplies carbons and nitrogen to metabolic pathways (Kovacević and Morris, 1972; Reitzer et al., 1979). Gln starvation or its hydrolysis inhibition suppresses tumor proliferation (Chen and Cui, 2015; Hoerner et al., 2018; Leone et al., 2019; LOBO et al., 2000) and increases sensitivity to chemotherapies (Chen et al., 2017; Mukhopadhyay et al., 2020) pinpointing gln metabolism as a promising target for cancer treatments.

Gln can affect organismal metabolism through different mechanisms. For example, gln attenuates the expression of inflammatory genes in the adipose tissue of obese mice (Petrus et al., 2020). Moreover, gln promotes the secretion of insulin by β-cells (Greenfield et al., 2009; Krause and Bittencourt, 2008; Samocha-Bonet et al., 2011) by a little-understood mechanism and is thus being beneficial for patients with diabetes mellitus. Interestingly, gln supplementation although beneficial, increased the levels of cholesterol, HDL, and LDL in rats (Rosa et al., 2015) and humans (Mansour et al., 2015), pinpointing a possible role of glutamine in lipid homeostasis *in vivo*. However, in these studies is not possible to distinguish a possible effect due to synthesis and SREBP2 activation or lipid uptake from the diet.

2.6. Glutamine metabolism rewiring

Mitochondrial diseases are characterized by energetic and metabolic impairments that affect diverse organs and cause neurological diseases and myopathies (Gorman et al., 2016). Cells with dysfunctional mitochondria must adapt to metabolic and energy deficiencies, including TCA cycle impairment and the lack of its intermediates, to survive. Gln quickly feeds the TCA cycle to compensate for mitochondrial dysfunctions and promotes survival (Chen et al., 2018; Motori et al., 2020). In the same way, mitochondrial dysfunction also affects lipid metabolism, resulting in diseases and triggering compensatory mechanisms (Vamecq et al.,

2012; Zhao et al., 2022). Interestingly, mitochondrial dysfunction due to lack of MFN2 (Chen et al., 2007; Lee et al., 2012; Misko et al., 2012; Pham et al., 2012) also undergoes gln metabolism proteome rewiring (Motori et al., 2020; Yao et al., 2019). Although *MFN2* mutations are associated with neuropathologies and cancer (Beręsewicz et al., 2018; Filadi et al., 2018; Larrea et al., 2019; Li et al., 2019; Stuppia et al., 2015; Xin et al., 2021; Züchner et al., 2006), it is not clear yet if they are caused by an individual role of MFN2 or the disruption of several of the cellular functions of MFN2.

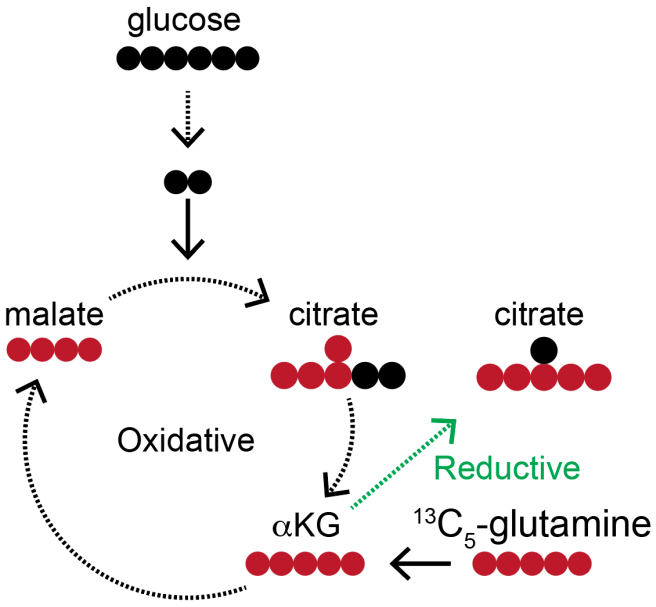

Figure 1.11. Oxidative and reductive forms of the TCA cycle. The TCA cycle starts with the donation of two carbons coming from the acetyl-CoA generated through glycolysis (shown here) or fatty acid oxidation. Acetyl-CoA together with the four-carbon oxaloacetate (OAA), will generate the six-carbon molecule citrate. The cycle will subsequently generate isocitrate, alpha-ketoglutarate (aKG), succinyl-CoA, succinate, fumarate, malate, and OAA, which will start the cycle again. This is the oxidative form of the cycle. Alternatively, aKG can be converted into isocitrate and further citrate. This is called the reductive form of the TCA cycle and is associated with mitochondrial dysfunction. Feeding the cells with labeled glutamine ($^{13}C_5$-glutamine) allows the distinction of the two forms of the TCA cycle and enables to assess which form is being used for anaplerosis in different conditions. Black dashed arrow: oxidative pathway; green dashed arrow: reductive pathway; black circles: ^{12}Carbons; and red circles: ^{13}Carbons.

The TCA (also known as Citric acid or the Krebs) cycle is a series of reactions inside mitochondria that generates energy substrates (NADPH and $FADH_2$) to the OXPHOS and intermediate metabolites (Figure 1.10) which play several functions from immunomodulation to anabolism substrates (Martínez-Reyes and Chandel, 2020). Two main carbon sources feed the TCA cycle: glucose and gln. In healthy cells, glucose is the major fuel for anaplerosis,

however, in cancer cells (Daye and Wellen, 2012; Tong et al., 2009) and under mitochondrial dysfunction (Chen et al., 2018; Ryan et al., 2021; Yang et al., 2014), gln becomes the main carbon donor. In these conditions, cells increase gln uptake and consumption to supply a higher demand. Interestingly, while glucose only feeds the cycle in one direction (oxidative), gln feeds the TCA cycle through the oxidative or reductive pathway (Figure 1.11). Although both pathways are increased under mitochondrial dysfunction, it was shown that the severity of the dysfunction dictates whether the gln-fueled TCA cycle will cycle in an oxidative or reductive way (Chen et al., 2018).

CHAPTER 2

SCOPE OF THE THESIS

Maintaining the correct levels of cholesterol is essential for life, and even small alterations in cholesterol homeostasis are related to several diseases and syndromes (Arenas et al., 2017; Escolà-Gil et al., 2014; Kolovou et al., 2006; Martins et al., 2009; Notkola et al., 1998; Nowaczyk and Irons, 2012; Scriver et al., 2001; Weiss, 2009; Wolozin et al., 2000) including cardiovascular disease (Liou and Kaptoge, 2020), the main cause of death worldwide (Nepogodiev et al., 2019). Consequently, cholesterol synthesis is under tight regulation by negative feedback through cholesterol itself or cholesterol derivatives (Luo et al., 2019). Mechanistically, cholesterol and its derivates promote the proteasome degradation of rate-limiting enzymes and the anchoring of SREBP2 at the ER. However, it is not known whether cholesterol precursors — such as glucose and glutamine — can also regulate cholesterol synthesis through positive or negative feedback. Moreover, the major approach to decrease cholesterol synthesis has been the administration of statins to inhibit HMGCR activity. However, statins also led to increased HMGCR expression through SREBP2 activation due to cholesterol starvation, potentially exacerbating cholesterol synthesis over time (Dorsch et al., 2021; Schonewille et al., 2016). Thus, a better understanding of the mechanisms that govern cholesterol synthesis would not just broaden our knowledge but also open new avenues for future interventions.

This thesis had two major aims: 1) Investigate whether cholesterol precursors regulate cholesterols synthesis and if so, define the underlying mechanism; 2) Define new approaches to decrease cholesterol levels.

CHAPTER 3

RESULTS

1. Glutamine is required for cholesterol synthesis

To investigate whether the cholesterol precursors glucose (glc) and glutamine (gln) could regulate cholesterol synthesis, I first starved U2OS (Human Bone Osteosarcoma Epithelial Cells) cells of gln or glc for 8h (Figure 3.1.1- A). The presence of FBS (Fetal Bovine Serum) inhibits cholesterol synthesis due to its lipid content (see Chapter 1.2) and thus to assess cholesterol synthesis, cells were always cultured in the absence of FBS or other sources of lipids.

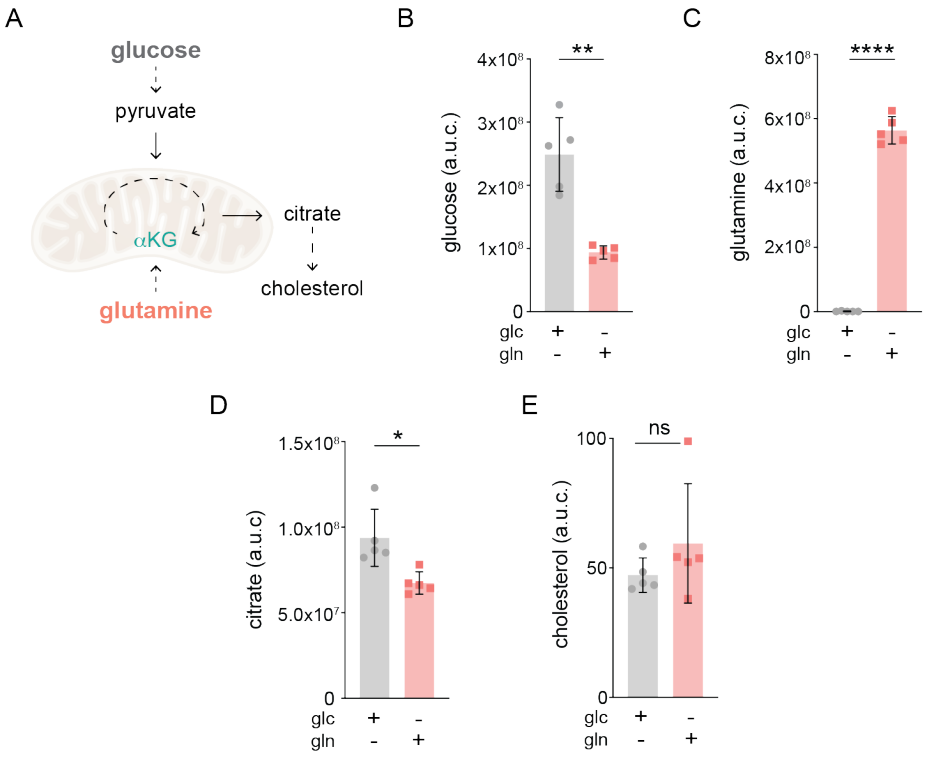

Figure 3.1.1. Cells cultured only in the presence of glutamine have lower levels of citrate and higher levels of cholesterol. The main carbons sources to generate citrate and cholesterol are glucose via the oxidation of pyruvate and glutamine via the oxidation of alpha-ketoglutarate (aKG) in the mitochondria **(A)**. The abundance of total glucose **(B)**, glutamine **(C)**, citrate **(D)**, and cholesterol **(E)** in U2OS cells cultured with only glucose (glc) or only glutamine (gln) for 8h. Data are mean ± s.d. of n=5 independent cultures; ns: non-significant, *p<0.05, **p<0.01, and ****p<0.0001 for t-test. For all experiments, gln was used at 2 mM and glucose at 25 mM. The area under the curve (a.u.c.).

Glc starvation reduced 60% of intracellular glc while gln starvation completely depleted gln levels in the respective experimental groups (Figure 3.1.1 – B and C). Cells cultured only in the presence of gln had reduced citrate levels while increased by ~ 20% cholesterol levels (Figure 3.1.1 – D and E). Since citrate is exported from mitochondria to feed the cholesterol synthesis, this result was surprising and suggested a role of gln — but not glc — in the regulation of cholesterol levels.

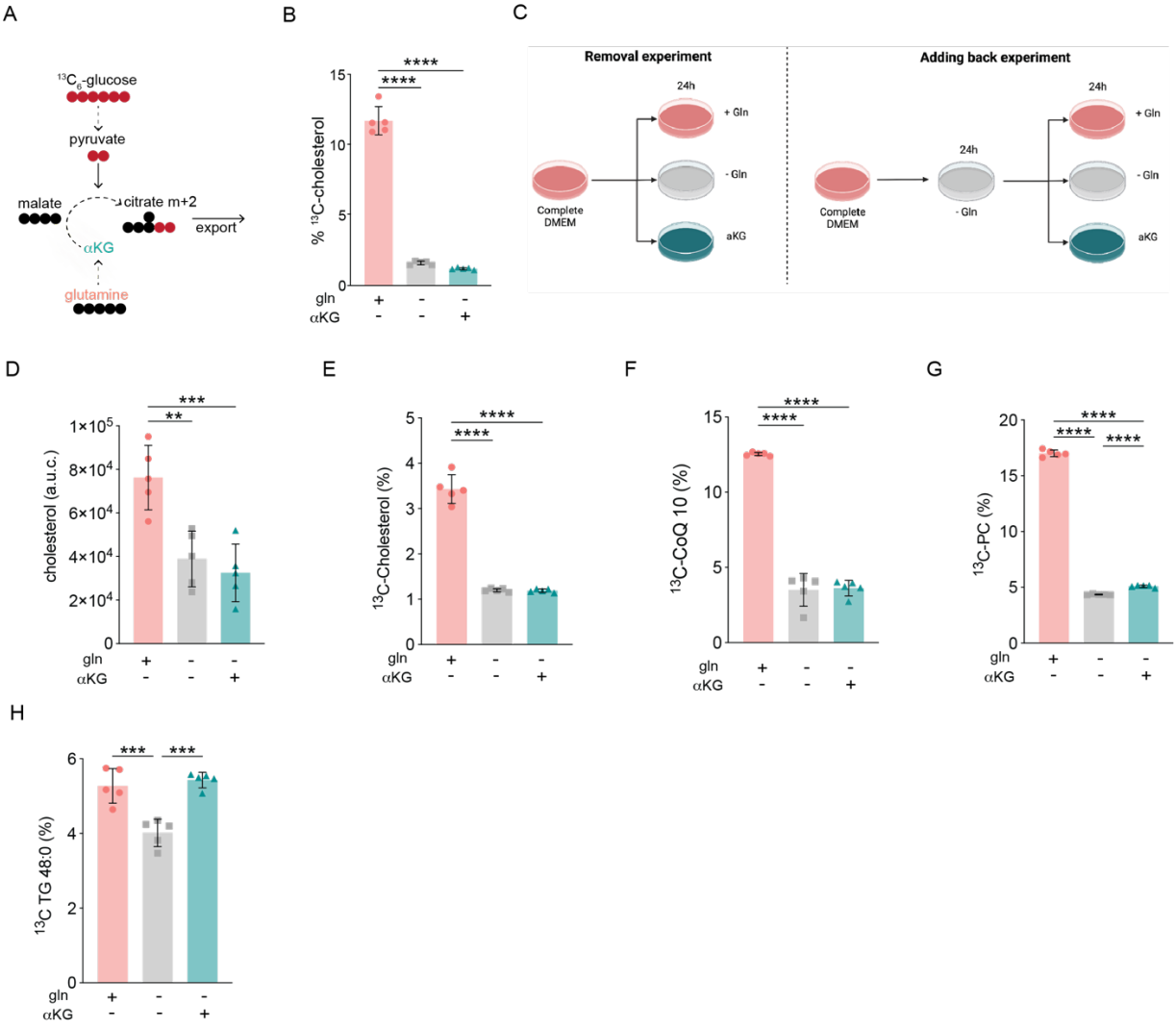

Figure 3.1.2. Glutamine licenses cholesterol synthesis. Simplified model of m+2 citrate efflux derived from $^{13}C_6$-glucose **(A)**. Red circles represent ^{13}C-carbons and black circles represent ^{12}C-carbons. Percentage of ^{13}C-cholesterol in U2OS cells after 24h treated as indicated **(B)**. Setup of removal and add back glutamine (gln) experiments **(C)**. The abundance of total cholesterol after adding back gln or alpha-ketoglutarate (aKG) as indicated for 24h **(D)**. Percentage of ^{13}C-cholesterol **(E)**, ^{13}C-coenzyme Q 10 **(F)**, ^{13}C-phosphatidylcholine **(G)**, and ^{13}C-triacylglyceride 48:0 **(H)** in U2OS after adding back gln or aKG as indicated for 24h. Data are mean ± s.d. of n=5 independent cultures; **p<0.01, ***p<0.001, and ****p<0.0001 for one-way ANOVA. For all experiments, gln was used at 2 mM, aKG at 1 mM, and glucose at 25 mM. The area under the curve (a.u.c.).

To measure cholesterol synthesis in cells in the presence or absence of gln I used isotope-labeled glc. Cells were cultured in the presence of glc uniformed labeled with ^{13}C (^{13}C-Glc) and deprived or fed with gln (Figure 3.1.2 – A). After 24h, the levels of ^{13}C in cholesterol were measured (Figure 3.1.2 – B) by mass spectrometry. Cells deprived of gln had >5-fold decrease in cholesterol synthesis. To exclude a potential effect of the TCA cycle anaplerosis, I added aKG to the cell culture media deprived of gln. Interestingly, although aKG rescued the levels of citrate (Figure 3.3- B; further discussed in chapter 3.3), it did not rescue the decrease in cholesterol levels (Figure 3.1.2 – B).

Next, I wondered whether the addition of gln to gln-starved cells was sufficient to promote again cholesterol synthesis (Figure 3.1.2 – C). To address this, I starved the cells of gln for 24h and added back gln or aKG for 24h. Gln — but not aKG — was sufficient to increase cholesterol levels and synthesis after gln starvation (Figure 3.1.2 – D and E). Interestingly, gln starvation also decreased the synthesis of coenzyme Q 10 (CoQ 10) and phospholipids (phosphatidylcholine — PC) by ~ 3-fold. The synthesis of triacylglycerides (TG) was less affected by gln starvation (~ 1.5-fold decrease). Interestingly, aKG supplementation was sufficient to rescue TG levels but not the synthesis of CoQ10 and PC (Figure 3.1.2 – F, G, and H). This result indicates that the effect of gln on TG is not directly linked to gln, but its derivatives. Moreover, it suggests that different mechanisms regulate cholesterol/phospholipids and TG synthesis.

2. Glutamine regulates HMGCR levels

To further understand how gln is required for cholesterol synthesis, I investigated the levels of the first rate-limiting enzyme in the pathway — HMGCR. I found that gln was required to sustain the levels of HMGCR (Figure 3.1.2 – A) in U2OS cells. Moreover, gln-starvation decreased the levels of HMGCR also in HeLa (human cancer cell line; Figure 3.1.2 – B), HFF (primary human cell line; Figure 3.1.2 – C), and MEF (murine embryonic fibroblasts; Figure 3.1.2 – D) cells indicating that the regulatory role of gln in HMGCR levels is conserved among species and cell types.

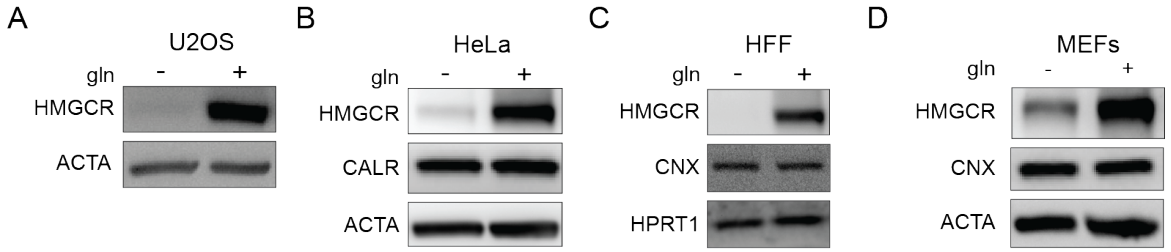

Figure 3.2.1. Glutamine regulates HMGCR levels. U2OS **(A)**, HeLa **(B)**, Primary human foreskin fibroblasts (HFFs) **(C)**, and Murine embryonic fibroblasts (MEFs) **(D)** cells were cultured ± glutamine (gln+, gln-) for 24h and analyzed by immunoblotting for HMGCR, calnexin (CNX), calreticulin (CALR), hypoxanthine phosphoribosyltransferase 1 (HPRT1), tubulin (TUBA) and actin (ACTA). For all experiments, gln was used at 2 mM.

Interestingly, the levels of HMGCR were reduced already at 2h of gln starvation, and after 24h the levels of HMGCR were completely lost in U2OS cells (Figure 3.2.2 – A). Adding back gln after 24h of gln starvation was sufficient to rescue the levels of HMGCR (Figure 3.2.2 – B) and is in accordance with the rescue of cholesterol levels in add-back experiments (Figure 3.1.2 – D and E). Interestingly, after only 2h, the levels of HMGCR started to increase getting the maximum expression at 12h of gln refeeding. To investigate whether HMGCR levels correlate with gln abundance, I refed cells with different concentrations of gln for 24h. Surprisingly, 0.125 mM of gln was sufficient to promote HMGCR levels, arriving at a plateau at 0.5 mM (Figure 3.2.2 – C) — which is ~ the gln concentration in the human plasma (see Chapter 2.1).

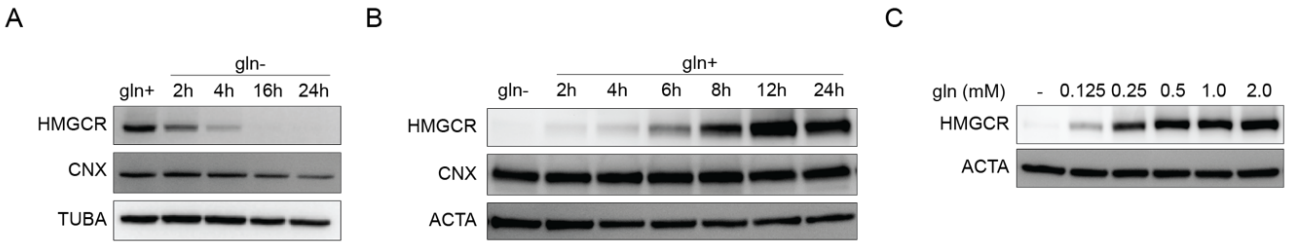

Figure 3.2.2. HMGCR levels are time and concentration-dependent of glutamine. U2OS cells were cultured ± glutamine (gln+, gln-) for the indicated times and analyzed by immunoblotting for HMGCR, calnexin (CNX), and tubulin (TUBA) **(A)**. U2OS cells were starved to gln for 24h and after cultured ± glutamine (gln+, gln-) for the indicated times and analyzed by immunoblotting for HMGCR, CNX, and actin (ACTA) **(B)**. U2OS cells were starved to gln for 24h and after cultured ± glutamine (gln+, gln-) for 24h with the indicated concentrations and analyzed by immunoblotting for HMGCR, and ACTA **(C)**. For all experiments, gln was used at 2 mM if not otherwise indicated.

3. Glutamine starvation promotes glucose oxidation into the TCA cycle

I hypothesized that gln starvation led to the retention of citrate inside mitochondria thereby inhibiting its use in cholesterol synthesis. To address this, I cultured cells with ^{13}C-Glc and gln or aKG. Gln starvation depleted intracellular levels of gln and it was not rescued by aKG addition (Figure 3.3 – A). On the other hand, aKG depletion mediated by gln starvation was rescued by aKG addition (Figure 3.3 –B).

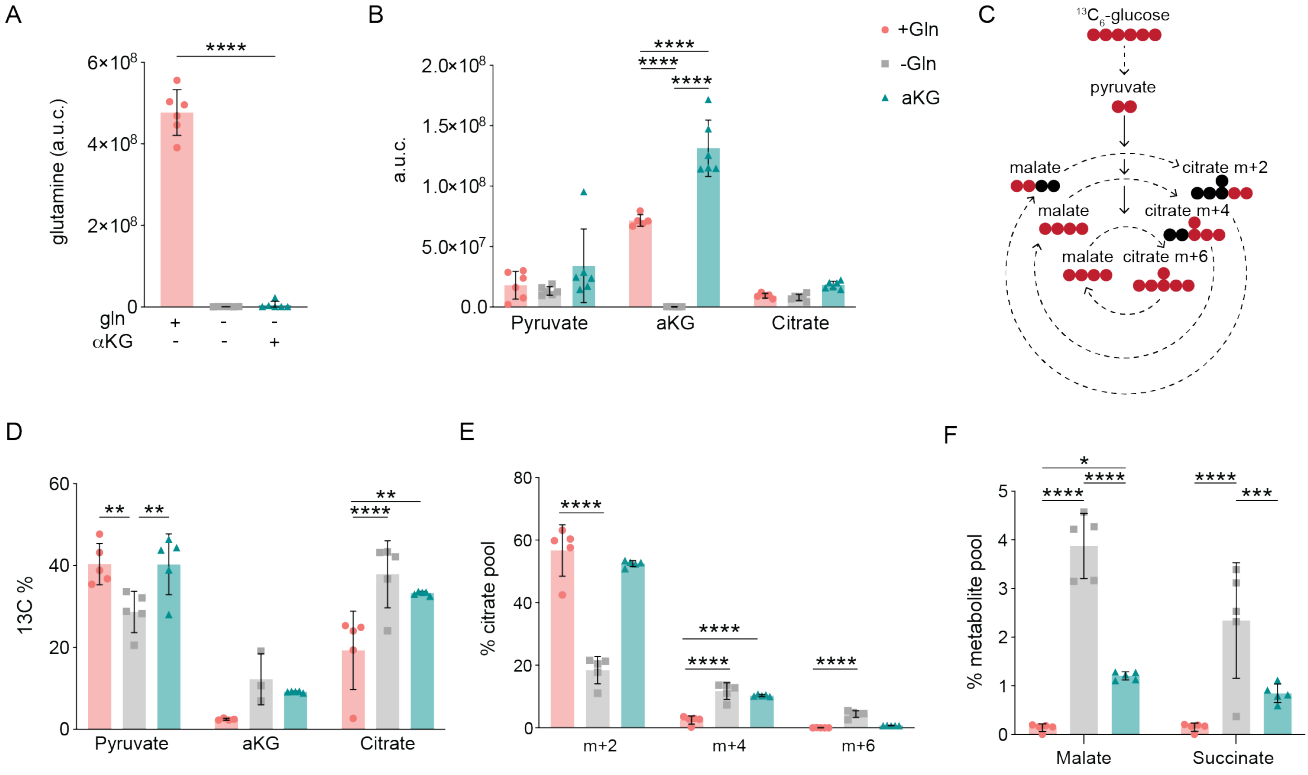

Figure 3.3. Glutamine starvation promotes glucose oxidation into the TCA cycle. The abundance of total glutamine (gln) **(A)** and pyruvate, alpha-ketoglutarate (aKG), and citrate **(B)** in U2OS cells cultured ± gln or aKG, as indicated, for 24h. Simplified model of ^{13}C-glucose (glc) oxidation into the TCA cycle intermediates **(C)**. Red circles represent ^{13}C-carbons and black circles represent ^{12}C-carbons; the dotted arrow represents 1+ steps. Percentage of ^{13}C-pyruvate, ^{13}C-aKG, and ^{13}C-Citrate in U2OS cells cultured ± gln or aKG, as indicated, for 24h **(D)**. Mass isotopologues of ^{13}C-Citrate in U2OS cells cultured ± gln or aKG, as indicated, for 24h **(E)**. Mass isotopologues of ^{13}C-Malate and ^{13}C-Succinate in U2OS cells cultured ± gln or aKG, as indicated, for 24h **(F)**. Data are mean ± s.d. of n=5 independent cultures; *p<0.05, **p<0.01, ***p<0.001, ****p<0.0001, for one or two-way ANOVA. For all experiments, gln was used at 2 mM, aKG at 1 mM, and glucose at 25 mM. The area under the curve (a.u.c.).

Interestingly, the absence of gln did not affect the total levels of citrate but increased the levels of newly synthesized citrate (^{13}C-Citrate), indicating that indeed citrate could be

retained inside mitochondria (Figure 3.3 – B, C, and D). To further investigate this, I analyzed the ^{13}C-Citrate isotopologue distribution. Citrate that incorporates 2 carbons from ^{13}C-Glc is exported for lipid synthesis, or retained inside mitochondria for oxidation in the TCA cycle (Figure 3.1.2 – A and Figure 3.3 – C). The absence of gln increased the isotopologues m+4 and m+6 and decreased the amount of isotopologue m+2 (Figure 3.3 – E). On the other hand, the presence of gln decreased the abundance of the isotopologue m+4 and m+6 and increased the amount of isotopologue m+2 (Figure 3.3 – E). This data indicate that citrate is more exported in the presence of gln, and under gln starvation, citrate cycled inside mitochondria instead of being exported to lipid synthesis. Surprisingly, although aKG also promoted citrate export (Figure 3.3 – E), it did not promote cholesterol synthesis (Figure 3.1.2 – B), disconnecting citrate levels and export from the gln effect in cholesterol synthesis regulation. Moreover, my results show that gln starvation promotes glc oxidation into the TCA cycle.

To address glc oxidation into other TCA cycle intermediates, I measured the isotopologue distribution of ^{13}C-Malate and ^{13}C-Succinate under gln starvation. Both metabolites are present as isotopologue m+2 after 1 round of the TCA, and if citrate is not exported, malate and succinate turn into m+4 in the next rounds (Figure 3.3 – C). Gln starvation also increased the abundance of m+4 ^{13}C-Malate and ^{13}C-Succinate (Figure 3.3 – F), supporting that citrate is not exported but oxidized in the TCA cycle.

4. Cholesterol synthesis regulation is uncoupled from citrate levels and export

My data indicate that the cholesterol synthesis regulation happens independently of citrate availability. This result was surprising, given the central role of citrate in cholesterol synthesis. To better understand the role of citrate in the regulation of cholesterol synthesis, I generated U2OS cells deficient for the enzyme citrate synthase (CS) and the mitochondrial citrate transporter (SLC25A1) by CRISPR-KO (Figure 3.4.1 – A and B). Further, I performed metabolomics in WT, CS-KO, and SLC25A1-KO cells cultured in the absence of FBS to quantify the levels of important metabolites for cholesterol homeostasis (Figure 3.4.2; 3.4.3; and 3.4.4) and lipids levels (Figure 3.4.5).

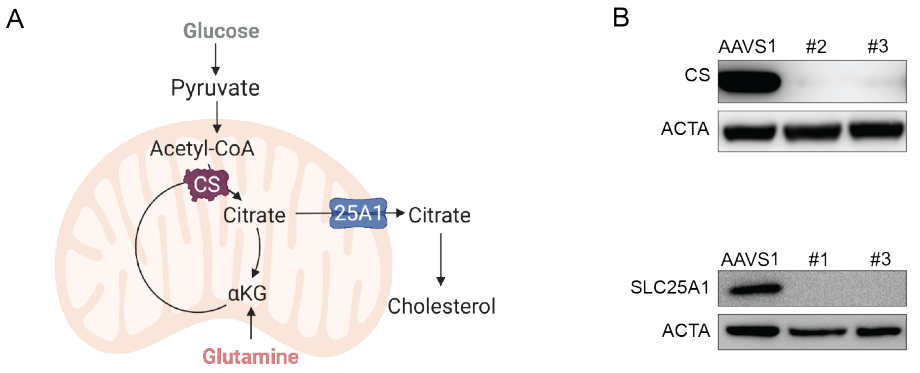

Figure 3.4.1. Validation of CS and SLC25A1-KO cells. Simplified model of citrate production and export from mitochondria **(A)**. Citrate synthase (CS) and the mitochondrial citrate transporter (SLC25A1) **(B)** were depleted in U2OS cells by CRISPR.

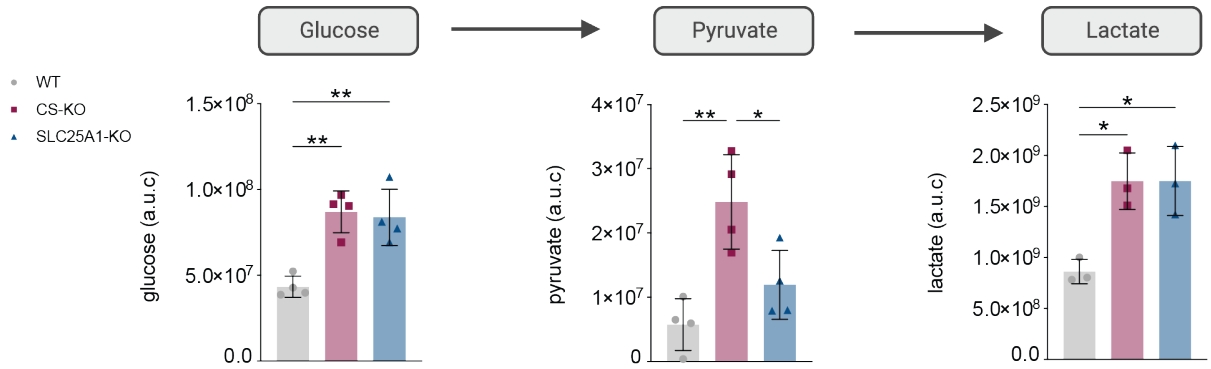

Figure 3.4.2. CS and SLC25A1-KO have increased glycolysis. The abundance of total glucose, pyruvate, and lactate in WT, CS-KO, and SLC25A1-KO U2OS cells. The area under the curve (a.u.c.). Data are mean ± s.d. of n=4 independent cultures; *p<0.05, and **p<0.01 for one-way ANOVA.

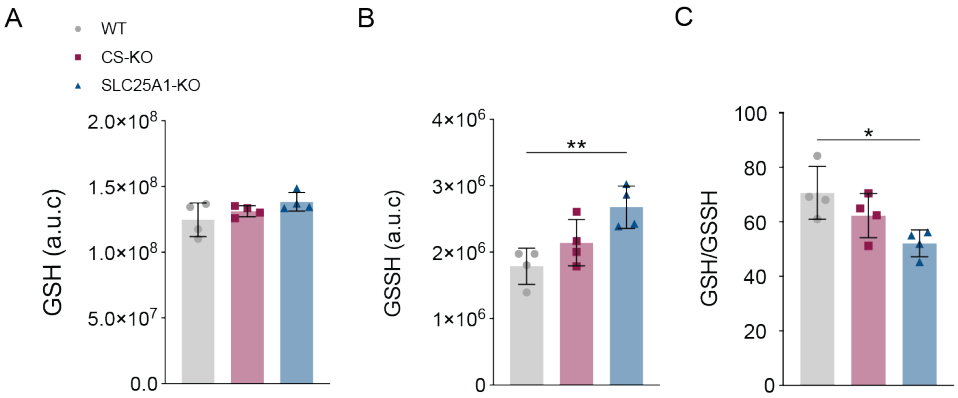

Figure 3.4.3. Loss of SLC25A1 results in oxidative stress. The abundance of total reduced glutathione (GHS), oxidized glutathione (GSSH), and the ratio GSH/GSSH in WT, CS-KO, and SLC25A1-KO U2OS cells. The area under the curve (a.u.c.). Data are mean ± s.d. of n=4 independent cultures; *p<0.05, and **p<0.01 for one-way ANOVA.

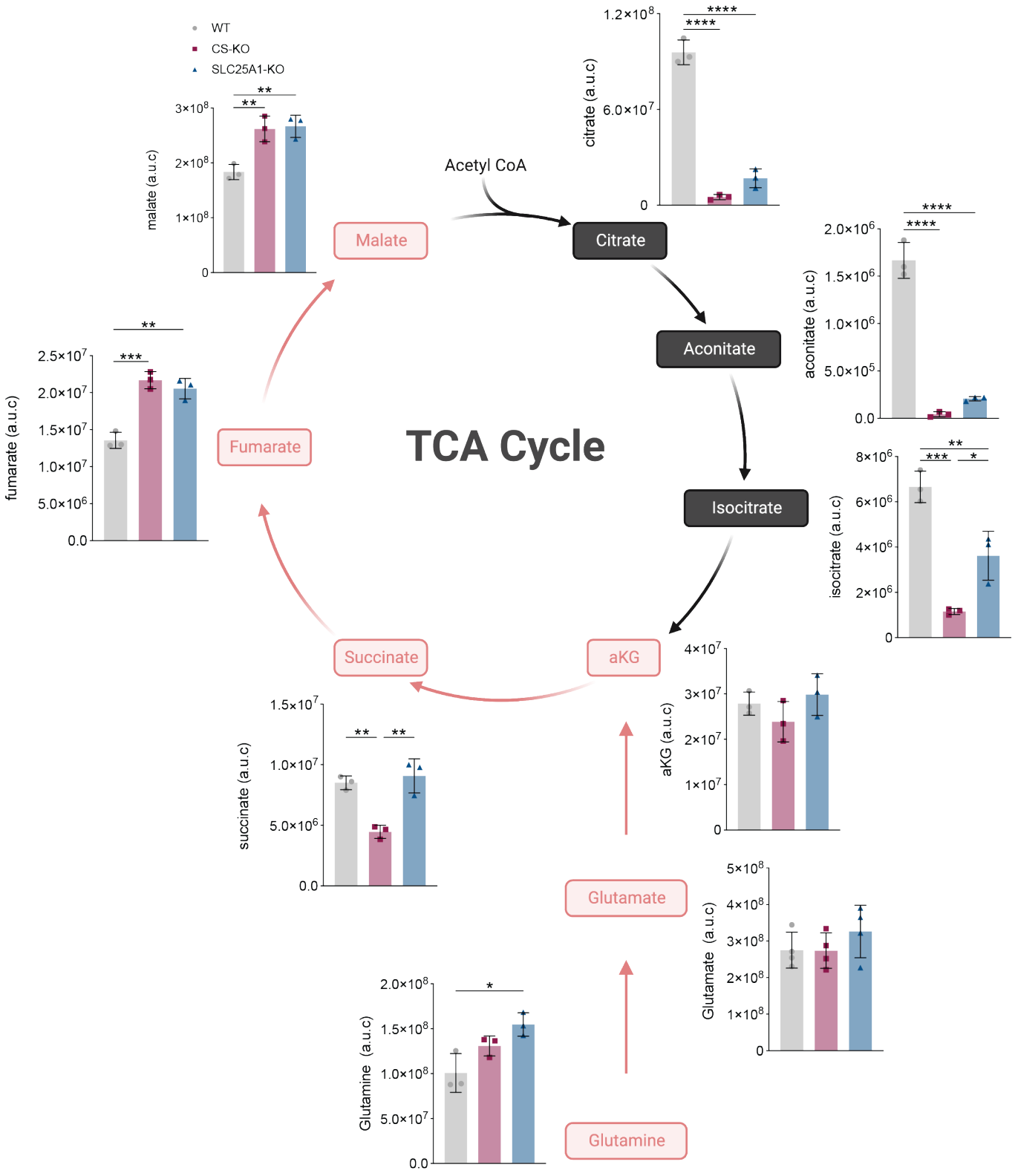

Figure 3.4.4. Lack of CS or SLC25A1 partially blocks the TCA cycle. The abundance of total TCA cycle intermediates in WT, CS-KO, and SLC25A1-KO U2OS cells. The area under the curve (a.u.c.). Data are mean ± s.d. of n=4 independent cultures; *p<0.05, **p<0.01, ***p<0.001, ****p<0.0001 for one-way ANOVA.

As expected, CS-KO and SLC25A1-KO cells had indications of mitochondrial dysfunction. First, the KO cells had a ~ 2-fold increase in glycolytic metabolites such as glc, pyruvate, and lactate (Figure 3.4.2). Second, the KO of CS and SLC25A1 affected the redox states of the cells, increasing the oxidized glutathione (GSSH) levels and the ratio GSH (reduced glutathione)/GSSH, indicating mitochondrial dysfunction and suggesting increased ROS (reactive oxygen species) production (Figure 3.4.3) (Chakrabarti et al., 2022; Dania C. Liemburg-Apers et al., 2015; Dania C. Liemburg-Apers et al., 2015; Rafikov et al., 2015).

To address the TCA cycle activity, I quantified the levels of the TCA intermediates in WT, CS-KO, and SLC25A1-KO cells. The lack of CS blocked citrate production and drastically reduced levels of the next intermediates in the cycle: aconitate and isocitrate (Figure 3.4.4). Surprisingly, the lack of SLC25A1 had the same effect, suggesting that the retention of citrate inside mitochondria may negatively regulate CS activity (Figure 3.4.4).

It is known that mitochondrial dysfunctions lead not only to increased glycolysis (Dania C. Liemburg-Apers et al., 2015) but also to a dependency on glutaminolysis to sustain the TCA cycle (Yang et al., 2014; Yoo et al., 2020). As expected, CS-KO and SLC25A1-KO cells had higher levels of gln uptake (Figure 3.4.4). Moreover, gln feeds the TCA cycle through aKG, and the levels of the next intermediates after aKG (succinate, fumarate, and malate) were unchanged or higher in CS-KO and SLC25A1-KO cells (Figure 3.4.4). This strongly suggests that gln feeds part of the TCA cycle when citrate production is impaired.

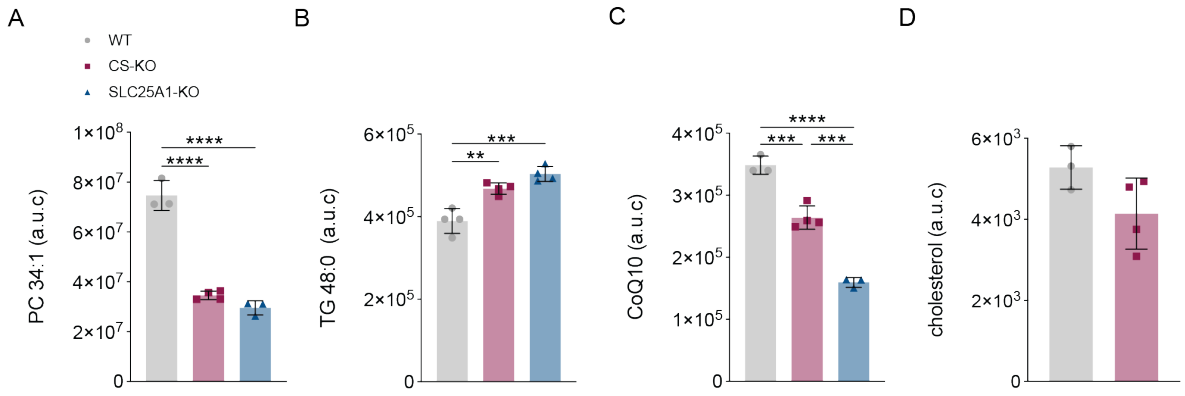

Figure 3.4.5. CS and SLC25A1-KO cells have low levels of lipids. The abundance of total phosphatidylcholine (PC) 34:1, triacylglycerol (TG) 48:0, coenzyme Q (CoQ) 10, and cholesterol in WT, CS-KO, and SLC25A1-KO U2OS cells. The area under the curve (a.u.c.). Data are mean ± s.d. of n=4 independent cultures, **p<0.01, ***p<0.001, and ****p<0.0001 for one-way ANOVA.

To understand the effects of CS and SLC25A1 in lipid homeostasis, I quantified the levels of PC 34:1 (phospholipid), TG 48:0 (fatty acid), Coenzyme Q 10 (CoQ10), and cholesterol in CS-KO and SLC25A1-KO cells. The KO cells had lower levels of PC 34:1 and higher TG 48:0 (Figure 3.4.5 – A and B). This data indicates different regulatory mechanisms governing the synthesis of different classes of lipids, as also my gln starvation data suggested (Figure 3.1.2).

Interestingly, levels of CoQ10 are decreased in the KO cells while no changes in cholesterol levels were found (Figure 3.4.1 – C and D), indicating that other products of the mevalonate pathway may be more sensitive to citrate levels.

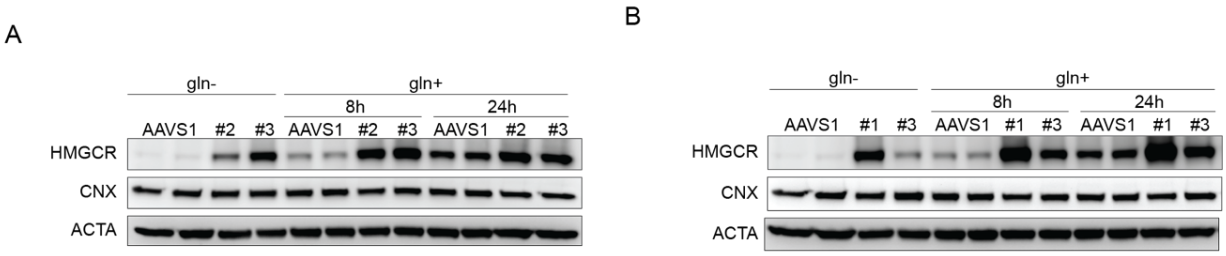

Figure 3.4.6. CS and SLC25A1-KO cells have higher levels of HMGCR and are responsive to glutamine starvation. U2OS WT, CS-KO **(A)**, and SLC25A1-KO **(B)** cells were cultured ± glutamine (gln+, gln-) for the indicated times and analyzed by immunoblotting for HMGCR, calnexin (CNX), and actin (ACTA). For all experiments, gln was used at 2 mM.

To assess the possible role of citrate levels and export from mitochondria in the regulation of the cholesterol synthesis enzymes, I quantified HMGCR levels in the CS-KO and SLC25A1-KO cells. Cells lacking CS and SLC25A1 had higher levels of HMGCR (Figure 3.4.6 – A and B) in the presence or absence of gln. This data shows that neither changes in citrate levels nor citrate export are required for HMGCR levels, disconnecting again citrate and the regulation of cholesterol synthesis. Moreover, the effect of gln on HMGCR levels is also citrate-independent.

5. Only glutamine, but not its derivatives, regulates HMGCR levels

Gln can be hydrolyzed and its derivatives feed several pathways in the cell (see Chapter 1.2.3) (Figure 3.5.1 – A). To further understand whether gln or its derivatives regulated cholesterol synthesis, I first measured which gln derivatives were decreased after 24h of gln starvation. All the main gln-derivatives were decreased after 24h of gln starvation (Figure

3.5.1 – B, C, and D). Moreover, aKG was sufficient to rescue only the TCA cycle intermediates, but not the UDP-GlnNac, NEAA, or nucleotide levels.

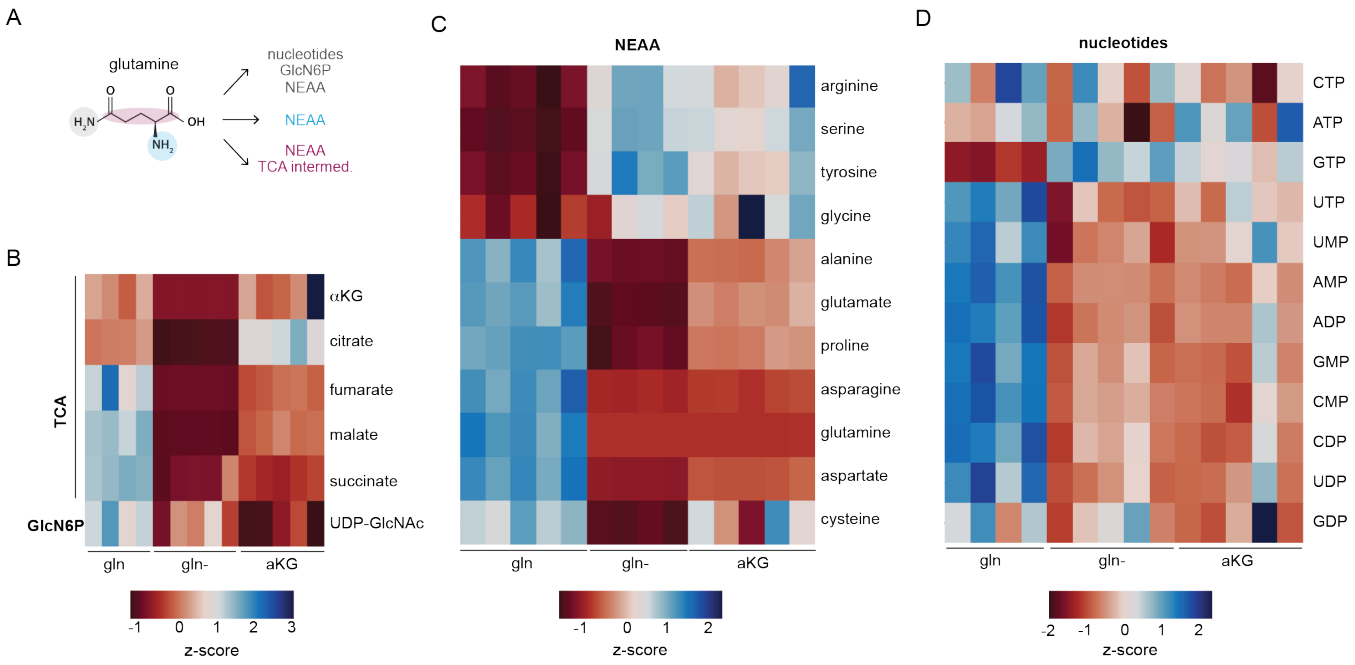

Figure 3.5.1. Glutamine starvation leads to decreased gln-derivatives levels. Glutamine (gln) supplies carbons and nitrogens for the synthesis of TCA intermediates, glucosamine-6-phosphate (GlcN6P) that is used for UDP-GlcNAc synthesis, non-essential amino acids (NEAA), and nucleotides **(A)**. Heat map of z-score normalization of the total pool size of TCA-cycle metabolites and UDP-GlcNAc **(B)**, non-essential amino acids (NEAA) **(C)**, and nucleotides **(D)** in U2OS cells cultured for 24h ± gln or aKG. Data are mean ± s.d. of n=5 independent cultures. For all experiments, gln was used at 2 mM and aKG at 1 mM.

To address the possibility that one of the gln derivatives regulates cholesterol synthesis, I starved cells were cultured in presence of gln or gln derivatives for 8h (Figure 3.5.2 – A). The addition of NEAA, nucleosides, and glucosamine (even in the presence of aKG) did not rescue HMGCR levels in the absence of gln, discarding a possible role of them in regulating HMGCR levels.

To address a boost of the TCA cycle in the presence of both glc and gln, cells starved to gln were also fed with glc and pyruvate (alone and in combination). However, only gln was sufficient to sustain HMGCR levels (Figure 3.4.6 – B) and a combination of glc and pyruvate had no effect on HMGCR levels. This data discards a glc or pyruvate combination role with gln in the regulation of cholesterol synthesis and pinpoint gln as the major regulator of HMGCR levels.

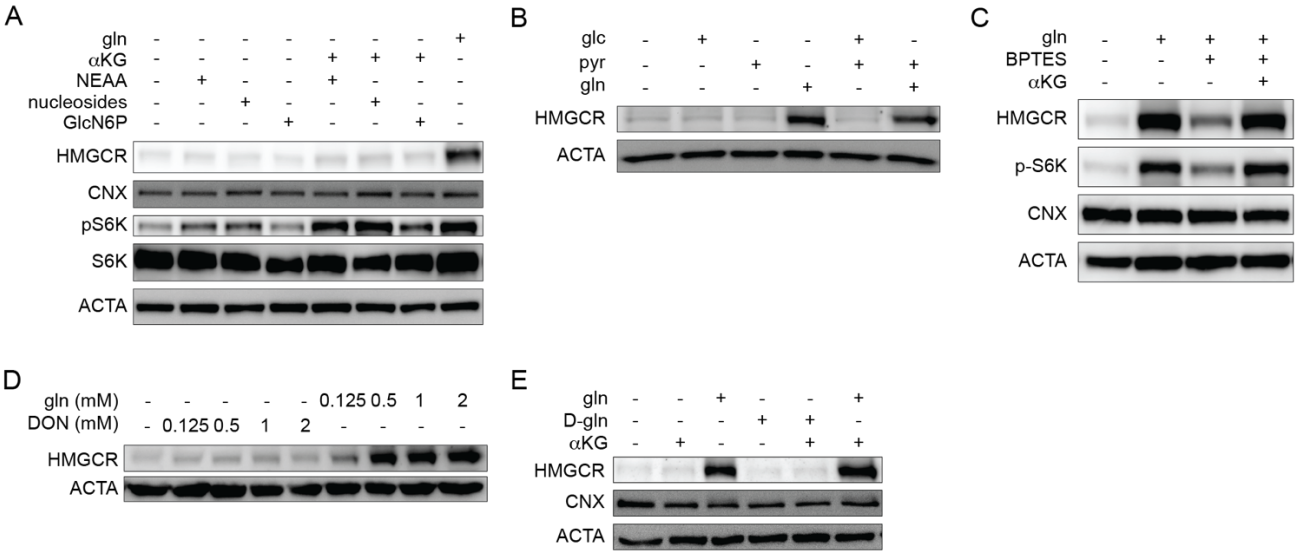

Figure 3.5.2. The addition of glutamine derivatives or variants does not rescue HMGCR levels under glutamine starvation. U2OS cells were cultured ± glutamine (gln) for 8 hours with the indicated supplements and concentrations; gln: 2 mM; aKG: 1mM; NEAA: 100 µM (glycine, alanine, asparagine, aspartate, glutamate, proline, and serine), nucleosides (cytidine 7.3 mg/L, guanosine 8.5 mg/L, uridine 7.3 mg/L, adenosine 8 mg/L, and thymidine 2.4 mg/L), and glucosamine (precursor to UDP-GlcNAc): 1 mM **(A)**. U2OS cells were cultured without gln for 24h and treated as indicated for 24h. Concentrations used: 1 mM sodium pyruvate (pyr), 2 mM gln, and 25 mM glucose (glc) **(B)**. U2OS cells were cultured as indicated for 8h. Concentrations used: 30 µM BPTES, 2 mM gln, and 1 mM aKG **(C)**. U2OS cells were cultured without gln for 24h and treated as indicated for 24h with gln or 6-diazo-5-oxo-L-norleucine (DON) with the indicated concentrations **(D)**. U2OS cells were cultured without gln for 24h and treated as indicated for 24h with 2 mM gln, 2 mM D-gln, or 1 mM aKG. Samples were analyzed by immunoblotting for HMGCR, calnexin (CNX), p70 S6 kinase (S6K), p70 phospho-S6K (pS6K), and actin (ACTA).

Gln activates mTORC1 through gln hydrolysis and aKG production (see Chapter 1.2.4). Thus, gln starvation inhibits mTORC1 and could affect HMGCR levels by blocking protein translation. To exclude a possible role for translation inhibition as a factor during gln hydrolysis inhibition, I cultured the cells in the presence of BPTES (X bis-2-(5-phenylacetamido-1,3,4-thiadiazol-2-yl)ethyl sulfide; glutaminolysis inhibitor) and aKG to sustain mTORC1 activity during impaired gln hydrolysis. I found that the inhibition of gln hydrolysis — and consequently glutamate, aKG, and NH_4^+ production — did not affect HMGCR levels (Figure 3.5.2 – C). Thus, the cholesterol synthesis regulatory effect of gln is independent of its hydrolysis. Moreover, structural variants of gln including D-gln and the gln antagonist DON (6-Diazo-5-oxo-L-norleucina) did not rescue HMGCR expression (Figure 3.5.2 – D and E). This data indicate that gln per se regulates cholesterol synthesis.

6. Glutamine regulates cholesterol synthesis through the SREBP2 pathway

There are two major pathways for HMGCR levels regulation: the SREBP2 pathway and degradation by proteasome machinery (see Chapter 1.1.2) (Figure 3.6.1– A). To better understand how gln increases HMGCR levels, I first assessed whether gln starvation promoted HMGCR degradation. To address this hypothesis, cells were treated with MG-132, a proteasome inhibitor that blocks protein degradation — as seen by the accumulation of ubiquitinated proteins (Figure 3.6.1– B) —, at the same time that gln withdrawal. Interestingly, blocking HMGCR degradation slightly increased the levels of HMGCR in gln-repleted and depletion conditions — showing that there is a basal degradation of this protein in both conditions. However, the inhibition of HMGCR degradation did not prevent HMGCR loss in gln-depletion (Figure 3.6.1– B). Thus, gln regulates HMGCR independently of its degradation.

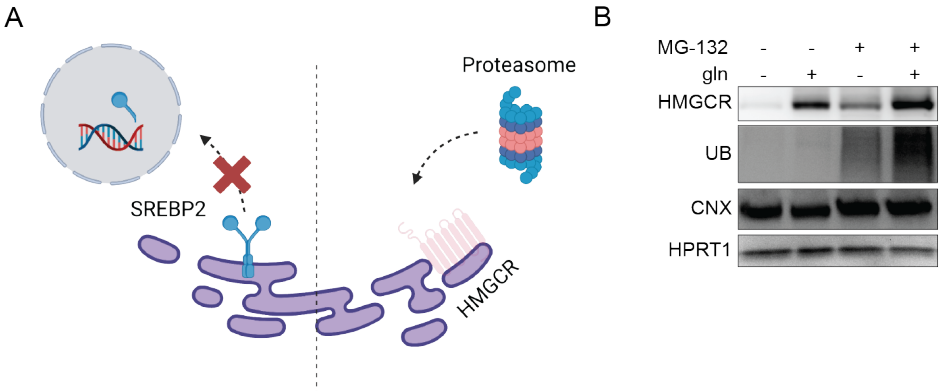

Figure 3.6.1. Glutamine does not affect HMGCR degradation. Simplified model of HMGCR levels regulation **(A)**. Glutamine-fed U2OS cells were cultured ± glutamine (gln+, gln-) and MG-132 (10 μM) for 8h **(B)**. Samples were analyzed by immunoblotting for HMGCR, ubiquitin (ub) calnexin (CNX), and hypoxanthine phosphoribosyltransferase 1 (HPRT1).

To assess whether gln affected the transcriptional regulation of HMGCR, I starved the cells to gln +/- aKG (to exclude the TCA cycle and mTORC1 activity effects) and performed RNAseq analysis (Figure 3.6.2– A). The enrichment pathway analysis showed that several pathways related to cholesterol synthesis and metabolism were decreased without gln (Figure 3.6.2– B). This data indicates that gln promotes the expression of cholesterol synthesis enzymes.

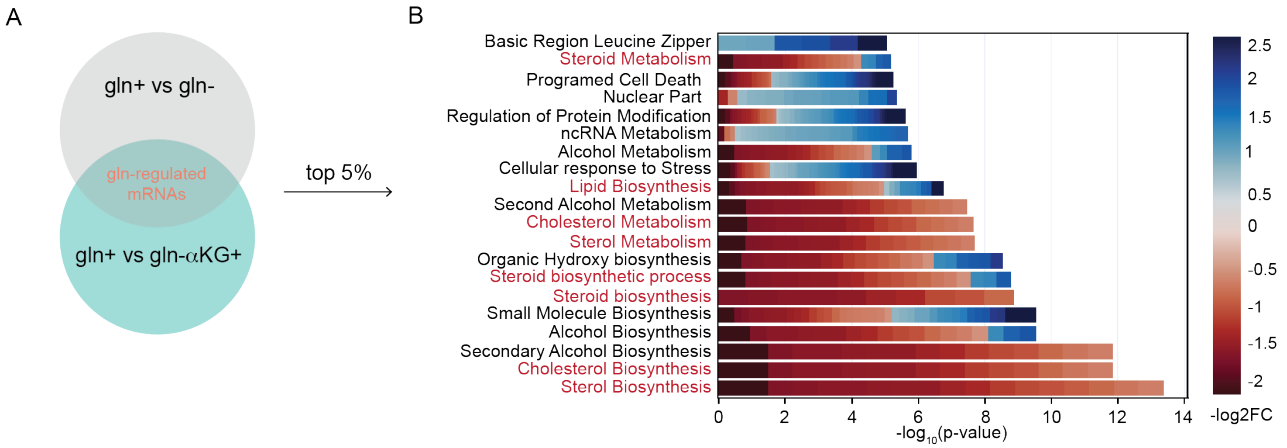

Figure 3.6.2. Glutamine changes the transcriptome of U2OS cells. U2OS cells were cultured with glutamine (gln+) or without glutamine ± aKG (gln-, aKG+) for 8h and analyzed by RNAseq analysis. Glutamine-responsive genes were those differentially regulated (FDR adjusted p-value of <0.01) between gln+ vs. gln- and gln+ vs. aKG+, but not significantly different between gln- vs. aKG+ sets; n=6 independent replicates **(A)**. GO analysis was performed on the top 5% of glutamine-responsive genes from analysis in (A); red text corresponds to cholesterol-related processes **(B)**.

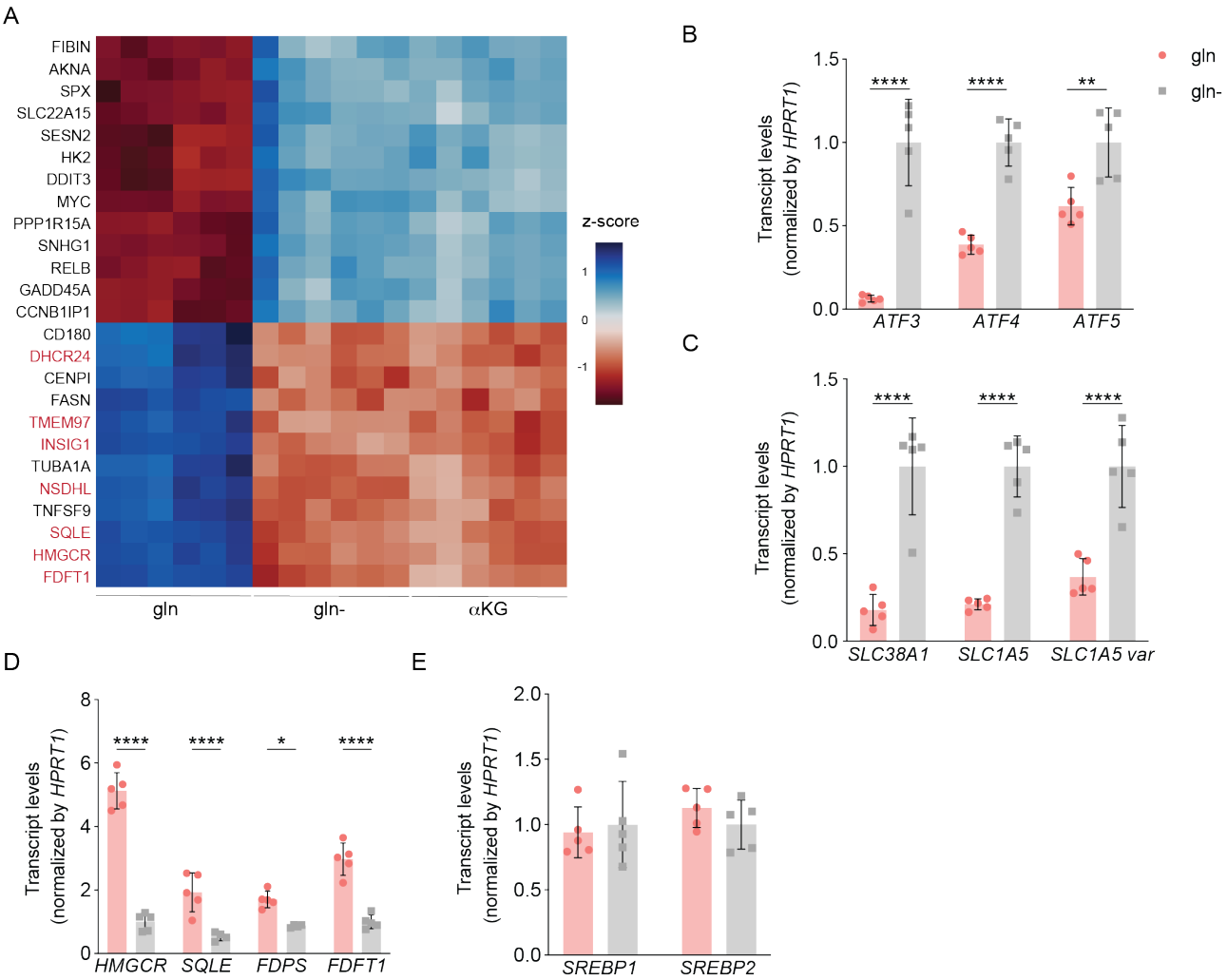

Figure 3.6.3. Glutamine is required for SREBP2 target genes expression. Heat map of z-score of expression values of the top 25 glutamine-regulated genes from the subset as described in (Figure 3.6.2 - A); genes in red are genes related to cholesterol synthesis regulation **(A)**. mRNA levels in U2OS cells that were cultured without gln for 24h, followed by gln- and gln+ culture for 8h. mRNA expression was measured by the standard curve method and normalized to HPRT1; the y-axis depicts the transcript levels related to cellular stress response **(B)**, glutamine uptake **(C)**, cholesterol synthesis **(D)**, and *SREBP1/2* **(E)**. Data are mean ± s.d. of n=5 independent cultures; *p<0.05, **p<0.01, ****p<0.0001, for two-way ANOVA. For all experiments, gln was used at 2 mM, and aKG at 1 mM.

To further investigate the gln transcriptional regulation, I selected the top 25 genes most affected by gln starvation. As no surprise, one of the top genes was c-Myc (see Chapter 1.2.4), a major regulator of gln metabolism (Figure 3.6.3 – A). Among the top 25 genes, 7 genes important for cholesterol synthesis were downregulated (Figure 3.6.3 – A; in red). Next, I assessed whether adding back gln was sufficient to promote the expression of cholesterol synthesis enzymes again. Interestingly, adding back gln was sufficient to decrease cellular stress programs (Figure 3.6.3– B) and decrease the expression of the gln transporters in the cell (Figure 3.6.3– C). Moreover, gln refeeding promoted the expression of the cholesterol synthesis enzymes *HMGCR*, *SQLE*, *FDPS,* and *FDFT1* (Figure 3.6.3– D). However, gln did not promote the expression of the *SREBP2* gene, or its variant *SREBP1* which regulates fatty acids synthesis. This data indicates that gln is required for transcription of the cholesterol synthesis enzymes, and its abundance is sensed by the SREBP2 pathway at the protein level.

7. Glutamine starvation blocks SCAP-SREP2 trafficking to Golgi

To investigate whether gln is sensed by the SREBP2 pathway at the protein level, I measured the levels of precursor (ER-resident) and mature SREBP2 (after trafficking and activation by proteolytic cleavage at Golgi) (see Chapter 1.1.2). In line with the RNAseq data, only gln, but not glc or aKG, promoted the activation of SREBP2 (Figure 3.7.1 – A and B). Other SREBP2 targets such as *HMGCR* and *FDFT1* were also increased in the presence of gln, confirming SREBP2 activation and transcriptional factor activity (Figure 3.7.1 – B). The overexpression of the mature version of SREBP2 in the absence of gln rescued the levels of SREBP2 and HMGCR (Figure 3.7.1 – C), pinpointing the lack of SREBP2 activation under gln starvation as the mechanism underlying the suppression of cholesterol synthesis.

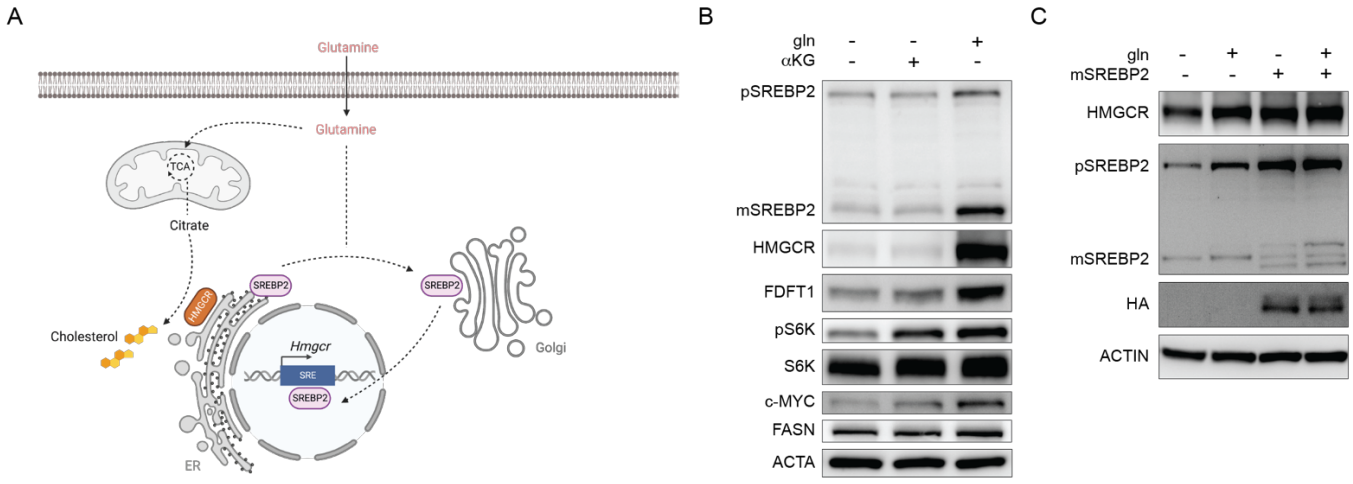

Figure 3.7.1. Glutamine is required for SREBP2 activation. Simplified hypothetical model of glutamine regulating HMGCR levels through SREBP2 **(A)**. U2OS cells were cultured ± glutamine or aKG for 8h and analyzed by immunoblotting **(B)**. mSREBP2-HA was expressed in CHO (Chinese hamster ovary) cells and cultured ± glutamine for 8h and analyzed by immunoblotting **(C)**. Samples immunoblotted for HMGCR, precursor (p) SREBP2, mature (m) SREBP2, FDFT1 (farnesyl-diphosphate farnesyltransferase 1), p70 S6 kinase (S6K), p70 phospho-S6K (pS6K), calnexin (CNX), c-MYC, fatty Acid Synthase (FASN), HA-tag (HA) and actin (ACTA).

To better understand how gln-starvation inhibits SREBP2 activation, I investigated the trafficking of proteins between ER and Golgi through COPII vesicles (see Chapter 1.1.2 and Figure 3.7.1 – A). A general impairment of the trafficking between the ER and Golgi could explain the effect of gln on SREBP2 maturation. To test this hypothesis, I first quantified the trafficking of other COPII cargos. ATF6 (Activating Transcription Factor 6) is another ER-resident transcription factor that undergoes cleavage at the Golgi by the same proteases as SREBP2 to be activated (Ye et al., 2000). Interestingly, the absence of gln did not affect ATF6 trafficking and activation under Tunicamycin treatment (Figure 3.7.2 – A).

To further measure the general trafficking between ER and Golgi, I applied the RUSH (Retention Using Selective Hooks) system. In this method, an ER-tagged protein (MAN2 – Alpha-Mannosidase 2) is reattained in the ER through a hook protein fused to streptavidin. The addition of biotin releases the ER protein from its hook and allows the measurement of ER-Golgi trafficking (Boncompain et al., 2012). The absence of gln did not affect the trafficking of MAN2 using the RUSH system (Figure 3.7.2 – B) as after 180 min the majority of MAN2 was Golgi-localized. Interestingly, at early time points as 1h (Figure 3.7.2 – B and C) a delay in the trafficking could be observed, suggesting that although not required, gln may facilitate the general ER-Golgi trafficking.

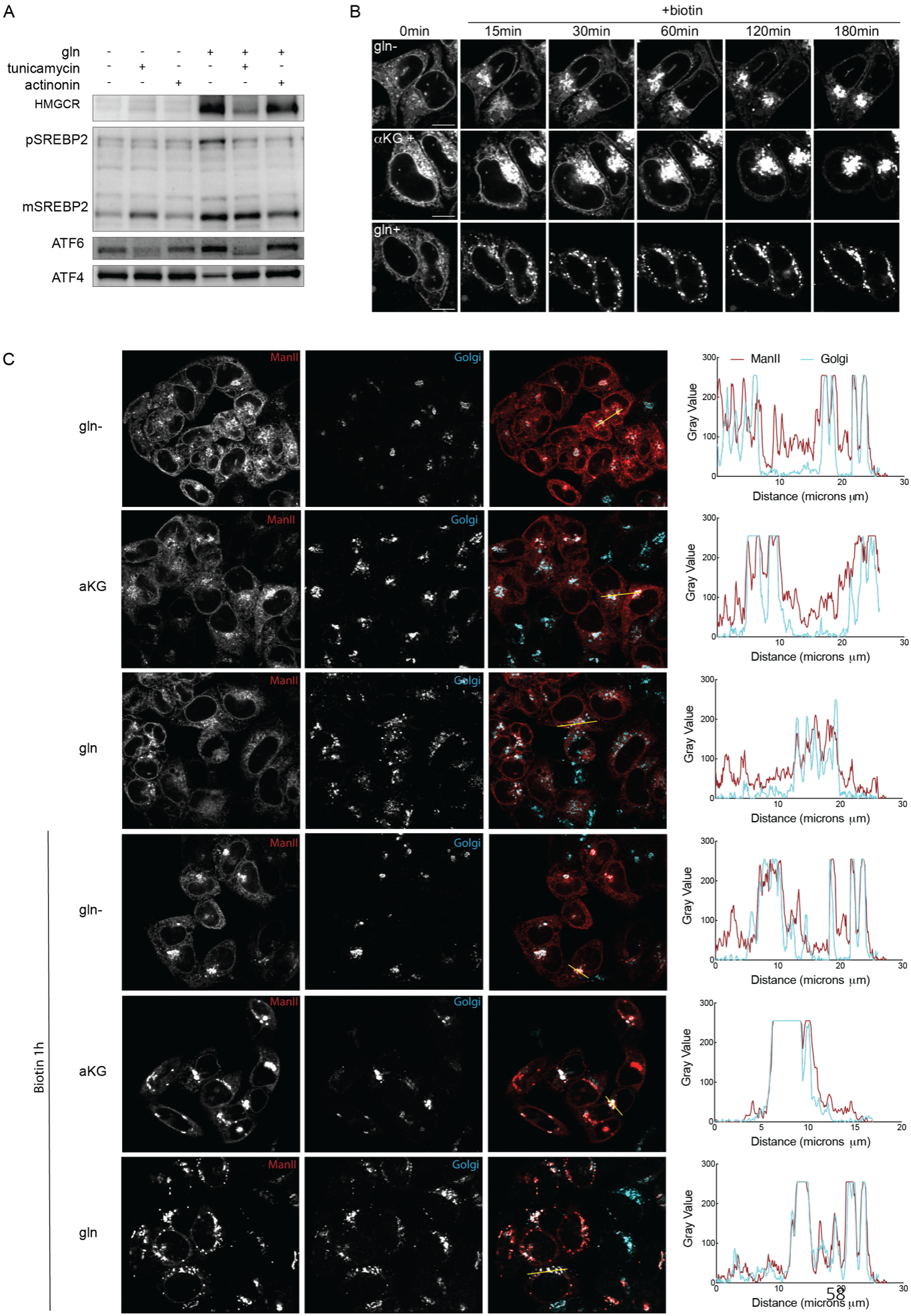
A
gln
tunicamycin
actinonin
HMGCR
pSREBP2
mSREBP2
ATF6
ATF4
B
+biotin
0min
15min
30min
60min
120min
180min
gln-
αKG +
gln+
C
ManII
Golgi
gln-
aKG
gln
Biotin 1h
Gray Value
Distance (microns μm)

Figure 3.7.2. Glutamine starvation does not affect the general ER-Golgi trafficking of proteins. U2OS cells were cultured without glutamine (gln) for 24h and treated as indicated for 8 hours. Concentrations used: 2 mM gln, 15 ug/mL tunicamycin,100 μM actinonin. Samples were analyzed by immunoblotting for HMGCR, precursor, and mature SREBP2 (pSREBP2, mSREBP2), ATF6, and ATF4 **(A)**. HeLas stably expressing mannosidase II-mCherry (MANII) fused to a streptavidin-binding peptide, and streptavidin fused KDEL which retains it in the ER were cultured without gln for 24h. Following 8h of treatment with gln (gln+) or without gln ± 1 mM aKG (gln-, aKG+, respectively), biotin was added as indicated. Representative live-cell images of mCherry-MANII at indicated time points following 40 μM biotin addition. Scale bar 10 μm **(B)**. HeLas stably expressing MANII-mCherry were treated as in (B), and cells were fixed and stained with anti-Golgi-488 antibody. Representative images of mCherry-MANII ± 40 μM of biotin for 1h. Co-localization of MANII with Golgi was measured using Fiji software. Scale bar 10 μm **(C)**.

Surprisingly, even after 24h of gln deprivation, the addition of biotin with aKG or gln had the same effect on ER-Golgi trafficking (Figure 3.7.3). After 180 min of refeeding, both metabolites promoted the trafficking of MAN2 to the Golgi. Collectively, these data indicate that the absence of gln does not impair ER-Golgi trafficking.

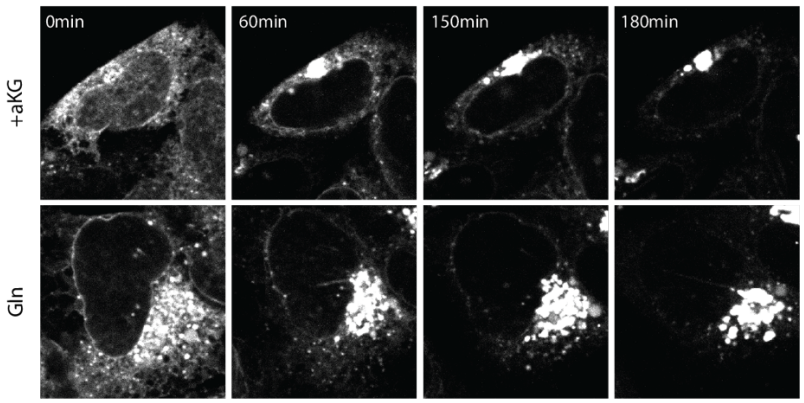

Figure 3.7.3. Refeeding of glutamine or aKG – simultaneously with biotin - promotes general ER-Golgi trafficking of proteins after glutamine starvation. HeLas stably expressing mannosidase II-mCherry (MANII) fused to a streptavidin-binding peptide, and streptavidin fused KDEL transmembrane domain which retains it in the ER were cultured without glutamine for 24h. Glutamine or aKG was added together with 40 μM of biotin. Representative live-cell images of mCherry-MANII at indicated time points.

To assess whether the ER-to-Golgi trafficking of SCAP-SREBP2 was specifically inhibited, I used CHO (Chinese hamster ovary cells) cells stable expressing SCAP-EGFP (Figure 3.7.4 – A). In the presence of gln, almost 80% of the cells had Golgi-localized SCAP, which represents an activated SREBP2 pathway and activated cholesterol synthesis (Figure 3.7.4 – A and B). However, in the absence of gln, with or without aKG, this percentage was reduced to <5%. Thus, the reduction in the SREBP2 pathway activation in the absence of gln is due to a specific block in the trafficking of the SCAP-SREBP2 complex from the ER to the Golgi.

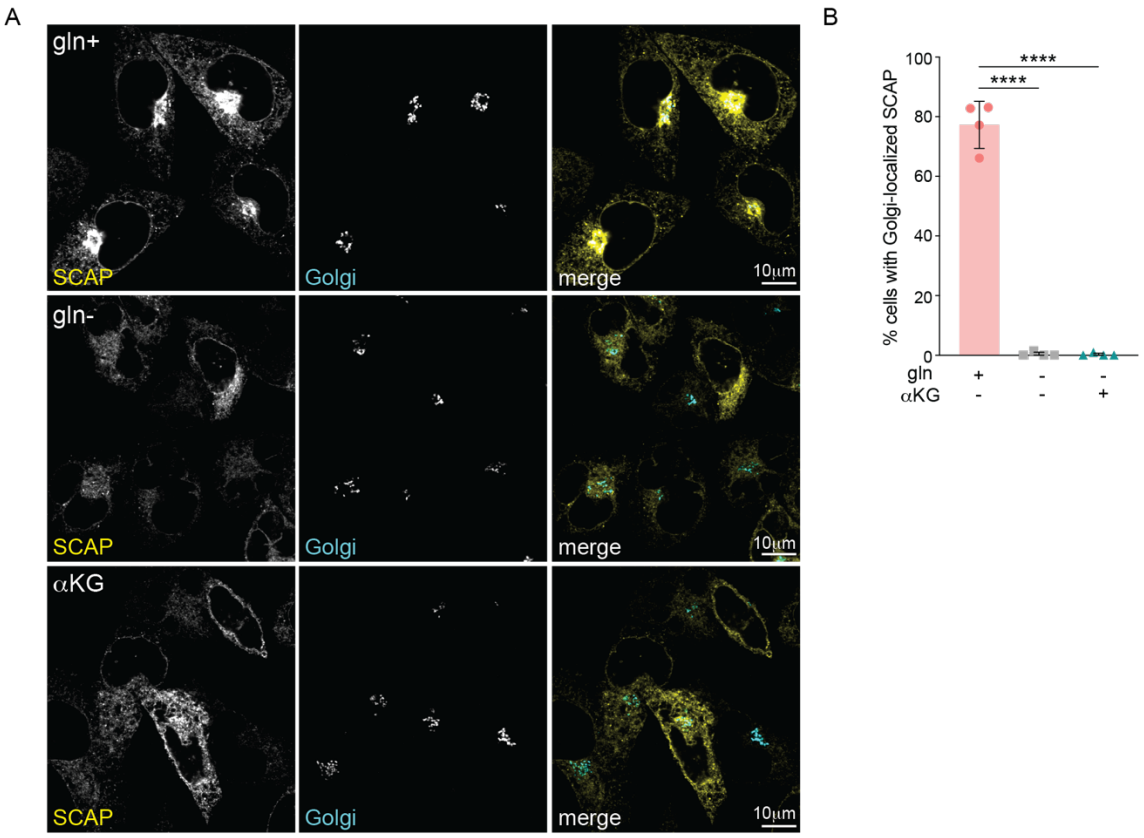

Figure 3.7.4. Glutamine is required for SCAP-SREBP2 trafficking. Representative images of eGFP-SCAP-expressing CHO cells cultured without gln for 24h, and then treated with gln (gln+) or without gln (gln-), or without gln with aKG (aKG+) in the presence of methionine sulfoximine (MSX; 500 μM) for 24h and processed for immunofluorescence analysis of the Golgi (using anti-golgin-97 antibody). Panels show localization of eGFP-SCAP relative to the Golgi, scale bar 10 μm **(A)**. Percentage of cells with Golgi-localized eGFP-SCAP **(B)** from experiments as in (A); data are mean ± s.d. of >100 cells counted from n=4 biological replicates; ****p<0.0001 for one-way ANOVA.

To rescue the SCAP-SREBP2 complex trafficking in the absence of gln, gln-starved cells were treated with Brefeldin A (BFA), which reallocates cis-Golgi proteins to the ER in the absence of ER-Golgi trafficking (Doms et al., 1989). Indeed, the redistribution of Golgi proteins to the ER (Figure 3.7.5 – A) rescued the cleavage and activation of SREBP2 in the absence of gln (Figure 3.7.5 – B), as well as HMGCR levels, demonstrating that gln starvation inhibits SREBP2 activity by preventing the trafficking of SCAP-SREBP2.

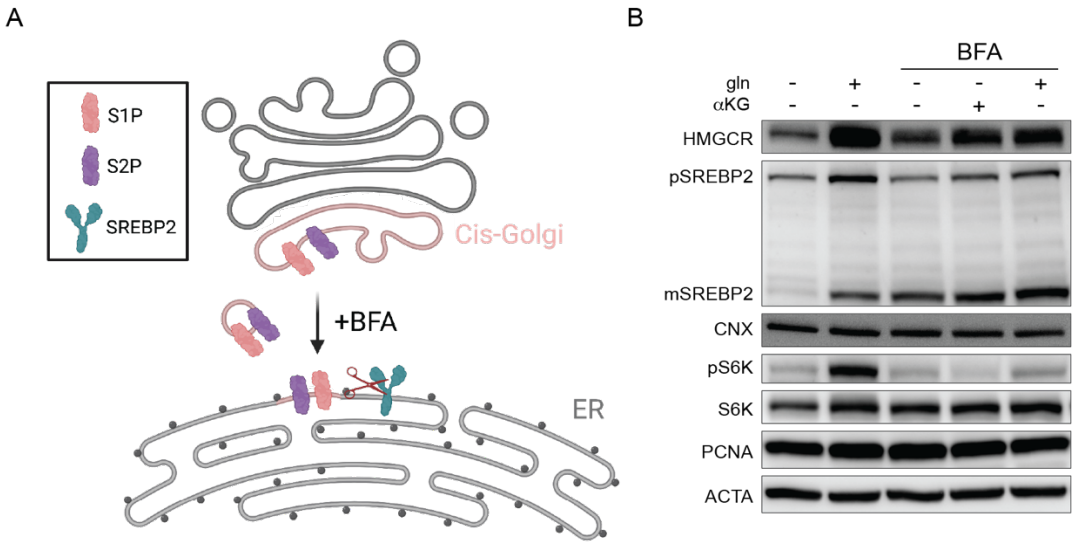

Figure 3.7.5. Forcing SREBP2 cleavage is sufficient to rescue the levels of mSREBP2 and HMGCR upon glutamine starvation. Simplified hypothetical model of S1P and S2P relocalization upon Brefeldin A (BFA) treatment. **(A)**. HepG2s were starved of glutamine (gln) for 24h and treated with ± gln or alpha-ketoglutarate (aKG) and BFA for 8h **(B)**. Samples were analyzed by immunoblotting for HMGCR, precursor and mature SREBP2 (pSREBP2 and mSREBP2), calnexin (CNX), p70 S6 kinase (S6K), p70 phospho-S6K (pS6K), proliferating cell nuclear antigen (PCNA) and actin (ACTA). For all experiments, gln was used at 2 mM, aKG at 1 mM, and BFA at 0.5 ug/mL.

8. MFN2-KO cells as a model to study the role of glutamine in the pathophysiological conditions

To better understand whether gln could play a role in regulating cholesterol in pathophysiological conditions, I took advantage of an *in vitro* model already known for promoting gln metabolism rewiring — the KO of MFN2 (see Chapter 1.3.1 and 1.3.2). First, I confirmed that the loss of MFN2 in U2OS resulted in mitochondrial dysfunction and gln metabolism rewiring (Figure 3.8.1 and Figure 3.8.2) in the absence of FBS.

I found that the loss of MFN2 in U2OS cells reduced the levels of other mitochondrial proteins such as SDHA, TOM20, and TOM40 (Figure 3.8.1 – A). MFN2-KO cells also had lower levels of GLS even though these cells undergo more glutaminolysis (Figure 3.8.2). Thus, the loss of MFN2 promotes a rewiring of the mitochondrial proteome. To assess mitochondrial dysfunction in the MFN2-KO cells, mitochondrial respiration was measured. As expected, cells lacking *MFN2* showed lower basal and maximum respiration (Figure 3.8.1 – B, C, and D) (Tur et al., 2020; Yao et al., 2019). The mitochondrial dysfunction in MFN2-KO cells was correlated with lower ATP production and spare respiratory capacity (Figure 3.8.1 –

E and D). Cells lacking MFN2 had higher gln consumption (Figure 3.8.2 – A) to promote anaplerosis through the reductive TCA cycle (Figure 3.8.2 – B). This data confirms that MFN2-KO is a viable model of enhanced gln dependence, with higher levels of gln consumption and metabolism.

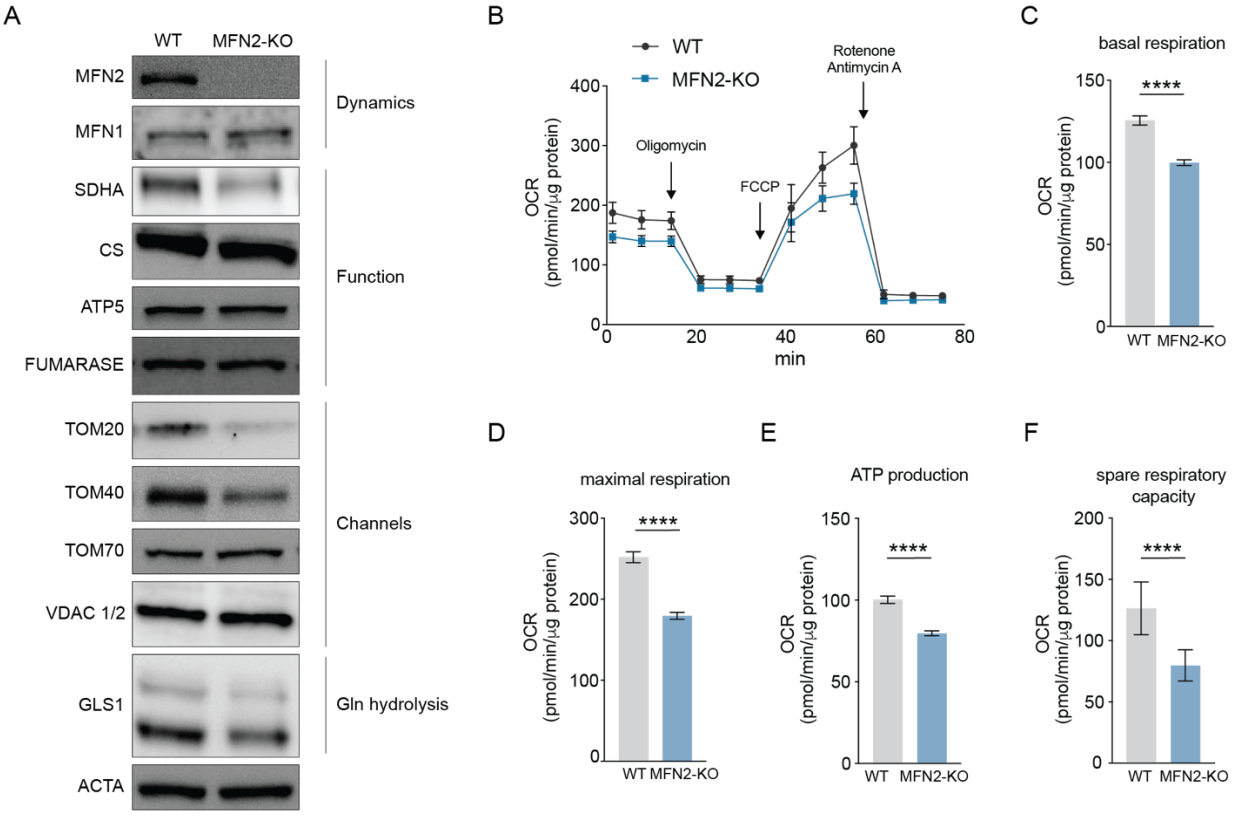

Figure 3.8.1. Loss of MFN2 leads to mitochondrial dysfunction. WT and MFN2 knockout (KO) U2OS cells were serum-starved for 24h and analyzed by immunoblot analysis for several mitochondrial proteins **(A)**. Oxygen consumption analyses in WT and MFN2-KO cells **(B)** including basal respiration **(C)**, maximal respiration **(D)**, ATP production **(E),** and spare respiratory capacity **(F)**. Data are mean ± s.d. of n≥17 independent cultures; ****p<0.0001 for t-test.

I hypothesized that MFN2-KO cells would have increased rates of cholesterol levels synthesis and hyperactivation of the SREBP2 pathway due to the higher levels of gln. To address this, I measured the levels of cholesterol in cells lacking *MFN2*. The loss of MFN2 increased cholesterol and cholesterol ester levels (Figure 3.8.3 – A and B). Similarly, the chronic loss of MFN2 increased HMGCR levels (Figure 3.8.3 – C), indicating increased activation of the SREBP2 pathway.

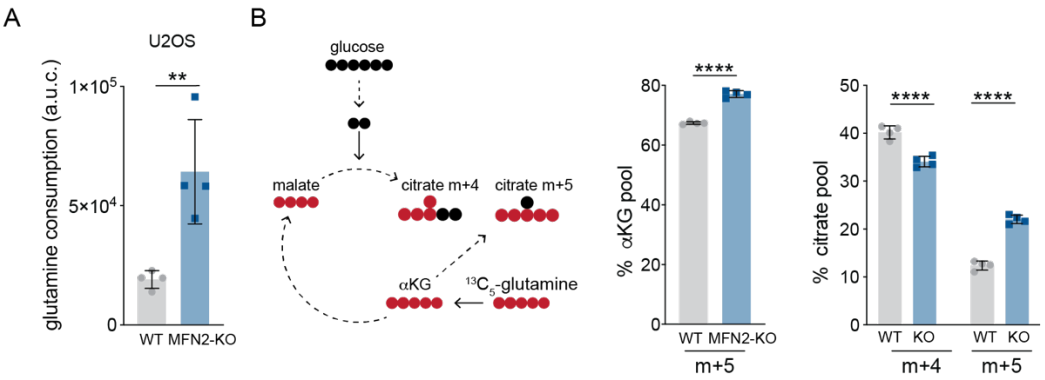

Figure 3.8.2. Lack of MFN2 increased glutamine metabolism. Total glutamine (gln) in DMEM versus gln in media 8 h after culture with WT or MFN2-KO cells **(A)**. During mitochondrial dysfunction, gln feeds citrate synthesis via reductive carboxylation of aKG. m+5 aKG and m+4/5 citrate in U2OSs cultured for 24h with 1 mM $^{13}C_5$-gln **(B)**. Data are mean ± s.d. of n=4 independent cultures, **p<0.01, ****p<0.0001 for t-test.

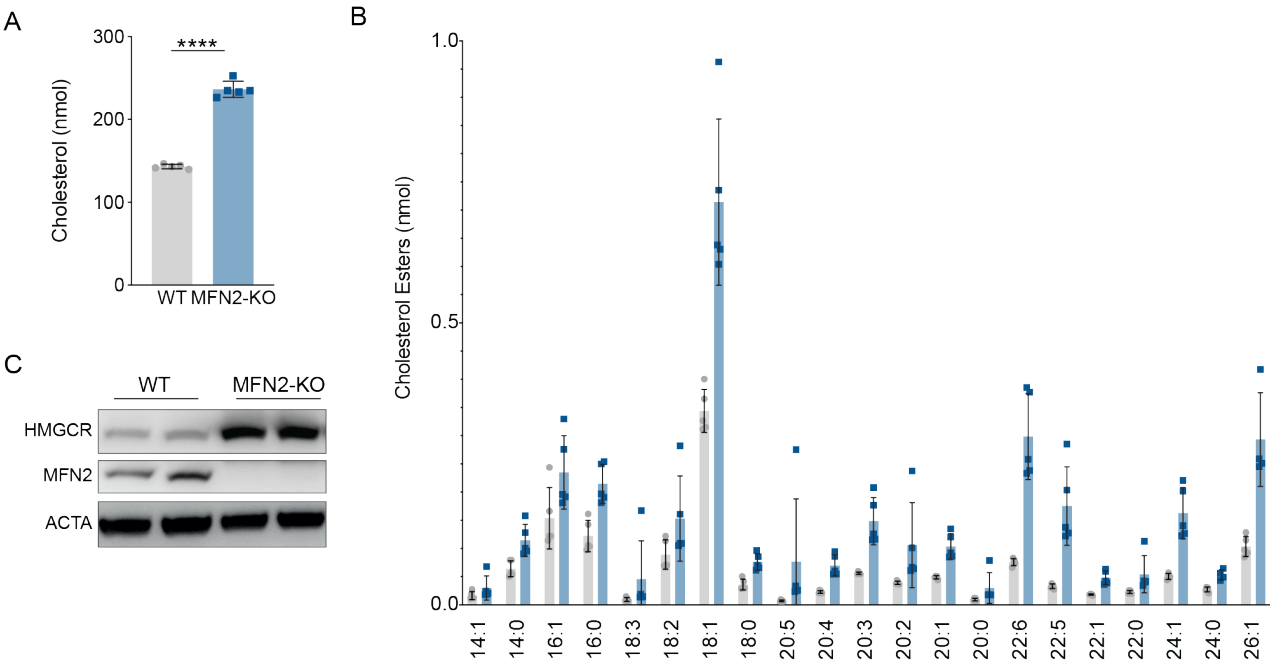

Figure 3.8.3. MFN2-KO cells have higher levels of cholesterol, cholesterol esters, and HMGCR expression. Total cholesterol **(A)** and cholesterol esters **(B)** levels in U2OS WT and MFN2-KO cells. Immunoblot analysis of U2OS WT and MFN2-KO cells for HMGCR, MFN2, and actin (ACTA) **(C)**. Data are mean ± s.d. of n=5 independent cultures, ****p<0.0001 for t-test. Significance is not shown in (B).

To dissect the mechanism underlying the higher levels of HMGCR, I first verified whether the loss of MFN2 resulted in increased HMGCR levels due to its impaired degradation (see Chapter 1.1.2). To address this hypothesis, I cultured WT and MFN2-KO cells in the presence of 25-HC (inducer of HMGCR degradation) and MG-132 (inhibitor of the

proteasomal machinery). 25-HC induced the degradation of HMGCR in WT and MFN2-KO cells (Figure 3.8.4 – A), indicating that MFN2 loss did not impair HMGCR degradation. MG-132 treatment, on the other hand, increased ub and HMGCR levels (Figure 3.8.4 – A). However, preventing HMGCR degradation in WT cells was not sufficient to normalize the levels of HMGCR to that of MFN2-KO cells. Thus, this data indicates that the increased levels of HMGCR in MFN2-KO are driven by SREBP2 activation.

To assess SREBP2 activation, I quantified the levels of precursor and mature SREBP2 in WT and MFN2-KO cells. The loss of MFN2 increased the levels of mature SREBP2 (Figure 3.8.4 – B). But this effect was lost in the presence of lipids indicating that the negative regulation of SREBP2 levels is intact in MFN2-KO (Figure 3.8.4 – B).

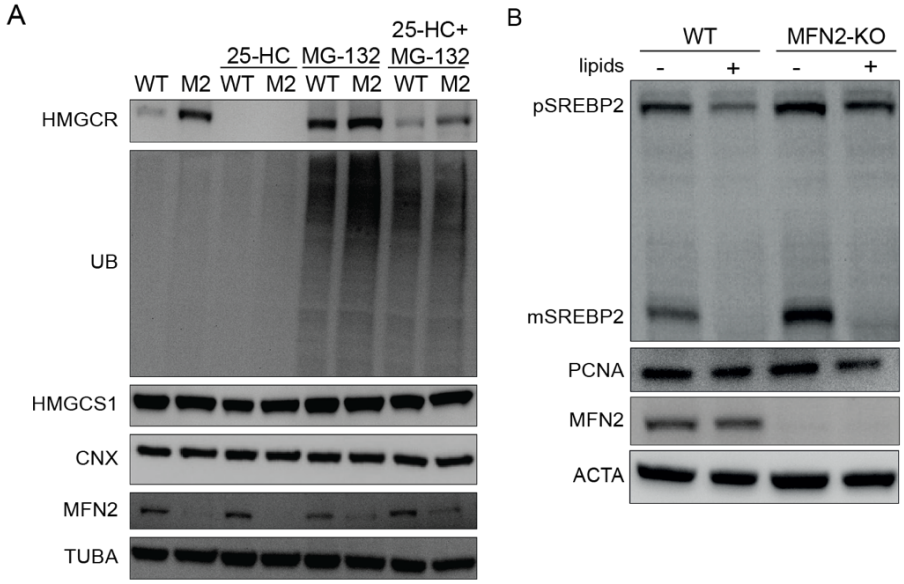

Figure 3.8.4. MFN2-KO cells have higher SREBP2 activation under lipid deprivation. WT and MFN2-KO U2OS cells were cultured ± 25HC (10uM) and MG-132 (10uM) for 6h and analyzed by immunoblotting **(A)**. WT and MFN2-KO U2OS cells were cultured overnight in DMEM without FBS and after cultured ± 10% FBS for 24h and analyzed by immunoblotting **(B).** Samples immunoblotted for HMGCR, precursor (p) SREBP2, mature (m) SREBP2, ubiquitin (UB), calnexin (CNX), mitofusin 2 (MFN2), tubulin (TUBA), proliferating cell nuclear antigen (PCNA), and actin (ACTA).

Next, I investigated whether known functions of MFN2 (see Chapter 1.3) could be responsible for the higher levels of HMGCR and mature SREBP2. First, I addressed the possible role of mitochondrial fusion in regulating HMGCR levels by comparing *Mfn1*$^{-/-}$ and *Mfn2*$^{-/-}$ MEFs cells (Figure 3.8.5). Interestingly, the KO of *Mfn1* in MEFs decreased HMGCR levels. *Mfn2*$^{-/-}$ MEFs cells on the other hand — similar to human cells — have higher levels of

the SREBP2 targets HMGCR and FDFT1 (Figure 3.8.5). This data shows that MFN2 loss exerts its effects on HMGCR independently of mitochondrial fusion.

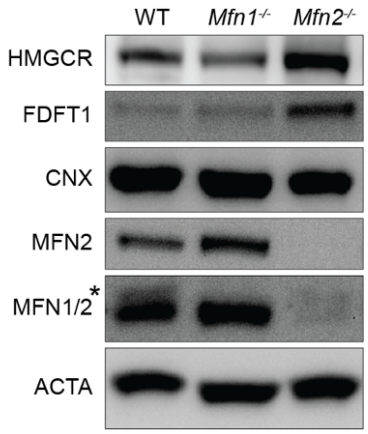

Figure 3.8.5. MEFs Mfn2$^{-/-}$ but not Mfn1$^{-/-}$ have higher levels of HMGCR. WT, MFN1-KO, and MFN2-KO MEF cells were cultured overnight in DMEM without FBS and after cultured ± 10% FBS for 24h and analyzed by immunoblotting. Samples immunoblotted for HMGCR, farnesyl-diphosphate farnesyltransferase 1 (FDFT1), calnexin (CNX), mitofusin 2 (MFN2), tubulin (TUBA), Mitofusin 1/2 (MFN1/2), and actin (ACTA). MFN1/2 antibody stains for both MFN1 and MFN2. * Indicates the MFN1 band.

In some cells line, the KO of MFN2 induces ER stress which may lead to the activation of ATF6 and SREBP2 (Ye et al., 2000). To assess whether MFN2-KO had higher levels of HMGCR due to activation of ER stress, I induced cellular stress with tunicamycin and actinonin in both WT and MFN2-KO. Tunicamycin is a well know ER stress inducer and promotes ATF6 cleavage by the same proteases that cleave SREBP2 in the Golgi. The cleavage of ATF6 activated a cascade response (Hillary and FitzGerald, 2018), together with other main players in the ER stress response — pEl2alpha, ATF4, ATF3, and GRP78 (Figure 3.8.6 – A). On the other hand, actinonin blocks mitochondrial translation (Escobar-Alvarez et al., 2010) which led to ATF4 and ATF3 activation independently of ATF6 cleavage (Figure 3.8.6 – B). Surprisingly, although cellular stress promoted SREBP2 cleavage, it also decreased the levels of SREBP2 target genes (HMGCR, FDPS, FDFT1, and HMGCS1) in U2OS (Figure 3.8.6 – B) and MEFs cells (Figure 3.8.6 – C). This data suggests that another regulatory mechanism downstream of SREBP2 cleavage regulates the levels of the SREBP2 target genes expression under cellular stress. Moreover, this data shows that ER stress does not drive the increased HMGCR levels in MFN2-KO cells.

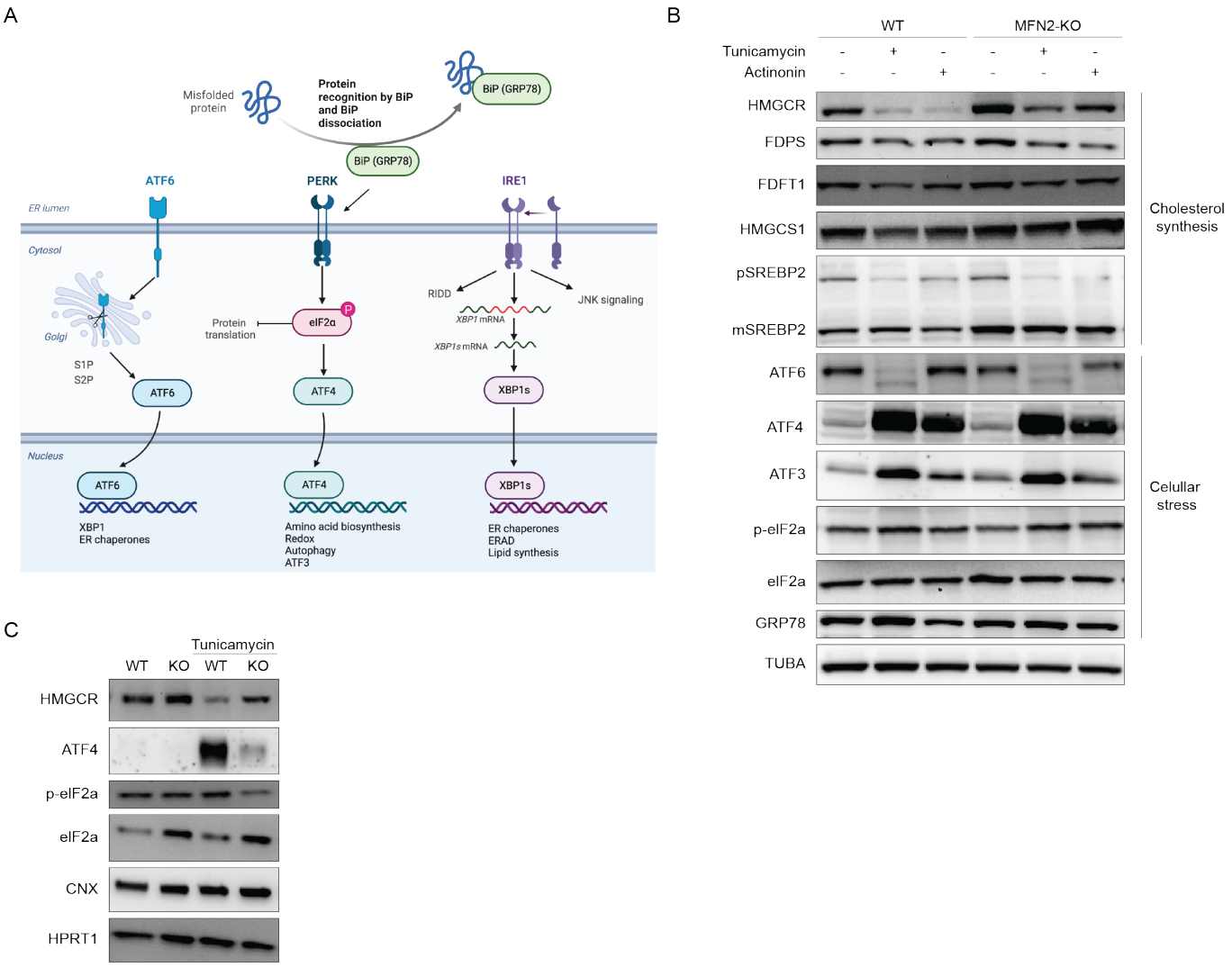

Figure 3.8.6. ER stress does not promote HMGCR levels. Simplified cartoon of ER stress showing ATF6 cleavage and activation by S1P and S2P in the Golgi and phosphorylation of eIF2alpha resulting in ATF4 activation and its downstream target ATF3, as well as, its downstream cellular effects. **(A)**. WT and MFN2-KO U20S **(B)** and MEFs **(C)**, FBS starved and analyzed by immunoblotting. Samples immunoblotted for cholesterol synthesis enzymes and cellular stress markers. The cartoon was made using a BioRender template.

To test the hypothesis that the hyperactivation of SREBP2 in MFN2-KO cells was due to the higher levels of gln in the KO cells, I cultured WT and MFN2-KO cells in the presence or absence of gln (Figure 3.8.7 – A). First, cells were starved for gln for 24h in order to ablate HMGCR levels in both groups (Figure 3.8.7 – B). After, gln was added in the medium for the time indicated (Figure 3.8.7 – B). Surprisingly, with 4h of gln addition HMGCR levels were detectable in both groups at similar levels. However, after 8h of gln addition, HMGCR levels were higher in MFN2-KO cells. This data supports that at earlier time points, WT and MFN2-KO had similar levels of gln. However, due to the higher gln uptake in MFN2-KO cells, cells

acquired more gln that promote activation of the SREBP2 pathway. Further studies are required to dissect the role of MFN2 in the gln levels regulation.

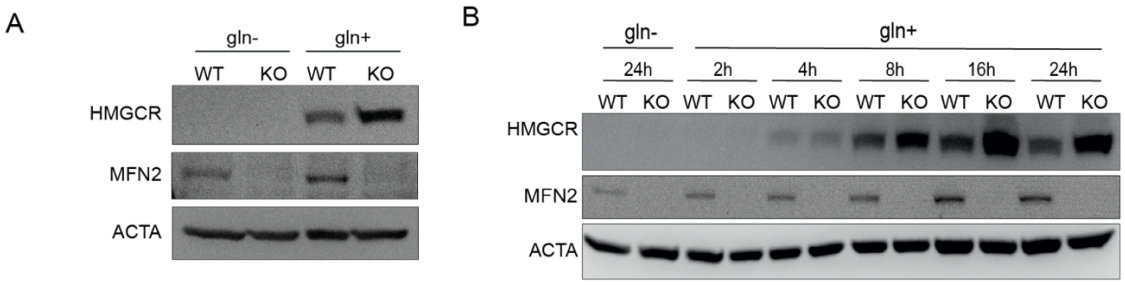

Figure 3.8.7.MFN2 effect on HMGCR levels is glutamine dependent. WT and MFN2-KO U2OS cells were starved for glutamine (gln) for 24h and after cultured ± gln for 24h **(A)** or the indicated time **(B)**. Samples immunoblotted for HMGCR, mitofusin 2 (MFN2), actin (ACTA). For all experiments, gln was used at 2 mM.

9. Acute mitochondrial dysfunction decreases HMGCR levels

I showed that cellular stress decreased SREBP2 target gene levels (Figure 3.8.6 – B). Moreover, acute mitochondrial dysfunction was previously shown to downregulate the SREBP2 target genes (see Chapter 1.3). To investigate whether mitochondrial dysfunction downregulated the SREBP2 pathway through activating integrate stress response (ISR), I induced mitochondrial dysfunction in the presence of ISRIB (ISR inhibitor) (Figure 3.9). In line with previous studies (Mick et al., 2020), oligomycin and CCCP activated ISR through ATF4 and decreased mature SREBP2 and HMGCR levels. The inhibition of ISR decreased ATF4 levels and partially rescued HMGCR levels (Figure 3.9 – A). Thus, suggesting that ATF4 plays a role in the downregulation of the SREBP2 targets upon mitochondrial dysfunction. However, this requires further investigation.

Gln starvation also activates ATF4 (Qing et al., 2012). To investigate whether ATF4 played a role in the loss of HMGCR in gln starvation, I starved cells of gln and added ISRIB simultaneously. Surprisingly, inhibition of ISR did not rescue the levels of HMGCR under gln depletion (Figure 3.9 – B). This data discards a possible role of ISR and ATF4 in the HMGCR levels under gln starvation, and suggest that different mechanism regulate the SREBP2 target genes under mitochondrial dysfunction/cellular stress and gln starvation.

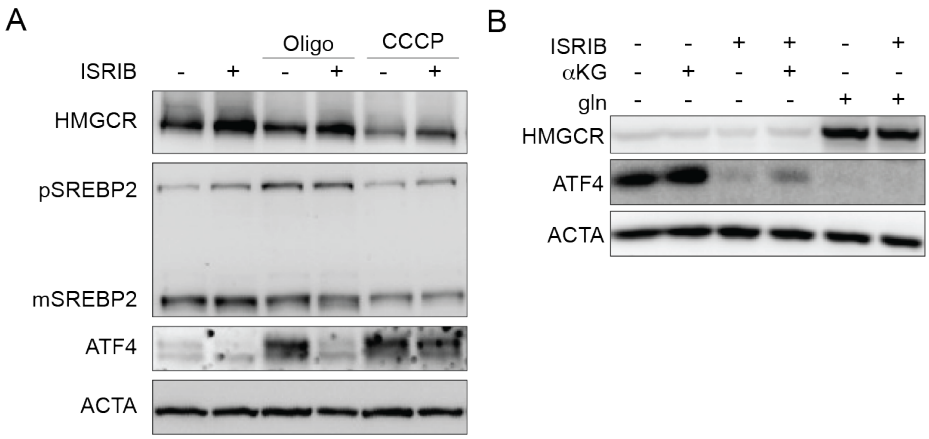

Figure 3.9.1. Acute mitochondrial dysfunction decreases mSREBP2 and HMGCR. U2OS cells were starved for FBS and treated with Oligomycin (Oligo) at 5 µM and carbonyl cyanide m-chlorophenyl hydrazone (CCCP) at 1 µM ± ISRIB for 4h **(A)**. U2OS cells were starved for glutamine (gln) for 24h and treated as indicated for 8h **(B)**. Samples were immunoblotted for HMGCR, precursor (p) SREBP2, mature (m) SREBP2, ATF4, and actin (ACTA). For all experiments, gln was used at 2 mM, alpha-ketoglutarate (aKG) at 1 mM, and ISRIB at 200nM.

To assess whether redox stress led to the gln-mediated effects on cholesterol synthesis, I quantified the levels of reduced and oxidized glutathione and NADH. However, no changes were found in these metabolites under gln starvation, supporting that gln starvation is not decreasing the cholesterol synthesis pathway activation through promoting a cellular redox imbalance.

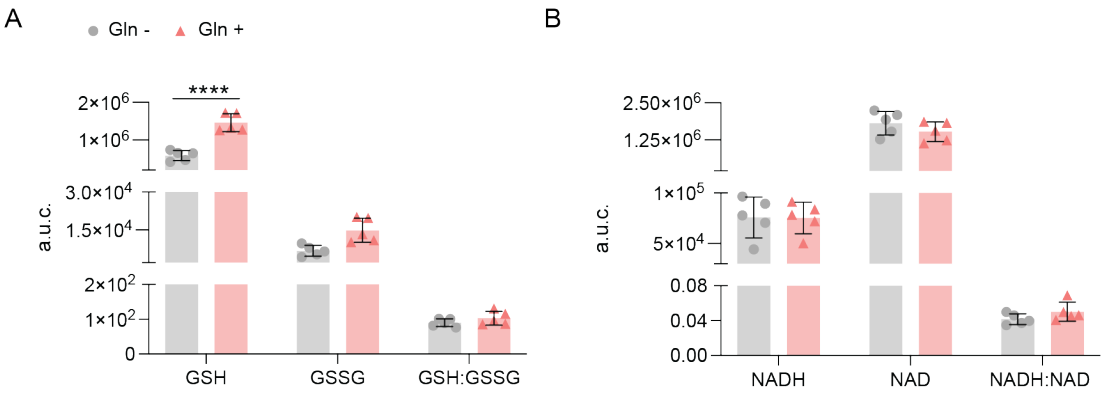

Figure 3.9.2. Glutamine starvation does not affect the redox cellular status. U2OS cells were starved for glutamine (gln) for 24h and treated ± gln for 8h. The redox status was assessed by quantification of reduced and oxidized glutathione (GSH) **(A)** and reduced and oxidized NADH **(B)**. For all experiments, gln was used at 2 mM. Data are mean ± s.d. of n=4 independent cultures, ****p<0.0001 for two-way ANOVA.

10. Glutamine depleted-diet decreases plasma cholesterol

To dissect the physiological relevance of my findings, I verified whether primary murine hepatocytes were sensitive to changes in gln levels (Figure 3.10.1 – A). As expected, primary murine hepatocytes had higher expression of SREBP1 and 2 target genes (Figure 3.10.1 B and C) in the presence of gln. The protein levels of HMGCR and SQLE were also increased in hepatocytes cultured in the presence of gln (Figure 3.10.1 – D), confirming that gln also promotes SREBP2 activation in primary hepatocytes.

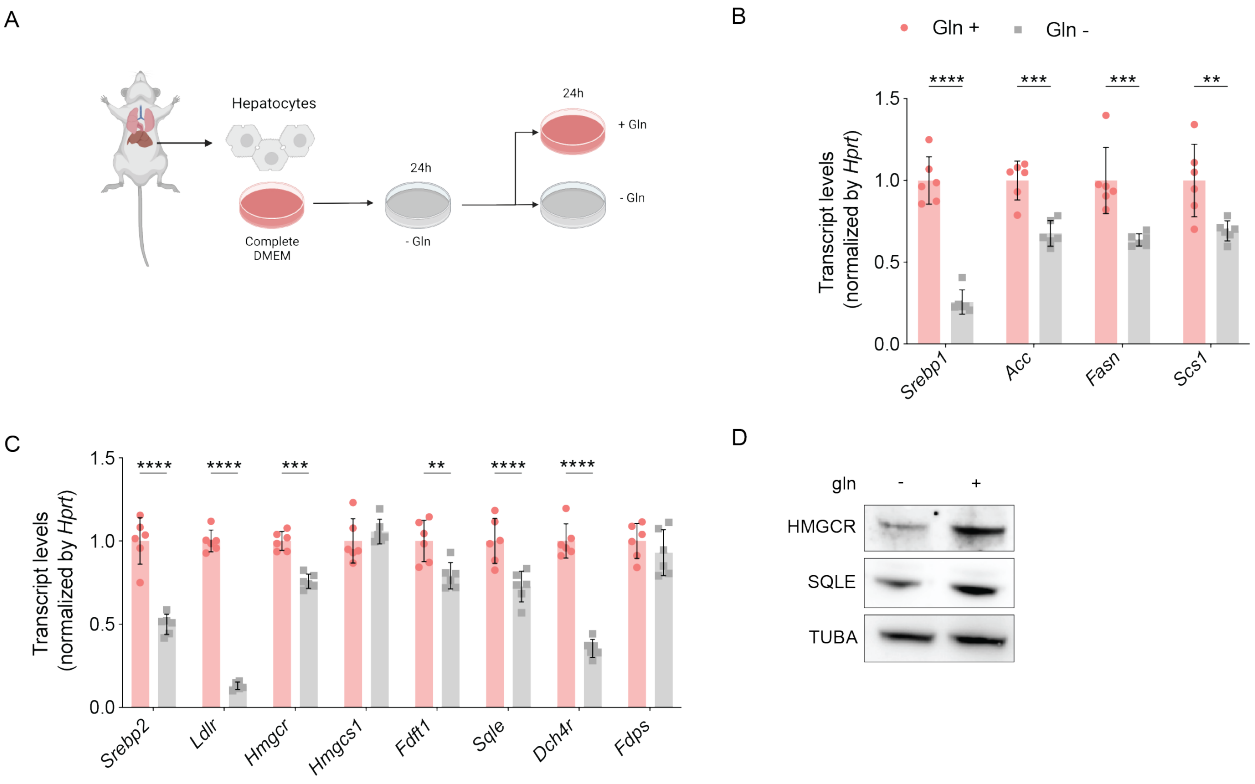

Figure 3.10.1. Glutamine promotes SREBP1/2 activation in primary hepatocytes. Primary mice hepatocytes were starved for glutamine (gln) for 24h and treated ± gln for 24h **(A)**. q-PCR of samples from (A) with the indicated primers **(B and C)**. Samples from (A) were immunoblotted for HMGCR, SQLE and tubulin (TUBA) **(D)**. gln was used at 2 mM.

To address whether manipulating gln levels affected cholesterol regulation *in vivo*, I fed mice with a repleted or depleted gln diet (1.8% or 0% of gln) for 12 weeks and assessed the changes in metabolism (Figure 3.10.2 – A). The lack of gln in the diet did not affect the food intake (Figure 3.10.2 – B) nor the total weight or weight gain after the 8 weeks (Figure 3.10.2 – C and D). Surprisingly, the gln-depleted diet did not affect the levels of gln in plasma (Figure 3.10.3 – A), suggesting that probably endogenous levels of gln are sufficient to sustain

the mice body's demands. On the other hand, while no changes in TGs were found (Figure 3.10.3 – B and D), cholesterol levels were decreased in the plasma after 8 and 12 weeks in the gln-depleted diet (Figure 3.10.3 – C). The majority of this change was due to decreased cholesterol-containing LDL (Figure 3.10.3 – D), which might indicate there was reduced cholesterol liver secretion. However, further experiments are required to assess this hypothesis.

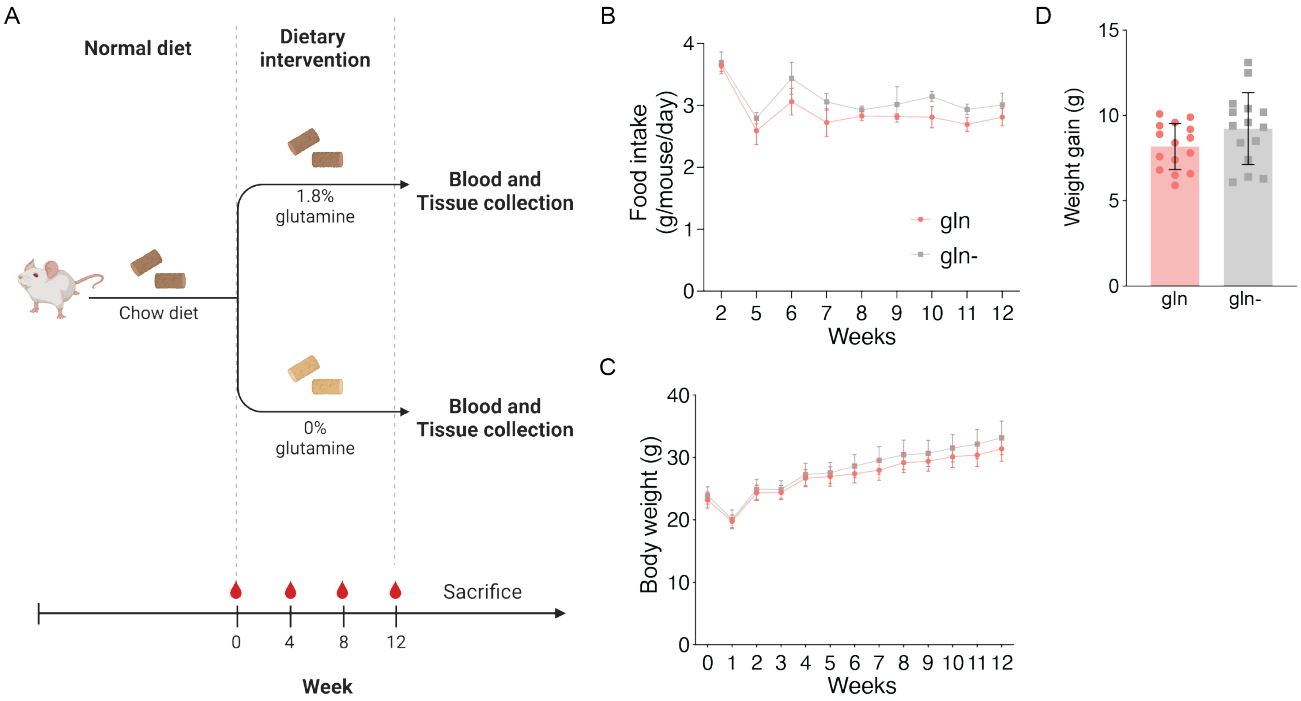

Figure 3.10.2. Mice fed with a gln-depleted diet for 12 weeks did not show changes in food intake or weight. Cartoon presenting the methodological strategy of the gln repleted and depleted diet *in vivo*. Male mice 7 weeks old were fed with diets containing 0 or 1.8% gln for 12 weeks. Blood samples were collected every 4 weeks and tissues were collected after 12 weeks **(A)**. Food intake **(B)**, total weight **(C),** and weight gain from mice in (A). Data are mean ± s.d. of n=15 mice per condition.

Next, I assessed the cholesterol content in different organs after 12 weeks in a gln-repleted or depleted diet. No changes were found in the cholesterol content in the liver, brain, or intestines (Figure 3.10.4). Strikingly, cholesterol levels in the lung were higher after 12 weeks on a gln-depleted diet. This result was surprising and raised some questions that will be further discussed. Although further investigation is required, my data indicates that the lack of gln in the diet can affect circulating cholesterol levels (Figure 3.10.3 – C) and there are probably other unrevealed mechanisms dictating gln and cholesterol levels *in vivo*.

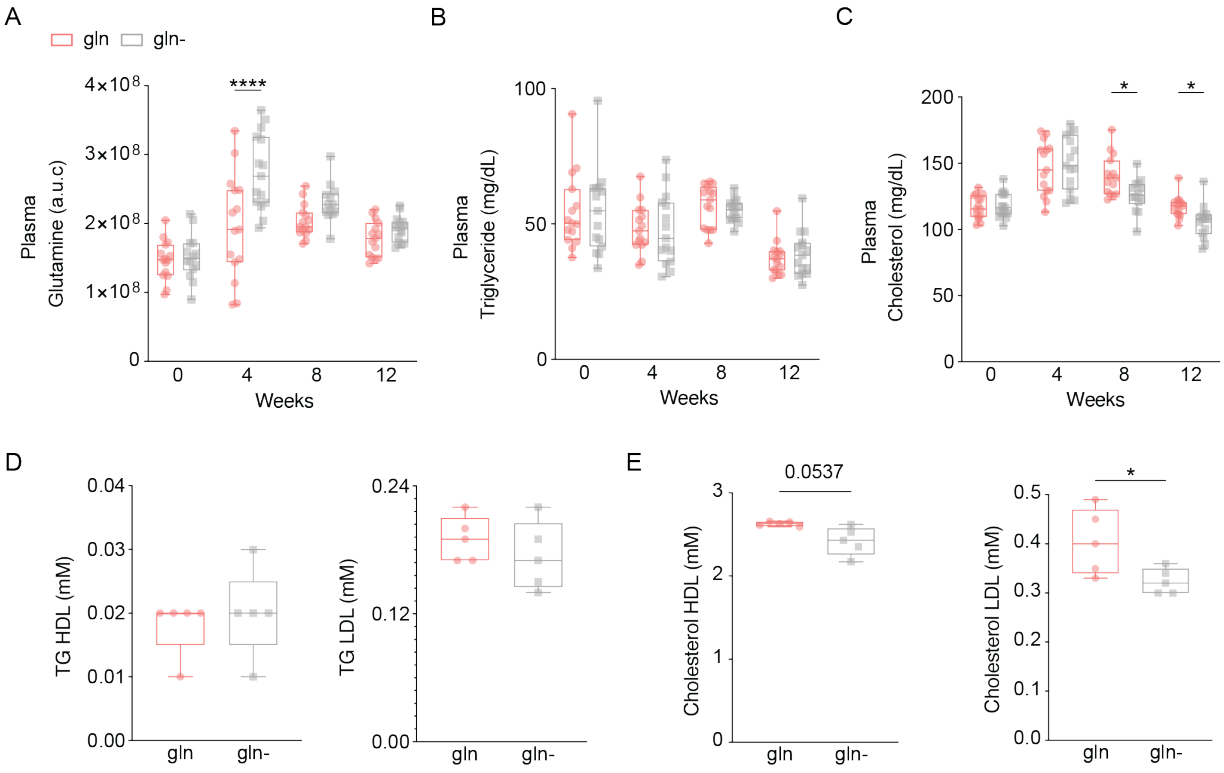

Figure 3.10.3. Plasma analysis of mice fed with gln-repleted or depleted diet. Male mice 7 weeks old were fed with diets containing 0 or 1.8% gln for 12 weeks. Blood samples were collected every 4 weeks and analyzed for glutamine **(A)**, triglycerides (TG) **(B)**, and cholesterol **(C).** Data are mean ± s.d. of n=15 mice per condition. *p<0.05, ****p<0.0001 for two-way ANOVA. Plasma samples of both mice groups were grouped for plasma fractionation analysis. TG **(D)** and cholesterol **(E)** present in HDL (high-density lipoprotein) and LDL (low-density lipoprotein) were measured. Data are mean ± s.d. of n=15 mice grouped into 4 groups per condition. *p<0.05 for t-test.

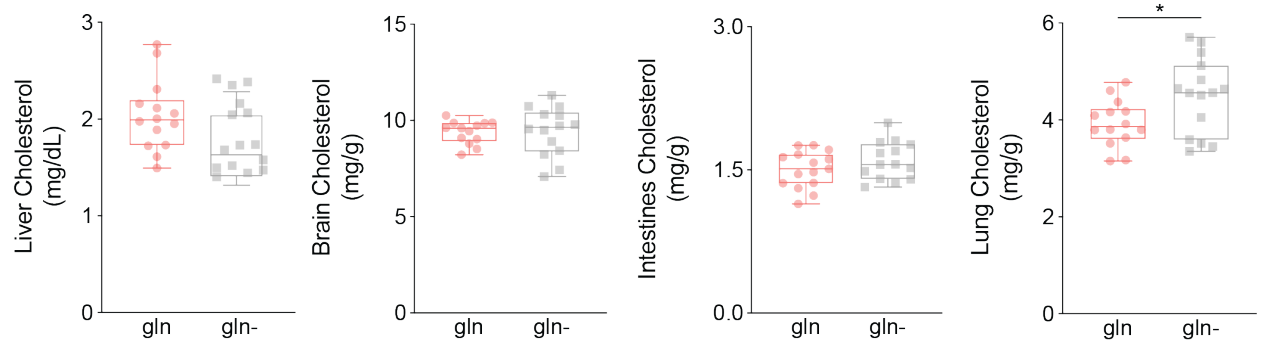

Figure 3.10.4. Lipid content in organs of mice fed with a replete or deplete gln-diet. Male mice 7 weeks old were fed with diets containing 0 or 1.8% gln for 12 weeks. Tissues samples were collected and analyzed for cholesterol levels. Data are mean ± s.d. of n=15 mice per condition. *p<0.05, for t-test.

11. Glutamine synthesis regulates HMGCR levels in a cell type-dependent manner

Gln is a conditional NEAA (see Chapter 1.2) and under normal conditions, gln synthesis is sufficient to sustain its demands. Could it explain why mice fed with a gln-depleted diet do not have changes in plasma gln? If yes, why does gln synthesis not sustain cholesterol synthesis in gln-starved U2OS cells? To address these questions, I first analyzed the GLUL expression levels in U2OS cells in data available at https://depmap.org/portal/ccle/ (Figure 3.11.1 – A and B). U2OS cells were among the 10% of cancer cells with lower levels of GLUL mRNA and protein. This data predict that U2OS cells are unable to sustain gln levels through synthesis.

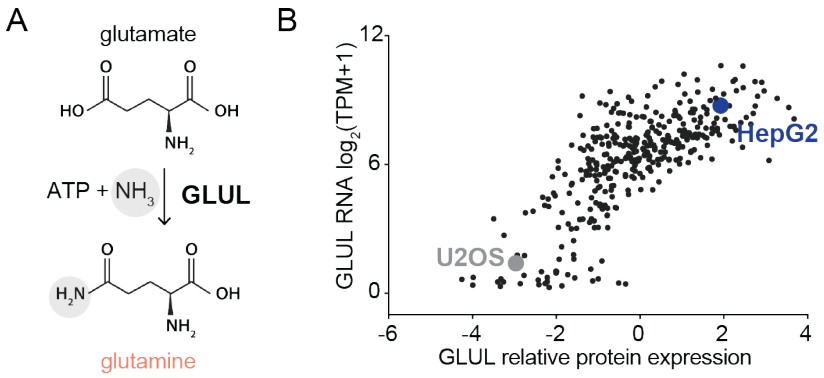

Figure 3.11.1. GLUL expression among cancer cell lines. Glutamine synthetase (GLUL) generates glutamine (gln) from ammonia and glutamate **(A)**. GLUL relative protein expression and RNA log2 TPM+1 in 347 cancer cell lines; data were obtained from previously generated data available at https://depmap.org/portal/ccle/ **(B)**.

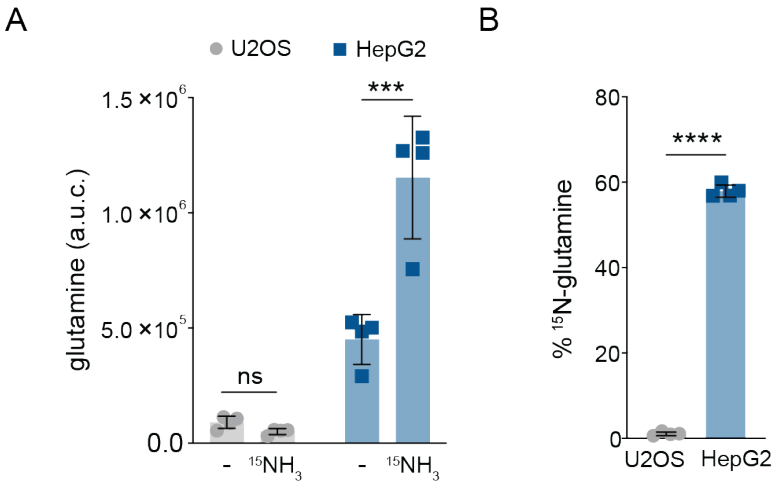

Figure 3.11.2. HepG2 but not U2OS cells synthesize glutamine. Total glutamine (gln) abundance in U2OS and HepG2 cultured without FBS and without gln ± 10 mM $^{15}NH_4Cl$ for 24h **(A)**. Percentage of ^{15}N-gln from cells

cultured as in (A) synthesized from $^{15}NH_4Cl$ **(B)**. Data are mean ± s.d. of n=4 independent cultures, ns: non-significant, ***p<0.001, ****p<0.0001 for t-test. The area under the curve (a.u.c.).

To address this hypothesis, I cultured U2OS cells and HepG2 cells — among the 10% cancer cells with higher levels of GLUL mRNA and protein — in the presence of ammonia (to promote gln synthesis) and measured gln synthesis. Ammonia supplementation had no effect in U2OS cells (Figure 3.11.2 – A and B) while in HepG2 it increased gln total levels and synthesis ratio. After 24h in the presence of $^{15}NH_4$, almost 60% of the gln pool in HepG2 cells was derived from de novo synthesis, while in U2OS it was approximately 0%. This data confirmed that U2OS are unable to synthesize gln due to a lack of GLUL expression.

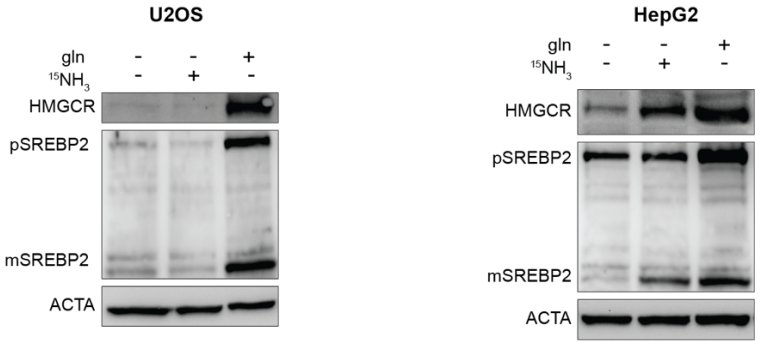

Figure 3.11.3. Ammonia only promotes mSREBP2 and HMGCR levels in HepG2 but not U2OS cells. U2OS and HepG2 cells were starved for glutamine (gln) for 24h and after cultured ±gln or $^{15}NH_4Cl$ for 24h. Samples immunoblotted for HMGCR, precursor (p) SREBP2, mature (m) SREBP2, and actin (ACTA). For all experiments, gln was used at 2 mM and 10 mM $^{15}NH_4Cl$.

To further investigate whether gln synthesis could promote cholesterol synthesis, I measured the levels of mature SREBP2 and HMGCR in U2OS and HepG2 under -/+ gln or ammonia. As expected, U2OS cells required exogenous gln to activate SREBP2 due to the lack of GLUL and gln synthesis (Figure 3.11.3). HepG2 cells however activated SREBP2 and promoted HMGCR expression in the presence of gln or ammonia (Figure 3.11.3). Thus, it might indicate that only cells able to synthesize gln — through GLUL expression — are able to sustain cholesterol synthesis in the absence of gln (Figure 3.11.3). To confirm this, I chemically inhibited GLUL activity (using MSX – Methionine sulfoximine) in cells that have high expression of GLUL (Figure 3.11.4). The chemical inhibition of GLUL prevented the activation of the SREBP2 pathway in the presence of ammonia (Figure 3.11.4 – A, B, and C). Thus, NH_4 promoted SREBP2 activation through gln synthesis and GLUL. The inhibition of GLUL in the presence of exogenous gln had no effect, discarding any unspecific effect of the

GLUL inhibitor. Surprisingly, CHO cells — which are frequently used as a model to study cholesterol synthesis regulation due to their high demand for cholesterol — were able to activate the SREBP2 through gln synthesis with the addition of only aKG (Figure 3.11.4 – C).

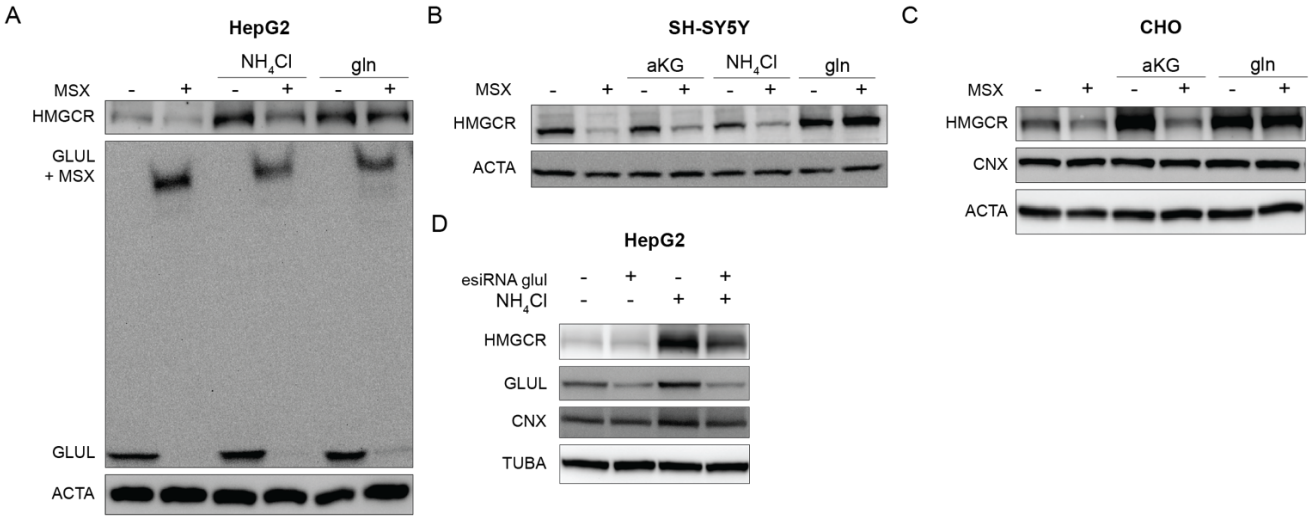

Figure 3.11.4. GLUL chemical or genetic ablation prevents ammonia or aKG effect on HMGCR levels. HepG2 **(A)**, SH-SY5Y **(B)**, and CHO **(C)** cells were starved for glutamine (gln) for 24h and cultured for 24h as indicated. Samples immunoblotted for HMGCR, glutamine synthetase (GLUL), calnexin (CNX), and actin (ACTA). HepG2 cells were transfected with esiRNA for 3 days and after treated as indicated for 8h **(B)**. Samples immunoblotted for HMGCR, GLUL, CNX, and ACTA. For all experiments, gln was used at 2 mM, aKG at 1 mM, 10 mM NH_4Cl at 10 mM, and MSX (methionine sulfoximine) at 500 μM.

The silencing of GLUL with esiRNA also decreased HMGCR levels in HepG2 cells (Figure 3.11.4 – D), indicating that chemical or genetic modulation of GLUL levels could be of great value to modulate HMGCR levels and cholesterol synthesis. Collectively, this data show that gln synthesis positively regulates cholesterol synthesis in a cell-type-dependent manner and sheds light on novel target approaches to regulate cholesterol synthesis.

12. Block of glutamine synthesis *in vivo* does not change plasma cholesterol

Since blocking gln synthesis was sufficient to downregulate the cholesterol synthesis enzymes *in vitro*, I investigated whether modulating gln synthesis *in vivo* would also have an effect on cholesterol. First, I verified whether primary hepatocytes were sensitive to MSX in culture. As immortalized cells, primary mice hepatocytes cultured with MSX had decreased HMGCR levels in the absence of exogenous gln or the presence of ammonia (Figure 3.12.1 – A).

Next, I investigated whether injecting MSX in mice fed with a gln-deplete diet for 1 week had an effect on cholesterol levels (Figure 3.12.1 – B). After 1 week of MSX+ gln-deplete diet, mice lost >15% of weight (Figure 3.12.1 – C). However, no changes were found in plasma cholesterol content (Figure 3.12.1 – D). Further studies are required to dissect the role of gln synthesis in cholesterol synthesis regulation *in vivo*.

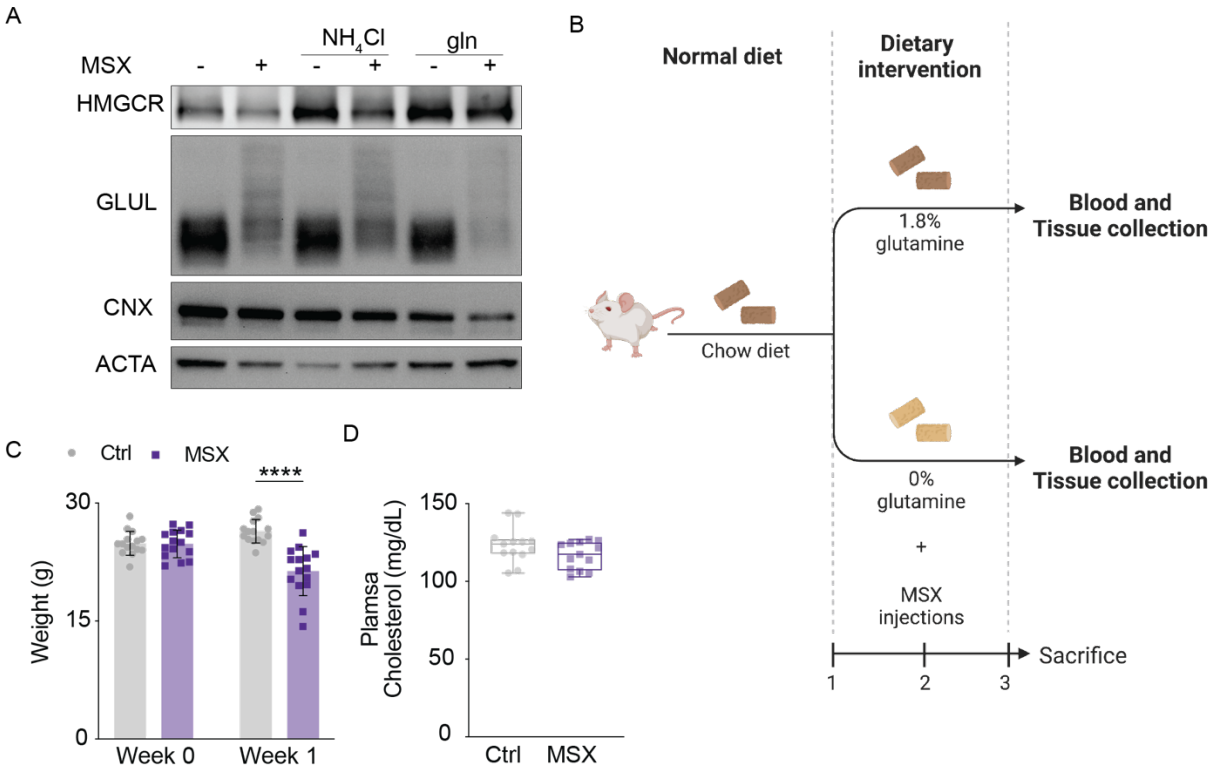

Figure 3.12.1. Block of glutamine synthesis *in vivo* does not change plasma cholesterol. Primary mice hepatocytes were starved for glutamine (gln) for 24h and treated as indicated for 24h. Samples immunoblotted for HMGCR, glutamine synthetase (GLUL), calnexin (CNX), and actin (ACTA) **(A)**. Cartoon presenting the methodological strategy of the MSX injections + gln depleted diet *in vivo*. Male mice 7 weeks old were fed with diets containing 0 or 1.8% gln for 1 week and injected 3x with MSX. Blood samples and tissues were collected. Total weight **(C)** from mice treated as (B). Plasma cholesterol content **(D)** from mice treated as (B). Data are mean ± s.d. of n= 15 ctr mice and n= 13 MSX mice. ****p<0.0001 for t-test.

CHAPTER 4

DISCUSSION AND FUTURE PERSPECTIVES

1. Why glutamine and not glucose?

Glc and gln are the main carbons sources for cellular anabolism, and their favoritism as substrate utilization is cell-type dependent (Lu et al., 2010; Reitzer et al., 1979). However, these two metabolites play also several other roles. Glc's main functions are a source of carbons, ATP generation (through glycolysis), and fuel for anaplerosis. Gln is more versatile than glc and is a source of carbons, ATP generation, fuel for anaplerosis, synthesis of nucleic acids, amino acids, and glutathione (Lu et al., 2010). In the absence of glc or gln, the other metabolite can oftentimes compensate (Le et al., 2012; Yoo et al., 2004), indicating that there is a communication between these two metabolite pathways. For example, c-Myc is a transcription factor that responds to gln levels regulating gln uptake and metabolism (see Chapter 1.2.4). Interestingly, c-Myc also upregulates glycolytic enzymes promoting both glc and gln utilization (Lu et al., 2010; Wang et al., 2018), showing that more than redundant, both pathways may act coordinated to promote growth and proliferation (DeBerardinis et al., 2007; Wasinski et al., 2014).

Glc is the main carbons donor to sustain lipid synthesis (DeBerardinis et al., 2007), however, my findings show that gln, but not glc, is required to activate the cholesterol synthesis pathway. Since cholesterol and gln are required for cellular growth and replication (see Chapter 1.1.2), a link between these two pathways would guarantee that the cells have all the resources required to grow at the same time. In other words, without gln, it would not be worth expending over one hundred ATP per molecule of cholesterol (Brown et al., 2021a), because there would not be enough resources to proliferate. So here, I speculate that the sensing of gln by the SREBP2 pathway would proportionate a coordinated replication.

2. Citrate is not required to activate the cholesterol synthesis pathway

Citrate is produced in the mitochondria and exported to the cytosol in order to feed the synthesis of cholesterol and fatty acids. Surprisingly, the lack of citrate activates the SREBP2 pathway (Figure 3.4.6). Several cholesterol derivatives or intermediates participate in the negative feedback of the SREBP2 pathway (see Chapter 1.1.2). However, it is the first time a cholesterol precursor is suggested as a negative regulator.

This result was surprising, since in most metabolic pathways, the precursor promotes the activation of the pathway — as gln promotes aKG synthesis, and glc promotes glycolysis — while the intermediates or end products play a role in the negative feedback (Locasale, 2018). Interestingly, citrate was already shown to negatively regulate important enzymes in the glycolytic pathway (Nissler et al., 1995; Williams and O'Neill, 2018), such as PFK1 and PFK2 (phosphofructokinase 1 and 2), and the TCA cycle enzymes SDH (succinate dehydrogenase) and PDH (pyruvate dehydrogenase) (Iacobazzi and Infantino, 2014; Martin and Vagelos, 1962; Taylor and Halperin, 1973). Thus, citrate might negatively regulate the SREBP2 pathway through protein-metabolite interaction.

In the absence of citrate, acetate can compensate for its deficiency and sustain lipid synthesis (Zhao et al., 2016). However, how the balance of these two metabolites is sensed by the cholesterol and fatty acid synthesis pathway is not known. Another possibility for the lack of citrate promoting the activation of the SREBP2 pathway is through changes in the acetate levels — or even acetylation of SREBP2. However, this requires more investigation.

3. Glutamine — and not its derivatives — is sensed to promote cholesterol synthesis

Glc is sensed through its derivative fructose-1,6-bisphosphate to activate the AMPK signaling to regulate cellular metabolism and homeostasis (C.-S. Zhang et al., 2017). In the same way, gln derivatives are sensed. For example, aKG is sensed to promote mTORC1 activity (Durán et al., 2012; Durán and Hall, 2012; Meng et al., 2020), promoting cellular growth and proliferation. However, whether glc and gln per se are sensed is not known yet.

Although the correlation between gln levels and SREBP2 activation was already described (Inoue et al., 2011), several questions were still open. Here I described for the first time that gln — and not its derivatives — is required for SREBP2 activation. During the development of this thesis, two other groups published similar findings (Cheng et al., 2022; Kong et al., 2023). However, the mechanism behind gln's role was divergent. While Cheng et al. claim that gln activates the SREBP2 pathway through the gln derivative ammonia, Kong et al. on the other hand, claim it is due to mTORC1-mediated autophagy.

In this thesis, I proved that ammonia is not sensed by the SREBP2 pathway and is not sufficient to promote SREBP2 activation. The effects that Cheng et al. found were mediated by gln synthesis after ammonia addition (Figure 3.11.2 and 3.11.4). Blocking gln synthesis in the presence of ammonia is sufficient to prevent SREBP2 activation (Figure 3.11.4). Moreover, U2OS cells (which lack GLUL) were not responsive to ammonia addition once these cells are not able to synthesize gln (Figure 3.11.2 and Figure 3.11.3). Moreover, inhibition of gln hydrolysis in the presence of aKG — and consequently ammonia production — did not affect SREBP2 activation (Figure 3.5.2). Thus, I can conclude that gln promotes SREBP2 activation independently of ammonia, or any other known derivative.

My findings also discarded a possible role of mTORC1 in the regulatory effect of gln in the cholesterol synthesis pathway. When U2OS cells were treated with aKG but not gln, mTORC1 was activated as previously described (Durán et al., 2012; Durán and Hall, 2012; Meng et al., 2020) but it did not sustain SREBP2 activation (Figure 3.7.1). Collectively, my data strongly suggest that gln per se is sensed to promote cholesterol synthesis. However, the mechanism of gln sensing remains unknown.

4. How is glutamine sensed by the cholesterol synthesis pathway?

Although in this thesis I have shown that gln can be sensed to promote cholesterol synthesis, the exact mechanism requires further investigation. Here I will discuss two of likely several possible models on how gln can promote SCAP-SREBP2 trafficking (Figure 4.4). First, gln may affect INSIG-SCAP interaction, promoting its dissociation and consequently, increasing SCAP-SREBP2 trafficking (Espenshade et al., 2002; Sun et al., 2007). Immunoprecipitation of SCAP in the presence and absence of gln would allow us to verify

this hypothesis. Moreover, cells lacking INSIG-SCAP interaction or an interaction permanently engineered would enable further investigation of whether gln affects INSIG-SCAP interaction.

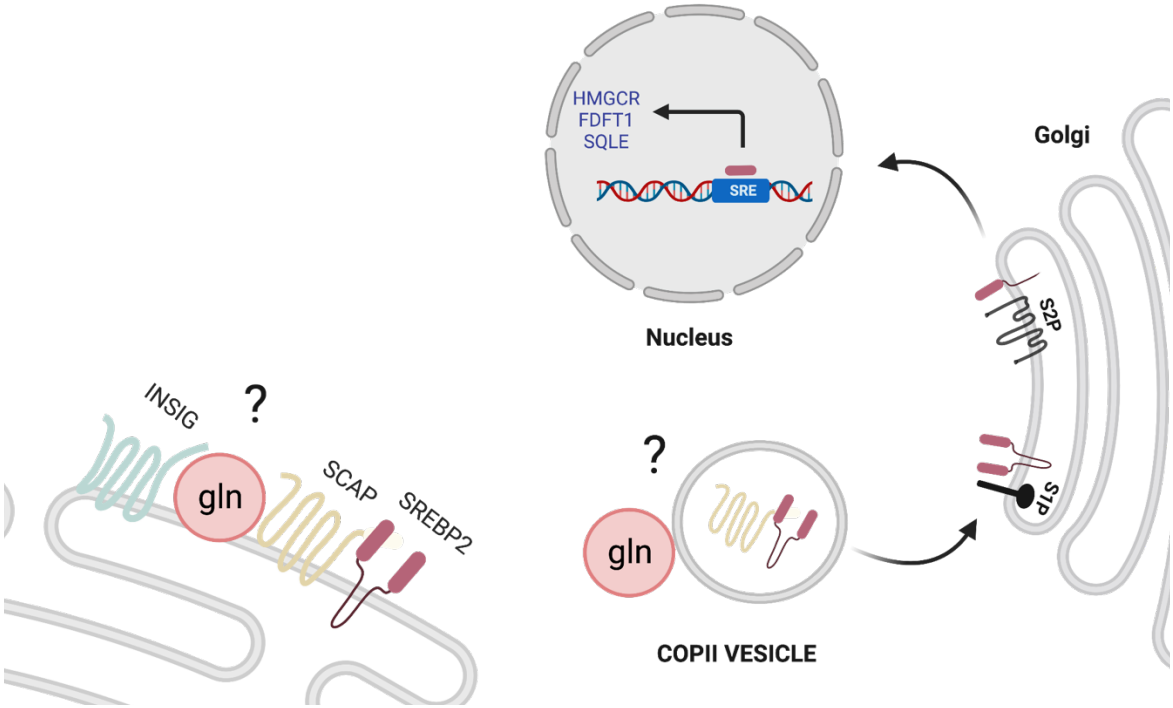

Figure 4.4. Hypothetic model of glutamine regulating SCAP-SREBP2 trafficking. Glutamine (gln) could promote cholesterol synthesis through two mechanisms: (1) gln may affect INSIG-SCAP interaction, consequently allowing SCAP-SREBP2 trafficking to Golgi, or (2) gln signals to COPII vesicles for selecting SCAP-SREBP2 as a cargo.

Second, gln could affect the COPII selection of cargos. Despite the major importance of protein trafficking between ER-Golgi for cellular function, it is not fully understood how the cargos at ER are selected. Moreover, little is known about whether this is a passive (dependent only on the viability of ER proteins) or an active (cargos are indeed selected based on external signals) process. Among the proteins required for the COPII formation, Sec23 and Sec24 are known for selecting the ER proteins which will be transported (Zanetti et al., 2013). However, what regulates the binding of these proteins is not known. Moreover, some proteins have been emerging as cargo receptors for the COPII vesicles, such as LMAN1 (Lectin, Mannose Binding 1) and SURF4 (Surfeit locus protein 4) (Shen et al., 2022; Zanetti et al., 2013). I hypothesize that gln might promote the selection of SCAP through its binding to Sec23/24 or other cargo receptors. However, further investigation is required to test this hypothesis.

5. Glutamine synthesis sustains cholesterol synthesis in a cell type-dependent manner

It was a surprise when Cheng et al. published their findings regarding gln regulating cholesterol synthesis through ammonia in HepG2 cells because I already had investigated this hypothesis in U2OS. Indeed, U2OS are not responsive to ammonia treatment while HepG2 cells are (Figure 3.11.3). I pinpointed that this difference is due to changes in GLUL expression. While HepG2 cells are able to synthesize gln from ammonia through GLUL activity, U2OS cells — which do not express GLUL — don't have this ability. Consequently, gln de novo synthesized in HepG2 cells regulates the cholesterol synthesis pathway and not ammonia per se. Chemical or genetic inhibition of GLUL in HepG2 prevents the effects of ammonia, confirming that ammonia alone cannot promote cholesterol synthesis (Figure 3.11.4).

Most studies and screenings that identified regulators of cholesterol synthesis were made in cells that are able to synthesize large amounts of gln from ammonia or aKG (Figure 3.11.4). Probably, in these studies, gln-related genes effects were sub-estimated. Performing these screenings in cell lines that cannot synthesize gln (such as U2OS) would allow the identification of new players in the cholesterol synthesis regulation, and possible to better understand how gln plays its regulatory role.

This finding brings questions regarding the differences in cholesterol synthesis regulation and gln dependence among cellular types. GLUL expression would decrease the cellular demand of gln for cellular growth and replication and is also important for the detoxification of ammonia (see Chapter 1.2.2). However, my findings suggest that these cells would also have autonomy regarding cholesterol synthesis, being able to produce its main nutrients for replication. On the other hand, cells with none or low GLUL expression would be dependent on extracellular sources of gln to produce cholesterol. However, why different cells would have different autonomies regarding gln and cholesterol synthesis remains an open interesting question.

The autonomy or external demand of gln to regulate cholesterol and promote growth and proliferation may play a role in high proliferative cells, such as cancer. It is known that

cancer cells have a higher dependence on gln and cholesterol to sustain the high ratio of proliferation (Altman et al., 2016). GLUL expression varies among cancer cell types and among patients with the same type of cancer (https://www.proteinatlas.org/). Inhibitors of GLUL were already tested as a possible cancer treatment (Kim et al., 2021; J. Zhang et al., 2017), however, in these studies, the inhibition was not always effective. My findings indicate that the different cancer cell types probably have different gln demands, and GLUL inhibition would only have an effect on cancer cells that relies on endogenous sources of gln to sustain metabolic anabolism and cellular proliferation.

6. The physiological relevance of glutamine to regulate cholesterol levels

Gln is a conditional NEAA that under certain conditions, such as high proliferation or increased demand due to cancer and exercise, turns essential. In these conditions, only endogenous synthesis of gln is not sufficient to supply the body's demand. Here, when gln was deprived of the diet, it was not sufficient to decrease gln levels in the plasma, which may indicate that endogenous synthesis is sufficient to sustain gln levels. Although the levels of cholesterol were decreased under a gln-depleted diet, the levels of cholesterol in the tissues were unchanged. This data suggests that although gln deprivation from the diet can affect systemic cholesterol homeostasis, it does not perturb the tissue microenvironment. This raised some questions such as: (1) May endogenous gln sustain cholesterol levels in the absence of gln from the diet? (2) Could other parameters not considered here — such as cholesterol and gln synthesis from the microbiota — be compensating for the loss of gln from the diet? and (3) May the body find new homeostasis by cholesterol flux from less to more affected organs by the gln-depleted diet?

Although I could not address all of them, to understand whether gln synthesis was compensating for the lack of gln from the diet, I inhibited gln synthesis in mice through MSX injections. Although plasma and organs were collected, until the completion of this thesis, only cholesterol in the plasma was analyzed. Further studies are required to dissect the role of gln synthesis in cholesterol level regulation *in vivo*.

CHAPTER 5

MATERIALS AND METHODS

Cell culture and cell lines

All cell lines (Table 1) were cultured in complete DMEM (cDMEM: DMEM 4.5 g/L glucose + 10% heat-inactivated FBS + 1% P/S) at 5% CO2 except for CHO cells and SH-SY5Y which were cultured in cDMEM/F12 media. For all the experiments, cells were plated and after cultivated without FBS (DMEM or DMEM/F12 and 10% H20 for cell culture + 1% P/S) to promote cholesterol synthesis. Cells were tested frequently for Mycoplasma infection by PCR. Primary hepatocytes were cultured with DMEM 1 g/L glucose + 100 nM of Insulin + 500 nM Dexamethasone.

Table 1. Immortalized cell lines used in this thesis.

Name	Specie	Source
CHO-SCAP-EGFP	Hamster	Drs. J Goldstein and M Brown (U of Texas Southwestern Medical Center, Texas, US)
HeLa	Human	ATCC - CCL-2
Hela-MANII	Human	Matteo Veronese (CECAD, Cologne, Germany)
HepG2	Human	ATCC - HB-8065
HFFs	Human	Hospital of University of Padova, Padova, Italy
HEK293T	Human	ATCC- CRL-1573
Mefs MFN1-KO	Mouse	ATCC - CRL-2992
Mefs MFN2-KO	Mouse	ATCC - CRL-2993
Mefs WT	Mouse	ATCC - CRL-2991
SH-SY5Y	Human	Dr. Hans Zempel (University of Cologne, Cologne, Germany)

U2OS MFN2-KO	Human	Dr. Edward A Fon (McGill University, Montreal, Canada)
U2OS WT	Human	Dr. Edward A Fon (McGill University, Montreal, Canada)
U2OS CS-KO	Human	This thesis
U2OS SLC25A1-KO	Human	This thesis

Reagents

The main reagents used in this thesis are described in Table 2 or indicated in the specific section.

Table 2. Reagents used in this thesis.

Name	Supplier	Catalog Number
13C- glucose	Sigma-Aldrich	389374
13C- glutamine	Sigma-Aldrich	605166
15-Nh4Cl	Sigma-Aldrich	299251
25-HC	Sigma-Aldrich	H1015
aKG	Sigma-Aldrich	349631
Ammonium carbonate	Sigma-Aldrich	379999
Benzonase® Nuclease	Millipore Sigma	70746-3
BFA	Sigma-Aldrich	B6542
Biotin	Sigma-Aldrich	B4639
BPTES	Sigma-Aldrich	SML0601
CCCP	Sigma-Aldrich	C2759
Chloroform	Merck	32211-1L-M
D-glutamine	Sigma-Aldrich	G9003
DMEM	Thermo Fisher Scientific	A1443001
DMEM 4.5 g/L glucose	Thermo Fisher Scientific	42430-082

DMEM F12	Thermo Fisher Scientific	11330032
DON	Sigma-Aldrich	D2141
Ethanol	Millipore Sigma	1.00983.2500
FBS	Thermo Fisher Scientific	A3840402
Glucosamine	Ultimate glucosamine®	
Glucose	Sigma-Aldrich	G7021
Glutamine	Thermo Fisher Scientific	25030081
Glycoblue	Thermo Fisher Scientific	AM9516
Lipofectamine RNAi Max	Thermo Fisher Scientific	13778075
Methanol	Thermo Fisher Scientific	A456-212
MG-132	Cell Signaling Technology	2194S
MSX	Sigma-Aldrich	M5379
NEAA	Thermo Fisher Scientific	11140035
Nh4Cl	Sigma-Aldrich	A9434
Nucleosides	Millipore Sigma	ES-008-D
Oligomycin	Sigma-Aldrich	75351
Opti-MEM™	Thermo Fisher Scientific	31985062
Paraformaldehyde	Thermo Fisher Scientific	28908
Polybrene	Millipore Sigma	TR-1003-G
Protease and Phosphatase Inhibitor tablets	Thermo Fisher Scientific	A32961
Phosstop™- phosphatase inhibitor tablets	Sigma-Aldrich	4906837001
Pyruvate	Thermo Fisher Scientific	11360070
Puromycin	Thermo Fisher Scientific	A1113803
SDS	Labochem	LC-10112.1
ISRIB	Sigma-Aldrich	SML0843
SYBR Green Master Mix	Thermo Fisher Scientific	A25742

Trizol	Thermo Fisher Scientific	15596018
Tunicamycin	Millipore Sigma	654380
XtremeGene9	Sigma-Aldrich	6365787001

Gene silencing

For gene silencing, Lipofectamine RNAi Max Reagent was used following the manufacturer's instructions. In brief, 40.000 cells were plated and transfected on the next day with a mix of Lipofectamine, Opti-MEM™, and esiRNA (3 μl:100 μl: 0.8 μg ratio). For the silencing of GLUL, Mission® esiRNA (sigma, EHU115441) was used. After 3 days, cells were treated as indicated.

Virus production and infections

To produce virus particles containing plasmids for transduction, HEK293T cells were transfected using Xtremegene9 and following the manufacturer's instructions. As a packing vector, pUMVC (gagpol) (addgene #14887) was used. For CRISPR-KO, pSPAX2 (addgene #12260) was used instead. As envelope vector, pCMV-VSVG (Addgene 8454) was used. After, 24h of the transfection, fresh DMEM + 10% FBS was added. In the next day, media from the transfected HEK293T cells was collected and passed through a 0.45 μM PES syringe filter and polybrene was added to the filtered viral supernatant to 5-8 μg/mL final concentration. Filtered media containing virus and polybrene was added to the target cells. After 24-48h, new fresh media was added to the cells and the experiments were performed as indicated.

CRISPR Knockout cell lines

To generate CS and SLC25A1 CRISPR KO cell lines, U2OS cells were transduced with lentiviral particles containing the following sgRNAs (Table 3) cloned into the pLenti CRISPRv2 (Addgene #5296) as previously described (Li et al., 2022). Cells were selected in 3 μg/mL puromycin and clones were isolated by FACs sorting. All clones were validated by immunoblotting for CS and SLC25A1.

Table 3. CRISPR guides used in this thesis.

CRISPR KO			
AAVS1	Human	F-1	CACCGGGGGCCACTAGGGACAGGAT
	Human	R-1	AAACATCCTGTCCCTAGTGGCCCCC
Cs	Human	F-1	CAACATGGCAAGACGGTGGT
	Human	R-1	ACCACCGTCTTGCCATGTTG
	Human	F-2	TTTTCCAAACCTTACCGTGG
	Human	R-2	CCACGGTAAGGTTTGGAAAA
Slc25a1	Human	F-1	AGATCTCGATGCCACCCGCC
	Human	R-1	GGCGGGTGGCATCGAGATCT
	Human	F-2	CTACGGTTCCATCCCCAAGG
	Human	R-2	CCTTGGGGATGGAACCGTAG

Immunofluorescence Assay

For immunofluorescence (IF) analysis of eGFP-SCAP-expressing CHOs, 2.5 x 10^3 cells were plated in a 24-well glass-bottom plate (Greiner Bio-One), starved of gln for 24h, and in the next day incubated with MSX at 0.5 mM with either no gln, 2 mM gln, or 1mM aKG. After 24h, cells were fixed in 4 paraformaldehyde (fresh) diluted in prewarmed DMEM/F12 for 20 min at 37°C, permeabilized for 20 min at RT with 0.2% triton in PBS, blocked in 3% bovine serum albumin (BSA) in PBS for 30 min, and incubated in golgin-97 (CST #13192) at 1:250 in 3% BSA overnight. On the next day, the samples were rinsed 3X in PBS, and incubated with secondary antibody anti-rabbit Alexa Fluor Plus 594 (Life Technologies, #A32740) at 1:1000 for 45 minutes. Following 3X rinses in PBS, images were taken using an Olympus IXplore SpinSR spinning disk confocal microscope (https://www.olympus-lifescience.com/en/microscopes/inverted/ixplore-spinsr/). All images were taken with a 100X/1.35 silicon oil objective and excitation with 488 and 561 lasers and processed via cellSens software (https://www.olympus-lifescience.com/pt/software/cellsens/).

Immunoblotting

For all experiments, unless otherwise indicated, cells were plated in cDMEM. The next day cell monolayers were rinsed with PBS and cultured in DMEM without FBS overnight (to

promote cholesterol synthesis), followed by treatments as indicated in the text. Whole cells were harvested in 200-400 µL of chilled lysis buffer (50mM Hepes-KOH pH 7.4, 40mM NaCl, 2mM EDTA, 1.5mM NaVO4, 50mM NaF, 10mM NaPyrophosphate, 10mM, NaBetaGlycerophosphate (disodium salt pentahydrate) and 1% Triton X-100) containing proteases and phosphatases inhibitors tablets (Table 2). 2 µL Benzonase® was added to the lysates which were subsequently shaken at 1500 rpm at 37°C for 15min, centrifuged for 5 min at 1200 rpm at 4°C, and the supernatant was transferred into a fresh tube. Protein concentration was quantified using Pierce™ BCA Protein Assay Kit and after diluted with 5X SDS added to a final of 1X SDS. The same amount of protein (10-20 ug, depending on the experiment) was applied in an SDS-PAGE gel and transferred to PVDF membranes. Membranes were blocked with PBS + 0.1% Tween 20 (PBS-T) and 5% non-fat milk for 30min at RT. Membranes were rinsed to remove the milk and were incubated in TBS-T + primary antibodies (1:1000 or 1:500) overnight. Following incubation, blots were washed three times in TBS-T and then incubated with horseradish peroxidase (HRP)-conjugated anti-mouse IgG (CST #7076) or anti-rabbit IgG (CST #7074) at a 1:10000 dilution for 60 minutes at RT and developed using a chemiluminescence system (Pierce™ ECL Western Blotting Substrate or Pierce SuperSignal™ West Atto Ultimate Sensitivity Substrate; ThermoFisher Scientific). The following antibodies were used (Table 4).

Table 4. Antibodies used in this thesis.

Name	Supplier	Catalog Number
ACTIN	Proteintech	66009-1-IG
ATF3	Abcam	ab207434
ATF4	Cell Signaling Technology	11815S
ATF6	Cell Signaling Technology	65880T
ATP5	Thermo Fisher Scientific	A21351
c-MYC	Cell Signaling Technology	5605S
CALNEXIN	GeneTex	GTX109669
CALRETICULIN	Cell Signaling Technology	12238S

CITRATE SYNTHASE	Proteintech	16131-1-AP
eIF2alpha	Cell Signaling Technology	9722S
p eIF2alpha	Cell Signaling Technology	9721S
FASN	Cell Signaling Technology	3180S
FUMARASE	Cell Signaling Technology	4567S
GLS1	Abcam	ab156876
GRP78	Cell Signaling Technology	3177S
HA	Cell Signaling Technology	3724S
HMGCR	Sigma-Aldrich	AMAB90619
HMGCS1	Novus Biologicals	NBP2-36554
HPRT1	Thermo Fisher Scientific	PA522281
MFN1	Cell Signaling Technology	14739S
MFN1/2	Abcam	ab57602
MFN2	Cell Signaling Technology	9482S
PCNA	BD Biosciences	610664
S6K	Cell Signaling Technology	9202S
pS6K	Cell Signaling Technology	97596S
SDHA	Cell Signaling Technology	11998S
SLC25A1	Proteintech	15235-1-AP
SQLE	Proteintech	12544-1-AP
SREBP2	BD Biosciences	557037
TOM20	Sigma-Aldrich	HPA011562
TOM40	Sigma-Aldrich	HPA036231
TOM70	Sigma-Aldrich	HPA048020
TUBULIN	Proteintech	66031-1-IG
UBIQUITIN	Cell Signaling Technology	3936S

VDAC1/2	Proteintech	0866-1-AP

Metabolomics and Isotope labeling sample preparation

2 x 10^5 cells were plated in cDMEM in 6 wells plates. On the following day, cells were rinsed with PBS and cultured in DMEM without FBS to promote cholesterol synthesis. After, cells were treated as indicated in the text. After the indicated treatments cells were washed twice with 75mM of ammonium carbonate pH =7.4 and the plates were frozen in liquid nitrogen and stored at -80°C until metabolite extraction. For metabolite extraction, 60% MeOH containing internal standards buffer (Amino acid standard - Cambridge isotopes MSK_A2-1.2, Citric acid D4 (Sigma 485438-1G), ATP $^{13}C_{10}$ (Sigma 710695), AMP $^{13}C_{10}{}^{15}N_5$ (Sigma 650676), and ADP $^{15}N_5$ (Sigma 741167)) was added to each well of the frozen plate. The cells were then scraped, transferred to a new tube containing MTBE and EquiSPLASH™ LIPIDOMIX® (Avanti 330731-1EA), and incubated for 30 min at 1500 rpm at 4°C. The samples were centrifuged for 10 min at 21.000 x g at 4°C. The supernatants were collected in a new tube with 100 µL LCMS-grade H2O, incubated for 10 min at 1500 rpm at 15°C, and further centrifuged for 5 min at 16.000 x g at 15°C to obtain a clear phase separation. The upper phase (apolar metabolites) and the down phase (polar metabolites) were collected in different tubes. After, the metabolite extracts were dried down in a speed vac and stored at -80°C until further analysis as described further. All metabolomics was performed by the metabolomics facility at the Max Planck Institute for Biology of Ageing, the lipidomics facility at CECAD (Cluster of Excellence for Aging Research), or the metabolomics facility at Max Planck Institute of Immunobiology and Epigenetics.

Semi-targeted liquid chromatography-high-resolution mass spectrometry-based (LC-HRS-MS) analysis of amine-containing metabolites

The LC-HRMS analysis of amine-containing compounds was performed using a QE-Plus high-resolution mass spectrometer coupled to a Vanquish UHPLC chromatography system (Thermo Fisher Scientific). In brief: 50 µL of the available 150 µL of the above-mentioned (AEX-MS method) polar phase were mixed with 25 µL of 100 mM sodium carbonate (Sigma),

followed by the addition of 25 µL 2% [v/v] benzoylchloride (Sigma) in acetonitrile (UPC/MS-grade, Biosove, Valkenswaard, Netherlands). The derivatized samples were thoroughly mixed and kept at a temperature of 20°C until analysis. For the LC-HRMS analysis, 1 µL of the derivatized sample was injected onto a 100 x 2.1 mm HSS T3 UPLC column (Waters). The flow rate was set to 400 µL/min using a binary buffer system consisting of buffer A (10 mM ammonium formate (Sigma-Aldrich), 0.15% [v/v] formic acid (Sigma-Aldrich) in UPC-MS-grade water (Biosove, Valkenswaard, Netherlands). Buffer B consisted of acetonitrile (IPC-MS grade, Biosove, Valkenswaard, Netherlands). The column temperature was set to 40°C, while the LC gradient was: 0% B at 0 min, 0-15% B 0- 4.1min; 15-17% B 4.1 – 4.5 min; 17-55% B 4.5-11 min; 55-70% B 11 – 11.5 min, 70-100% B 11.5 - 13 min; B 100% 13 - 14 min; 100-0% B 14 - 14.1 min; 0% B 14.1-19 min; 0% B. The mass spectrometer (Q-Exactive Plus) was operating in positive ionization mode recording the mass range m/z 100-1000. The heated ESI source settings of the mass spectrometer were: Spray voltage 3.5 kV, capillary temperature 300°C, sheath gas flow 60 AU, aux gas flow 20 AU at 330°C, and the sweep gas was set to 2 AU. The RF-lens was set to a value of 60. The LC-MS data analysis was performed using the TraceFinder software (Version 5.1, Thermo Fisher Scientific). The identity of each compound was validated by authentic reference compounds, which were measured at the beginning and the end of the sequence. For data analysis the area of the protonated [M + nBz + H]+ (nBz stands for the number of benzoyl moieties attached to each compound) isotopologue mass peaks of every required compound were extracted and integrated using a mass accuracy <3 ppm and a retention time (RT) tolerance of <0.05 min as compared to the independently measured reference compounds. If no independent ^{12}C experiments were carried out, where the pool size is determined from the obtained peak area of the 1^2C monoisotopologue, the pool size determination was carried out by summing up the peak areas of all detectable isotopologues per compound. These areas were then normalized, as performed for un-traced ^{12}C experiments, to the internal standards, which were added to the extraction buffer, followed by normalization to the protein content or the cell number of the analyzed samples. The relative isotope distribution of each isotopologue was calculated from the proportion of the peak area of each isotopologue towards the sum of all detectable isotopologues. The ^{13}C enrichment, namely the area attributed to ^{13}C molecules traced in the detected isotopologues, was calculated by multiplying the peak area of each isotopologue

with the proportion of the ^{13}C and the ^{12}C carbon number for the corresponding isotopologue (the ^{12}C and ^{13}C monoisotopologue areas were multiplied with 0 and 1 respectively). The obtained ^{13}C area of each isotopologue are summed up, providing the peak area fraction associated to ^{13}C atoms in the compound. Dividing this absolute ^{13}C area by the summed area of all isotopologues provides the relative ^{13}C enrichment factor.

Anion-Exchange Chromatography Mass Spectrometry (AEX-MS) for the analysis of anionic metabolites

Extracted metabolites were re-suspended in 150 µL of UPLC/MS grade water (Biosolve), of which 100 µL were transferred to polypropylene autosampler vials (Chromatography Accessories Trott, Germany) before AEX-MS analysis. The samples were analysed using a Dionex ionchromatography system (Integrion Thermo Fisher Scientific) as described previously. In brief, 5 µL of the resuspended polar metabolite extract were injected in push-partial mode, using an overfill factor of 1, onto a Dionex IonPac AS11-HC column (2 mm × 250 mm, 4 µm particle size, Thermo Fisher Scientific) equipped with a Dionex IonPac AG11-HC guard column (2 mm × 50 mm, 4 µm, Thermo Fisher Scientific). The column temperature was held at 30°C, while the auto sampler temperature was set to 6°C. A potassium hydroxide gradient was generated using a potassium hydroxide cartridge (Eluent Generator, Thermo Scientific), which was supplied with deionized water (Milli-Q IQ 7000, Millipore). The metabolite separation was carried at a flow rate of 380 µL/min, applying the following gradient conditions: 0-3 min, 10 mM KOH; 3-12 min, 10−50 mM KOH; 12-19 min, 50-100 mM KOH; 19-22 min, 100 mM KOH, 22-23 min, 100-10 mM KOH. The column was re-equilibrated at 10 mM for 3 min. For the analysis of metabolic pool sizes the eluting compounds were detected in negative ion mode using full scan measurements in the mass range m/z 77 – 770 on a Q-Exactive HF high resolution MS (Thermo Fisher Scientific). The heated electrospray ionization (ESI) source settings of the mass spectrometer were: Spray voltage 3.2 kV, capillary temperature was set to 300°C, sheath gas flow 50 AU, aux gas flow 20 AU at a temperature of 330°C and a sweep gas glow of 2 AU. The S-lens was set to a value of 60. The LC-MS data analysis was performed using the TraceFinder software (Version 5.1, Thermo Fisher Scientific). The identity of each compound was validated by authentic reference compounds, which were measured at the beginning and the end of the sequence.

For data analysis the area of the deprotonated [M-H+]-1 or doubly deprotonated [M-2H]-2 isotopologues mass peaks of every required compound were extracted and integrated using a mass accuracy <3 ppm and a retention time (RT) tolerance of <0.05 min as compared to the independently measured reference compounds. If no independent ^{12}C experiments were carried out, where the pool size is determined from the obtained peak area of the ^{12}C monoisotopologue, the pool size determination was carried out by summing up the peak areas of all detectable isotopologues per compound. These areas were then normalized, as performed for un-traced ^{12}C experiments, to the internal standards, which were added to the extraction buffer, followed by a normalization to the protein content or the cell number of the analyzed samples. The relative isotope distribution of each isotopologue was calculated from the proportion of the peak area of each isotopologue towards the sum of all detectable isotopologues. The ^{13}C enrichment, namely the area attributed to ^{13}C molecules traced in the detected isotopologues, was calculated by multiplying the peak area of each isotopologue with the proportion of the ^{13}C and the ^{12}C carbon number for the corresponding isotopologue (the ^{12}C and ^{13}C monoisotopologue areas were multiplied with 0 and 1, respectively). The obtained ^{13}C area of each isotopologue are summed up, providing the peak area fraction associated to ^{13}C atoms in the compound. Dividing this absolute ^{13}C area by the summed area of all isotopologues provides the relative ^{13}C enrichment factor.

UPLC-HRMS-based measurement of cholesterol

The UPLC-HRMS analysis of cholesterol was performed using a modified method described by McDonald et al (McDonald et al., 2007). In brief: The lipid fraction of the two-phase metabolite extract was re-suspended in 100 µL of 95% methanol (Optima-Grade, Thermo Fisher Scientific) and incubated at 4°C for 15 min on a thermomixer. The re-suspended extract was centrifuged for 5 min at 16.000 x g at 4°C and the cleared supernatant were transferred to auto-sampler vials with 200 µL glass inserts (Chromatography Accessories Trott, Germany). For the LC-HRMS analysis, 3 µL of the sample were injected onto a 100 x 2.1 mm HSS T3 UPLC column (Waters). The flow rate was set to 300 µL/min using a binary buffer system consisting of buffer A (5 mM ammonium acetate (Sigma), in 85% LC-MS-grade methanol (Optima-Grade, Thermo Fisher Scientific)), while buffer B consisted of 5 mM ammonium acetate (Sigma), in 100% LC-MS-grade methanol. The column temperature was set to 40°C,

while the LC gradient was: 0 min 0% B, 2 min, 0% B 15 min; 100% B, 25 min 100% B, 25.1 min 0% B and 30 min 0% B. The mass spectrometer (Q-Exactive HF, Thermo Fisher Scientific) was operating in positive ionization mode recording the mass range m/z 250-600. The heated ESI source settings of the mass spectrometer were: Spray voltage 3.5 kV, capillary temperature 300°C, sheath gas flow 60 AU, aux gas flow 20 AU at a temperature of 340°C and the sweep gas to 2 AU. The S-lens was set to a value of 60 arbitrary units. Semi-targeted data analysis for the samples was performed using the TraceFinder software (Version 4.1, Thermo Fisher Scientific). The identity of each compound was validated by authentic reference compounds, which were run before and after every sequence. Peak areas of [M - H2O + H]+ ions were extracted using a mass accuracy (<3 ppm) and a retention time tolerance of <0.05 min. Areas of the cellular pool sizes were normalized to the internal standards (Cholesterol D7 Avanti Polar Lipids), which were added to the extraction buffer, followed by a normalization to the cell number of the analyzed sample. Enrichment analysis and isotope distribution were calculated as described in the IC/Bz section.

Total levels of cholesterol quantification in WT and MFN2-KO cells

Cholesterol levels were determined by Liquid Chromatography coupled to Electrospray Ionization Tandem Mass Spectrometry (LC-ESI-MS/MS). 1.5 to 5 x 10^6 U2OS cells were homogenized in 300 µL of Milli-Q water using the Precellys 24 Homogenisator (Peqlab) at 6.500 rpm for 30 sec. The protein content of the homogenate was routinely determined using bicinchoninic acid. To 70 µL of homogenate 430 µL of Milli-Q water, 1.875 mL of chloroform/methanol/37% hydrochloric acid 5:10:0.15 (v/v/v), and 1.26 nmol of deuterated cholesterol-D7 (Avanti Polar Lipids) as internal standard was added. Lipids were extracted using the "One-Step Extraction" described in Özbalci et al (Özbalci et al., 2013), a method modified from Bligh and Dyer (Bligh and Dyer, 1959). Dried lipid extracts were resolved in 300 µL of methanol and sonicated for 5 min. After centrifugation (12.000 × g, 5 min, 4 °C), 40 µL of the clear supernatants were transferred to autoinjector vials. LC-MS/MS analysis of cholesterol was performed as previously described (Mourier et al., 2015).

Mice diet and MSX injections

Male C57BL/6 mice (n=30) at 7 weeks of age were blindly randomized into two dietary groups: (1) Control diet (1.8% gln; Ssniff diet, #S9159-E764) and (2) Test diet (0% gln; Ssniff diet, #S9159-E762) for 12 weeks. Blood samples were collected at t=0,4,8, and 12 weeks for glucose and lipids measurements. Mice were weight weekly to assess weight and weight gain (weight at 12 weeks – weight at 0 weeks). After 12 weeks, mice were fasted for 4h and euthanatized by anesthesia (166,7 mg/kg of Ketamin and 23,8 mg/kg of Xylazine in 0.9% NaCl) injection followed by cervical dislocation. Tissues were collected, watched with PBS, snap-frozen in liquid nitrogen, and stored at -80 °C until subsequent analysis.

For assessing the effects of MSX *in vivo*, mice were treated and fed as mentioned above for 1 week and injected 3x with saline or MSX (20 mg/kg diluted in saline) as previously described (Ghoddoussi et al., 2010). After, mice were euthanatized as mentioned and blood and organs collect for future analysis.

Cholesterol and TG quantification in plasma

Blood was collected from mice and spun down for 5min at 300 rpm. Plasma was transferred to a new tube and used for cholesterol and triglycerides measurement. Cholesterol was measured with CHOLESTEROL CHOD-PAP reagent (Biolobo, #87356) and the triglycerides with TRIGLYCERIDES FS reagent (Biolobo, #80019). For it, 5 µL of plasma and a standard curve was pipette into a 96-well plate in duplicate. After, 200 µL and 100 µL of CHOLESTEROL CHOD-PAP and TRIGLYCERIDES FS, respectively, were added. Plates were incubated for 20 min at RT and read at 490 nm in a plate reader.

Plasma fractionation

Fast protein liquid chromatography (FPLC) was used to measure cholesterol and triglycerides content in VLDL, LDL, and HDL lipoprotein as described by Gerdes et al. (Gerdes et al., 1992). In brief: plasma lipoproteins were eluted in Tris-buffered Saline pH=7.4 and pumped at a flow rate of 0.31 mL/min by a PU-4180 quaternary pump into a Superose 6 increase 10/30 column (GE Healthcare). Diode Array Detector (DAD MD 4015, Jasco) was used (detection at 505 nm). Calibration curves for the quantitative analysis (SKZL) of the separated lipoprotein

fractions were made with lipid plasma standards. Chrom Nav chromatographic software (version 2.0, Jasco) was used for chromatographic analysis.

Lipid extraction and cholesterol quantification in tissues

Tissues were weight and ~100 mg of tissues were lysate with 1 mL of RIPA buffer (#BP-115; Boston BioProducts) supplemented with Protease inhibitor (PI; P8340 Merck; 1:100 dilution) and Phenylmethanesulfonlyflouride (PMSF; P7626 Merck; 1:100 dilution of lab-stock; 1mM final concentration) in microtubes with metal beads. QIAGEN TissueLyser II was used for lysis, using 45-60 sec cycles. 200 µL of the lysate was used for lipid extraction by adding 6 mL of chloroform/methanol (2:1) to the lysates. The lysates + chloroform/methanol was shaken overnight at 4°C. On the next day, phase separation was promoted by adding 1.5 mL of 0.9% NaCl. After, the samples were vortexed and spun down for 5 min at 1000 rpm. The lower layer (chloroform layer) — contained lipids — was pipetted into a clean tube and added 2 µL of 100% Triton. The samples were dried with nitrogen gas in a fume hood. 100 µL of water was added to the samples, and the lipids were dissolved by shaking and incubating the samples at 37°C for 30 min. Samples were stored at -20°C. For protein quantification, the remained lysate was spun down for 10 min at 4°C and 20.000 x g and the supernatant was transferred into a new tube. Protein concentration was quantified using Pierce™ BCA Protein Assay Kit.

For cholesterol quantification in the tissues, the extracted lipids were diluted 20x, and 10 µL were used. Cholesterol levels were determined as described above, using the CHOLESTEROL CHOD-PAP reagent (Biolobo, #87356).

Glutamine consumption

Cells were cultured in DMEM without FBS, pelleted, and stored at -80°C until extraction. Samples were resuspended in extraction solution (ice-cold 80% methanol), incubated for 5 min on ice, and centrifuged for 3 min, 20.000 x g, at -9°C. The supernatant was collected and kept on dry ice. Samples were further resuspended two more times with extraction solution and treated as previously described to further collect supernatants. Samples were finally dried using a Genevac EZ2 speed vac and further processed following protocols previously

described (Edwards-Hicks et al., 2020). Targeted metabolite quantification by LC-MS was carried out using an Agilent 1290 Infinity II UHPLC in line with an Agilent 6495 QQQ-MS operating in MRM mode. MRM settings were optimized separately for all compounds using pure standards. LC separation was on a Phenomenex Luna propylamine column (50 x 2 mm, 3 µm particles) as described previously (Edwards-Hicks et al., 2020). Briefly, a solvent gradient of 100% buffer B (5 mM ammonium carbonate in 90% acetonitrile) to 90% buffer A (10 mM NH_4 in water) was used. The flow rate was from 1000 to 750 µL/min. The autosampler temperature was 5°C and the injection volume was 2 µL. Raw data were analyzed using the R package automRm (Eilertz, Mitterer, Büscher, in preparation). Further analysis was performed using MassHunter software (Bruker). The amount of gln consumed by the cells was calculated as the difference between the starting gln concentration in DMEM and the gln concentration in DMEM after 8h of culturing cells of the indicated genotype. The gln consumption was normalized to the average cell density.

Quantitative real-time PCR

Total RNA was prepared from U2OS treated as indicated in the text using TriZol (Table 2) according to the manufacturer's instructions. RNA was quantified by spectrophotometry using Nanodrop One (ThermoFisher) and purity was assessed by the absorbance ratios of 260:280 and 260:230. From an equal amount of total RNA, complementary DNA was generated with SuperScript™ VILO™ Master Mix (Thermo Fischer Scientific; # 11755050). Real-time quantitative PCR (qPCR) was based on the SYBR green (Table 2) chemistry and carried out using the StepOne™ Real-Time PCR System . The Ct levels were calculated using Software StepOne™ and the average of CTs of each sample was calculated (n=3). The mean CT of each sample was linearized (=2^{-CT}) and normalized by the *Hprt1* expression of the same sample as previously described (Garcia et al., 2020). The following primer sequences were used (Table 5).

Table 5. The q-PCR primers used in this thesis.

Gene	Species	Sense	Sequence (5′-3′)
Atf3	Human	F	GGA GCC TGG AGC AAA ATG ATG
		R	AGG GCG TCA GGT TAG CAA AA
Atf4	Human	F	TTC TCC AGC GAC AAG GCT AAG G
		R	CTCCAACATCCAATCTGTCCCG
Atf5	Human	F	GAG CCC CTG GCA GGT GAT
		R	CAG AGG GAG GAG AGC TGT GAA
Fdft1	Human	F	GGA AAG GGC AAG CAG TGA CC
		R	GGA TGG TGG AGA TGA TCT GCC TT
Fdps	Human	F	GCT GGT GGT TCA GTG TCT GC
		R	GCA AGA ACA CTG CTG GCA GAT C
Hmgcr	Human	F	AGG CCT GTT TGC AGA TGC TAG G
		R	GAT GTC CTG CTG CCA ATG CT
Hprt1	Human	F	TGA CAC TGG CAA AAC AAT GCA
		R	CGT CCT TTT CAC CAG CAA GCT
Slc1a5	Human	F	CTC GAT TCG TTC CTG GAT CTT
		R	GTT CCG GTG ATA TTC CTC TCT TC
Slc1a5var	Human	F	GCC CTC CCA CTA TGT ACT CTA
		R	CTA CCA AGC CCA GGA TGT TC
Slc38a1	Human	F	CAC AGA CCA GGA TGG AGA TAA AG
		R	GGA ATG CTG ACC AAG GAG AA
Sqle	Human	F	TGG GCT GCT TTC TGT ATT GTC TCC
		R	CAC CAC TAC TGA GAA GGG CTG G
Srebp1	Human	F	TGT CCA CAA AAG CAA ATC TCT
		R	AGT GTG TCC ACC TCA GTC T

Srebp2	Human	F	GTT GTA TGT CCT GTG CCT TTT
		R	TGG GAC ACA GTG ACT GAT TGA
Srebp2	Mouse	F	ACC TAG ACC TCG CCA AAG GT
		R	GCA CGG ATA AGC AGG TTT GT
Ldlr	Mouse	F	AGG CTG TGG GCT CCA TAG G
		R	TGC GGT CCA GGG TCA TCT
Hmgcr	Mouse	F	GCT CGT CTA CAC AAA CTC CAC G
		R	GCT TCA GCA GTG CTT TCT CCG T
Hmgcs1	Mouse	F	GGA AAT GCC AGA CCT ACA GGT G
		R	TAC TCG GAG AGC ATG TCA GGC T
Fdft1	Mouse	F	TCC AAA CAG GAC TGG GAC A
		R	AGA CGA GAA AGG CCA ATT CC
Sqle	Mouse	F	TGT GCG GAT GGA CTC TTC TCC
		R	GTT GAC CAG AAC AAG CTC CGC A
Dch4r	Mouse	F	GGT CAT GAC GGA CGA CGT A
		R	AGG GCT TGT AGT AAC TGC CAA T
Fdps	Mouse	F	GGT GGT TCA GTG TCT GCT ACG A
		R	CGC CTC ATA CAG TGC TTT CAC C
Srebp1	Mouse	F	GGA GCC ATG GAT TGC ACA TT
		R	GGC CCG GGA AGT CAC TGT
Acc	Mouse	F	GGA GAT GTA CGC TGA CCG AG
		R	TAC CCG ACG CAT GGT TTT CA
Fasn	Mouse	F	GCT GCG GAA ACT TCA GGA AAT
		R	AGA GAC GTG TCA CTC CTG GAC TT
Scd1	Mouse	F	CCA AGC TGG AGT ACG TCT GG
		R	CAG AGC GCT GGT CAT GTA GT

Hprt1	Mouse	F	GTT GGG CTT ACC TCA CTG CT
		R	TCA TCG CTA ATC ACG ACG CT

RNAseq extraction and analysis

For RNAseq analysis cells were plated and cultured as indicated in the text. Two independent experiments were performed with n=3. RNA was extracted and quantified, and purity was assessed as mentioned above. The RNAseq was performed for the Cologne Center for Genomics (CCG) following the protocols previously described (George et al., 2015; Peifer et al., 2015). In brief: Libraries were prepared using the Illumina® Stranded TruSeq® RNA sample preparation Kit. Library preparation started with 500ng total RNA. After poly-A selection (using poly-T oligo-attached magnetic beads), mRNA was purified and fragmented using divalent cations under elevated temperature. The RNA fragments underwent reverse transcription using random primers. This was followed by second-strand cDNA synthesis with DNA Polymerase I and RNase H. After end repair and A-tailing, indexing adapters were ligated. The products were then purified and amplified (15 PCR cycles) to create the final cDNA libraries. After library validation and quantification (Agilent Tape Station), equimolar amounts of library were pooled. The pool was quantified by using the Peqlab KAPA Library Quantification Kit and the Applied Biosystems 7900HT Sequence Detection System. The pool was sequenced on an Illumina NovaSeq6000 sequencing instrument with a PE100 protocol. For the RNAseq analysis, Ensembl Homo sapiens release 105/ hg38 was used for genomes and annotations. rRNA transcripts were removed and cDNA fasta was generated using `gffread` (cufflinks/2.2.1) (Trapnell et al., 2012). cDNA index was built using kallisto (kallisto/0.46.1) (Bray et al., 2016). 4 million reads were pseudoaligned to reference transcriptome using kallisto/0.46.1 and RSeQC/4.0.0 used to identify mapping strand (Wang et al., 2012). A strand was identified by having more than 60% of reads mapped to it. Cases with less than 60% of reads in each strand were defined as unstranded. Reads were pseudoaligned to reference transcriptome and quantified using kallisto/0.46.1. After the removal of batch effects, differential expression was performed between "Control" and "Treatment" samples using limma/3.54.0 (Love et al., 2014). Gln+ samples were classified as

Control whereas gln- samples and aKG+ samples were classified as Treatment. Pathway enrichment analysis was performed using the DAVID API (Sherman et al., 2022). Data visualization was performed with Flaski (Iqbal 2021).

RUSH assay

MannII-SBP-mCherry HeLa stable cell lines were generated via lentivirus transduction and sequential puromycin selection. A second-generation lentivirus packaging system was used. The plasmids for the lentivirus production were obtained from addgene, psPAX2 (Addgene plasmid #12260), pMD2.G (Addgene plasmid #12259) and pCDH_Str-KDEL_ManII-SBP-mCherry (Addgene plasmid #65259). For Lentivirus production, 10 x 10^6 HEK293T cells were seeded on a 15 cm plate and after 24 h, cells were transfected with pCDH_Str-KDEL_ManII-SBP-mCherry, psPAX2, and pMD2.G mix in a ratio 4:2:1 using $CaPO_4$ precipitation. The virus-containing medium was collected, centrifuged, and filtered with 0.2 µM filters. 2 x 10^6 HeLa cells were infected in a 10 cm plate on two consecutive days. Polybrene at a final concentration of 10 µg/mL was added to the medium to increase the infection efficiency. After 24h from the last infection, the cells were selected with puromycin at the final concentration of 1 µg/mL. For life imaging, HeLas stably expressing pCDH_Str-KDEL_ManII-SBP-mCherry were plated on 6-well CELLview glass-bottom cell culture dishes (Greiner Bio-One) and treated as indicated in the text and imaged at the start and following biotin addition using an Olympus IXplore SpinSR 50 mm spinning disk confocal microscope. Live cell imaging was performed in DMEM without FBS with incubation at 37°C and 5% CO2. For fixed images, cells were fixed and incubated as previous described. All images were taken with a 100X/1.35 silicon oil objective and excitation with 488 and 561 lasers and processed via cellSens software (https://www.olympus-lifescience.com/pt/software/cellsens/).

OCR measurement

Oxygen consumption rate (OCR) was measured using Seahorse XF Analyzer. A total of 32.000 cells per well were plated in XF 96 cell culture microplates in DMEM medium supplemented with 10% FBS. The next day, DMEM was replaced by Seahorse XF medium without FBS and

supplemented with pyruvate (1 mM), glutamine (1 mM), and either glucose or galactose (10 mM). The OCR was measured according to the manufacturer's protocol (XF Cell Mito Stress Test Kit) at basal level and after injections with oligomycin (2 µM), FCCP (0.5 µM), and a combination of antimycin A (0.5 µM) and rotenone (0.5 µM). To normalize OCR data, protein concentration per well was determined using a bicinchoninic acid assay. The data were analyzed by Seahorse Wave Desktop software.

Primary hepatocytes isolation and culture

Primary hepatocyte isolation and culture were performed as previously described (Maslansky and Williams, 1982). In brief: mice were anesthetized and liver perfusion was performed first with perfusion solution and after with collagenase solution. The liver was removed from the animal, transferred to a Petri dish containing perfusion solution, and gently combed until turned into a homogenate. The liver homogenate was passed through a sieve into 50 mL tubes. Hepatocytes were washed, counted, and plated in commercial collagen-coated plates (Corning, Cat no# 734-0274 or 734-0295). The cells were left to attach to the dish for 3h and the medium was replaced with DMEM 1 g/L glucose + 100 nM of Insulin + 500 nM Dexamethasone.

Statistical analyses

All statistical analyses were performed using one-way ANOVA, two-way ANOVA, or t-test in GraphPad Prism 9 software (https://www.graphpad.com/features) and are indicated accordingly.

Data visualization

All graphs and heatmaps were generated with GraphPad Prism 9 software and Flaski (https://flaski.age.mpg.de/home/). Cartoons were made with Biorender (https://www.biorender.com/). Figures were made with Adobe Illustrator 2023 (https://www.adobe.com/products/illustrator.html). For image analysis and WB figures Fiji (https://imagej.net/software/fiji/downloads) was also used.

Grammar correction

The grammar of this thesis was checked with Grammarly (https://www.grammarly.com/).

REFERENCES

Adams, C.M., Reitz, J., Brabander, J.K.D., Feramisco, J.D., Li, L., Brown, M.S., Goldstein, J.L., 2004. Cholesterol and 25-Hydroxycholesterol Inhibit Activation of SREBPs by Different Mechanisms, Both Involving SCAP and Insigs*. J. Biol. Chem. 279, 52772–52780. https://doi.org/10.1074/jbc.m410302200

Ahn, E., Kumar, P., Mukha, D., Tzur, A., Shlomi, T., 2017. Temporal fluxomics reveals oscillations in TCA cycle flux throughout the mammalian cell cycle. Mol Syst Biol 13, 953. https://doi.org/10.15252/msb.20177763

Altman, B.J., Stine, Z.E., Dang, C.V., 2016. From Krebs to clinic: glutamine metabolism to cancer therapy. Nat Rev Cancer 16, 619–634. https://doi.org/10.1038/nrc.2016.71

Amores-Sánchez, M.I., Medina, M.Á., 1999. Glutamine, as a Precursor of Glutathione, and Oxidative Stress. Mol Genet Metab 67, 100–105. https://doi.org/10.1006/mgme.1999.2857

Andersen, J.M., Dietschy, J.M., 1977. Regulation of sterol synthesis in 15 tissues of rat. II. Role of rat and human high and low density plasma lipoproteins and of rat chylomicron remnants. J Biol Chem 252, 3652–3659. https://doi.org/10.1016/s0021-9258(17)40302-4

Andersson, M., Elmberger, P.O., Edlund, C., Kristensson, K., Dallner, G., 1990. Rates of cholesterol, ubiquinone, dolichol and dolichyl-P biosynthesis in rat brain slices. Febs Lett 269, 15–18. https://doi.org/10.1016/0014-5793(90)81107-y

Arenas, F., Garcia-Ruiz, C., Fernandez-Checa, J.C., 2017. Intracellular Cholesterol Trafficking and Impact in Neurodegeneration. Front Mol Neurosci 10, 382. https://doi.org/10.3389/fnmol.2017.00382

Bakalar, B., Duska, F., Pachl, J., Fric, M., Otahal, M., Pazout, J., Andel, M., 2006. Parenterally administered dipeptide alanyl-glutamine prevents worsening of

insulin sensitivity in multiple-trauma patients. Crit Care Med 34, 381–386. https://doi.org/10.1097/01.ccm.0000196829.30741.d4

Barle, H., Ahlman, B., Nyberg, B., Andersson, K., Essén, P., Wernerman, J., 1996. The concentrations of free amino acids in human liver tissue obtained during laparoscopic surgery. Clin Physiol 16, 217–227. https://doi.org/10.1111/j.1475-097x.1996.tb00570.x

Beręsewicz, M., Charzewski, Ł., Krzyśko, K.A., Kochański, A., Zabłocka, B., 2018. Molecular modelling of mitofusin 2 for a prediction for Charcot-Marie-Tooth 2A clinical severity. Sci Rep-uk 8, 16900. https://doi.org/10.1038/s41598-018-35133-9

Bergström, J., Fürst, P., Norée, L.O., Vinnars, E., 1974. Intracellular free amino acid concentration in human muscle tissue. J Appl Physiol 36, 693–697. https://doi.org/10.1152/jappl.1974.36.6.693

Besseling, J., Kastelein, J.J.P., Defesche, J.C., Hutten, B.A., Hovingh, G.K., 2015. Association Between Familial Hypercholesterolemia and Prevalence of Type 2 Diabetes Mellitus. Jama 313, 1029–1036. https://doi.org/10.1001/jama.2015.1206

Billig, H., Furuta, I., Hsueh, A.J., 1993. Estrogens inhibit and androgens enhance ovarian granulosa cell apoptosis. Endocrinology 133, 2204–2212. https://doi.org/10.1210/endo.133.5.8404672

Bjo□rkhem, I., Meaney, S., 2004. Brain Cholesterol: Long Secret Life Behind a Barrier. Arteriosclerosis Thrombosis Vasc Biology 24, 806–815. https://doi.org/10.1161/01.atv.0000120374.59826.1b

Bligh, E.G., Dyer, W.J., 1959. A RAPID METHOD OF TOTAL LIPID EXTRACTION AND PURIFICATION. Can J Biochem Phys 37, 911–917. https://doi.org/10.1139/o59-099

Bodineau, C., Tomé, M., Courtois, S., Costa, A.S.H., Sciacovelli, M., Rousseau, B., Richard, E., Vacher, P., Parejo-Pérez, C., Bessede, E., Varon, C., Soubeyran, P., Frezza, C., Murdoch, P. del S., Villar, V.H., Durán, R.V., 2021. Two parallel pathways connect glutamine metabolism and mTORC1 activity to regulate glutamoptosis. Nat Commun 12, 4814. https://doi.org/10.1038/s41467-021-25079-4

Boncompain, G., Divoux, S., Gareil, N., Forges, H. de, Lescure, A., Latreche, L., Mercanti, V., Jollivet, F., Raposo, G., Perez, F., 2012. Synchronization of secretory

protein traffic in populations of cells. Nat Methods 9, 493–498. https://doi.org/10.1038/nmeth.1928

Boutant, M., Kulkarni, S.S., Joffraud, M., Ratajczak, J., Valera-Alberni, M., Combe, R., Zorzano, A., Cantó, C., 2017. Mfn2 is critical for brown adipose tissue thermogenic function. Embo J 36, 1543–1558. https://doi.org/10.15252/embj.201694914

Bowtell, J.L., Bruce, M., 2002. Glutamine: an anaplerotic precursor. Nutrition 18, 222–224. https://doi.org/10.1016/s0899-9007(01)00795-x

Boza, J.J., Dangin, M., Moe□nnoz, D., Montigon, F., Vuichoud, J., Jarret, A., Pouteau, E., Gremaud, G., Oguey-Araymon, S., Courtois, D., Woupeyi, A., Finot, P.-A., Ballèvre, O., 2001. Free and protein-bound glutamine have identical splanchnic extraction in healthy human volunteers. Am J Physiol-gastr L 281, G267–G274. https://doi.org/10.1152/ajpgi.2001.281.1.g267

Bray, N.L., Pimentel, H., Melsted, P., Pachter, L., 2016. Near-optimal probabilistic RNA-seq quantification. Nat Biotechnol 34, 525–527. https://doi.org/10.1038/nbt.3519

Brown, A.J., Coates, H.W., Sharpe, L.J., 2021a. Biochemistry of Lipids, Lipoproteins and Membranes 317–355. https://doi.org/10.1016/b978-0-12-824048-9.00005-5

Brown, A.J., Sharpe, L.J., Rogers, M.J., 2021b. Oxysterols: From physiological tuners to pharmacological opportunities. Brit J Pharmacol 178, 3089–3103. https://doi.org/10.1111/bph.15073

Brown, M.S., Goldstein, J.L., 1980. Multivalent feedback regulation of HMG CoA reductase, a control mechanism coordinating isoprenoid synthesis and cell growth. J. Lipid Res. 21, 505–517. https://doi.org/10.1016/s0022-2275(20)42221-7

Brown, M.S., Ho, Y.K., Goldstein, J.L., 1980. The cholesteryl ester cycle in macrophage foam cells. Continual hydrolysis and re-esterification of cytoplasmic cholesteryl esters. J Biological Chem 255, 9344–52.

Bruneau, E.G., McCullumsmith, R.E., Haroutunian, V., Davis, K.L., Meador-Woodruff, J.H., 2005. Increased expression of glutaminase and glutamine synthetase mRNA in the thalamus in schizophrenia. Schizophr Res 75, 27–34. https://doi.org/10.1016/j.schres.2004.12.012

Capel, E., Vatier, C., Cervera, P., Stojkovic, T., Disse, E., Cottereau, A.-S., Auclair, M., Verpont, M.-C., Mosbah, H., Gourdy, P., Barraud, S., Miquel, A., Züchner, S.,

Bonnefond, A., Froguel, P., Christin-Maitre, S., Delemer, B., Fève, B., Laville, M., Robert, J., Tenenbaum, F., Lascols, O., Vigouroux, C., Jéru, I., 2018. MFN2-associated lipomatosis: Clinical spectrum and impact on adipose tissue. J Clin Lipidol 12, 1420–1435. https://doi.org/10.1016/j.jacl.2018.07.009

Carvalho, K.F., Machado, T.S., Garcia, B.M., Zangirolamo, A.F., Macabelli, C.H., Sugiyama, F.H.C., Grejo, M.P., Neto, J.D.A., Tostes, K., Ribeiro, F.K.S., Sarapião, F.D., Pandey, A.K., Nociti, R.P., Tizioto, P., Coutinho, L.L., Meirelles, F.V., Guimarães, F.E.G., Pernas, L., Seneda, M.M., Chiaratti, M.R., 2020. Mitofusin 1 is required for oocyte growth and communication with follicular somatic cells. Faseb J 34, 7644–7660. https://doi.org/10.1096/fj.201901761r

Casellas-Díaz, S., Larramona-Arcas, R., Riqué-Pujol, G., Tena-Morraja, P., Müller-Sánchez, C., Segarra-Mondejar, M., Gavaldà-Navarro, A., Villarroya, F., Reina, M., Martínez-Estrada, O.M., Soriano, F.X., 2021. Mfn2 localization in the ER is necessary for its bioenergetic function and neuritic development. Embo Rep 22, e51954. https://doi.org/10.15252/embr.202051954

Chakrabarti, R., Fung, T.S., Kang, T., Elonkirjo, P.W., Suomalainen, A., Usherwood, E.J., Higgs, H.N., 2022. Mitochondrial dysfunction triggers actin polymerization necessary for rapid glycolytic activation. J. Cell Biol. 221, e202201160. https://doi.org/10.1083/jcb.202201160

Chandhok, G., Lazarou, M., Neumann, B., 2018. Structure, function, and regulation of mitofusin-2 in health and disease. Biol Rev 93, 933–949. https://doi.org/10.1111/brv.12378

Chang, T.-Y., Li, B.-L., Chang, C.C.Y., Urano, Y., 2009. Acyl-coenzyme A:cholesterol acyltransferases. Am J Physiol-endoc M 297, E1–E9. https://doi.org/10.1152/ajpendo.90926.2008

Chen, H., Huang, W., Li, X., 2022. Structures of oxysterol sensor EBI2/GPR183, a key regulator of the immune response. Structure 30, 1016-1024.e5. https://doi.org/10.1016/j.str.2022.04.006

Chen, H., McCaffery, J.M., Chan, D.C., 2007. Mitochondrial Fusion Protects against Neurodegeneration in the Cerebellum. Cell 130, 548–562. https://doi.org/10.1016/j.cell.2007.06.026

Chen, L., Cui, H., 2015. Targeting Glutamine Induces Apoptosis: A Cancer Therapy Approach. Int J Mol Sci 16, 22830–22855. https://doi.org/10.3390/ijms160922830

Chen, Q., Kirk, K., Shurubor, Y.I., Zhao, D., Arreguin, A.J., Shahi, I., Valsecchi, F., Primiano, G., Calder, E.L., Carelli, V., Denton, T.T., Beal, M.F., Gross, S.S., Manfredi, G., D'Aurelio, M., 2018. Rewiring of Glutamine Metabolism Is a Bioenergetic Adaptation of Human Cells with Mitochondrial DNA Mutations. Cell Metab 27, 1007-1025.e5. https://doi.org/10.1016/j.cmet.2018.03.002

Chen, R., Lai, L.A., Sullivan, Y., Wong, M., Wang, L., Riddell, J., Jung, L., Pillarisetty, V.G., Brentnall, T.A., Pan, S., 2017. Disrupting glutamine metabolic pathways to sensitize gemcitabine-resistant pancreatic cancer. Sci Rep-uk 7, 7950. https://doi.org/10.1038/s41598-017-08436-6

Chen, W., Sun, Y., Sun, Q., Zhang, J., Jiang, M., Chang, C., Huang, X., Wang, C., Wang, P., Zhang, Z., Chen, X., Wang, Y., 2020. MFN2 Plays a Distinct Role from MFN1 in Regulating Spermatogonial Differentiation. Stem Cell Rep 14, 803–817. https://doi.org/10.1016/j.stemcr.2020.03.024

Cheng, C., Geng, F., Li, Z., Zhong, Y., Wang, H., Cheng, Xiang, Zhao, Y., Mo, X., Horbinski, C., Duan, W., Chakravarti, A., Cheng, Xiaolin, Guo, D., 2022. Ammonia stimulates SCAP/Insig dissociation and SREBP-1 activation to promote lipogenesis and tumour growth. Nat Metabolism 1–14. https://doi.org/10.1038/s42255-022-00568-y

Chiang, J.Y.L., 2013. Comprehensive Physiology. Compr Physiol 3, 1191–1212. https://doi.org/10.1002/cphy.c120023

Choi, B.-H., Coloff, J.L., 2019. The Diverse Functions of Non-Essential Amino Acids in Cancer. Cancers 11, 675. https://doi.org/10.3390/cancers11050675

Chung, K.-P., Hsu, C.-L., Fan, L.-C., Huang, Z., Bhatia, D., Chen, Y.-J., Hisata, S., Cho, S.J., Nakahira, K., Imamura, M., Choi, M.E., Yu, C.-J., Cloonan, S.M., Choi, A.M.K., 2019. Mitofusins regulate lipid metabolism to mediate the development of lung fibrosis. Nat Commun 10, 3390. https://doi.org/10.1038/s41467-019-11327-1

Cohen, J.J., Duke, R.C., 1984. Glucocorticoid activation of a calcium-dependent endonuclease in thymocyte nuclei leads to cell death. J Immunol Baltim Md 1950 132, 38–42.

Cruzat, Vinicius Fernandes, Krause, M., Newsholme, P., 2014. Amino acid supplementation and impact on immune function in the context of exercise. J Int Soc Sport Nutr 11, 61. https://doi.org/10.1186/s12970-014-0061-8

Cruzat, Vinicius F., Pantaleão, L.C., Donato, J., Bittencourt, P.I.H. de, Tirapegui, J., 2014. Oral supplementations with free and dipeptide forms of l-glutamine in endotoxemic mice: effects on muscle glutamine-glutathione axis and heat shock proteins. J Nutritional Biochem 25, 345–352. https://doi.org/10.1016/j.jnutbio.2013.11.009

Cruzat, V.F., Rogero, M.M., Tirapegui, J., 2010. Effects of supplementation with free glutamine and the dipeptide alanyl-glutamine on parameters of muscle damage and inflammation in rats submitted to prolonged exercise. Cell Biochem Funct 28, 24–30. https://doi.org/10.1002/cbf.1611

Daye, D., Wellen, K.E., 2012. Metabolic reprogramming in cancer: Unraveling the role of glutamine in tumorigenesis. Semin Cell Dev Biol 23, 362–369. https://doi.org/10.1016/j.semcdb.2012.02.002

DeBerardinis, R.J., Mancuso, A., Daikhin, E., Nissim, I., Yudkoff, M., Wehrli, S., Thompson, C.B., 2007. Beyond aerobic glycolysis: Transformed cells can engage in glutamine metabolism that exceeds the requirement for protein and nucleotide synthesis. Proc. Natl. Acad. Sci. 104, 19345–19350. https://doi.org/10.1073/pnas.0709747104

Dietschy, J.M., 1984. Regulation of cholesterol metabolism in man and in other species. Klin Wochenschr 62, 338–345. https://doi.org/10.1007/bf01716251

Dietschy, J.M., Turley, S.D., 2004. Thematic review series: Brain Lipids. Cholesterol metabolism in the central nervous system during early development and in the mature animal. J Lipid Res 45, 1375–1397. https://doi.org/10.1194/jlr.r400004-jlr200

Doms, R.W., Russ, G., Yewdell, J.W., 1989. Brefeldin A redistributes resident and itinerant Golgi proteins to the endoplasmic reticulum. J. cell Biol. 109, 61–72. https://doi.org/10.1083/jcb.109.1.61

Dongiovanni, P., Petta, S., Mannisto, V., Mancina, R.M., Pipitone, R., Karja, V., Maggioni, M., Kakela, P., Wiklund, O., Mozzi, E., Grimaudo, S., Kaminska, D., Rametta, R., Craxi, A., Fargion, S., Nobili, V., Romeo, S., Pihlajamaki, J., Valenti, L., 2015. Statin use and non-alcoholic steatohepatitis in at risk individuals. J Hepatol 63, 705–712. https://doi.org/10.1016/j.jhep.2015.05.006

Dorsch, M., Kowalczyk, M., Planque, M., Heilmann, G., Urban, S., Dujardin, P., Forster, J., Ueffing, K., Nothdurft, S., Oeck, S., Paul, A., Liffers, S.T., Kaschani, F., Kaiser, M., Schramm, A., Siveke, J.T., Winslow, M.M., Fendt, S.-M., Nalbant, P., Grüner, B.M., 2021. Statins affect cancer cell plasticity with distinct consequences

for tumor progression and metastasis. Cell Reports 37, 110056. https://doi.org/10.1016/j.celrep.2021.110056

Durán, R.V., Hall, M.N., 2012. Glutaminolysis feeds mTORC1. Cell Cycle 11, 4107–4108. https://doi.org/10.4161/cc.22632

Durán, R.V., MacKenzie, E.D., Boulahbel, H., Frezza, C., Heiserich, L., Tardito, S., Bussolati, O., Rocha, S., Hall, M.N., Gottlieb, E., 2013. HIF-independent role of prolyl hydroxylases in the cellular response to amino acids. Oncogene 32, 4549–4556. https://doi.org/10.1038/onc.2012.465

Durán, R.V., Oppliger, W., Robitaille, A.M., Heiserich, L., Skendaj, R., Gottlieb, E., Hall, M.N., 2012. Glutaminolysis Activates Rag-mTORC1 Signaling. Mol Cell 47, 349–358. https://doi.org/10.1016/j.molcel.2012.05.043

Edwards-Hicks, J., Mitterer, M., Pearce, E.L., Buescher, J.M., 2020. Metabolic Dynamics of In Vitro CD8+ T Cell Activation. Metabolites 11, 12. https://doi.org/10.3390/metabo11010012

Eid, T., Ghosh, A., Wang, Y., Beckström, H., Zaveri, H.P., Lee, T.-S.W., Lai, J.C.K., Malthankar-Phatak, G.H., Lanerolle, N.C. de, 2008. Recurrent seizures and brain pathology after inhibition of glutamine synthetase in the hippocampus in rats. Brain 131, 2061–2070. https://doi.org/10.1093/brain/awn133

Eid, T., Thomas, M., Spencer, D., Rundén-Pran, E., Lai, J., Malthankar, G., Kim, J., Danbolt, N., Ottersen, O., Lanerolle, N. de, 2004. Loss of glutamine synthetase in the human epileptogenic hippocampus: possible mechanism for raised extracellular glutamate in mesial temporal lobe epilepsy. Lancet 363, 28–37. https://doi.org/10.1016/s0140-6736(03)15166-5

Escobar-Alvarez, S., Gardner, J., Sheth, A., Manfredi, G., Yang, G., Ouerfelli, O., Heaney, M.L., Scheinberg, D.A., 2010. Inhibition of Human Peptide Deformylase Disrupts Mitochondrial Function. Mol. Cell. Biol. 30, 5099–5109. https://doi.org/10.1128/mcb.00469-10

Escolà-Gil, J.C., Quesada, H., Julve, J., Martín-Campos, J.M., Cedó, L., Blanco-Vaca, F., 2014. Sitosterolemia: Diagnosis, Investigation, and Management. Curr Atheroscler Rep 16, 424. https://doi.org/10.1007/s11883-014-0424-2

Espenshade, P.J., Li, W.-P., Yabe, D., 2002. Sterols block binding of COPII proteins to SCAP, thereby controlling SCAP sorting in ER. Proc National Acad Sci 99, 11694–11699. https://doi.org/10.1073/pnas.182412799

Ferreira, C., Mesquita, I., Barbosa, A.M., Osório, N.S., Torrado, E., Beauparlant, C.-J., Droit, A., Cunha, C., Carvalho, A., Saha, B., Estaquier, J., Silvestre, R., 2020. Glutamine supplementation improves the efficacy of miltefosine treatment for visceral leishmaniasis. Plos Neglect Trop D 14, e0008125. https://doi.org/10.1371/journal.pntd.0008125

Filadi, R., Pendin, D., Pizzo, P., 2018. Mitofusin 2: from functions to disease. Cell Death Dis 9, 330. https://doi.org/10.1038/s41419-017-0023-6

FLÄRING, U.B., ROOYACKERS, O.E., WERNERMAN, J., HAMMARQVIST, F., 2003. Glutamine attenuates post-traumatic glutathione depletion in human muscle. Clin Sci 104, 275. https://doi.org/10.1042/cs20020198

Frick, K.M., Kim, J., Tuscher, J.J., Fortress, A.M., 2015. Sex steroid hormones matter for learning and memory: estrogenic regulation of hippocampal function in male and female rodents. Learn Memory 22, 472–493. https://doi.org/10.1101/lm.037267.114

Fuchs, M., 2003. III. Regulation of bile acid synthesis: past progress and future challenges. Am J Physiol-gastr L 284, G551–G557. https://doi.org/10.1152/ajpgi.00468.2002

Fujimoto, M., Hayashi, T., Su, T.-P., 2012. The role of cholesterol in the association of endoplasmic reticulum membranes with mitochondria. Biochem Bioph Res Co 417, 635–639. https://doi.org/10.1016/j.bbrc.2011.12.022

Garcia, B.M., Machado, T.S., Carvalho, K.F., Nolasco, P., Nociti, R.P., Collado, M. del, Bianco, M.J.D.C., Grejo, M.P., Neto, J.D.A., Sugiyama, F.H.C., Tostes, K., Pandey, A.K., Gonçalves, L.M., Perecin, F., Meirelles, F.V., Ferraz, J.B.S., Vanzela, E.C., Boschero, A.C., Guimarães, F.E.G., Abdulkader, F., Laurindo, F.R.M., Kowaltowski, A.J., Chiaratti, M.R., 2020. Mice born to females with oocyte-specific deletion of mitofusin 2 have increased weight gain and impaired glucose homeostasis. Mol. Hum. Reprod. 26, 938–952. https://doi.org/10.1093/molehr/gaaa071

Garcia-Ruiz, C., Mari, M., Colell, A., Morales, A., Caballero, F., Montero, J., Terrones, O., Basañez, G., Fernández-Checa, J.C., 2008. Mitochondrial cholesterol in health and disease. Histol Histopathol 24, 117–32. https://doi.org/10.14670/hh-24.117

George, J., Lim, J.S., Jang, S.J., Cun, Y., Ozretić, L., Kong, G., Leenders, F., Lu, X., Fernández-Cuesta, L., Bosco, G., Müller, C., Dahmen, I., Jahchan, N.S., Park, K.-S., Yang, D., Karnezis, A.N., Vaka, D., Torres, A., Wang, M.S., Korbel, J.O.,

Menon, R., Chun, S.-M., Kim, D., Wilkerson, M., Hayes, N., Engelmann, D., Pützer, B., Bos, M., Michels, S., Vlasic, I., Seidel, D., Pinther, B., Schaub, P., Becker, C., Altmüller, J., Yokota, J., Kohno, T., Iwakawa, R., Tsuta, K., Noguchi, M., Muley, T., Hoffmann, H., Schnabel, P.A., Petersen, I., Chen, Y., Soltermann, A., Tischler, V., Choi, C., Kim, Y.-H., Massion, P.P., Zou, Y., Jovanovic, D., Kontic, M., Wright, G.M., Russell, P.A., Solomon, B., Koch, I., Lindner, M., Muscarella, L.A., Torre, A. la, Field, J.K., Jakopovic, M., Knezevic, J., Castaños-Vélez, E., Roz, L., Pastorino, U., Brustugun, O.-T., Lund-Iversen, M., Thunnissen, E., Köhler, J., Schuler, M., Botling, J., Sandelin, M., Sanchez-Cespedes, M., Salvesen, H.B., Achter, V., Lang, U., Bogus, M., Schneider, P.M., Zander, T., Ansén, S., Hallek, M., Wolf, J., Vingron, M., Yatabe, Y., Travis, W.D., Nürnberg, P., Reinhardt, C., Perner, S., Heukamp, L., Büttner, R., Haas, S.A., Brambilla, E., Peifer, M., Sage, J., Thomas, R.K., 2015. Comprehensive genomic profiles of small cell lung cancer. Nature 524, 47–53. https://doi.org/10.1038/nature14664

Gerdes, L.U., Gerdes, C., Klausen, I.C., Faergeman, O., 1992. Generation of analytic plasma lipoprotein profiles using two prepacked superose 6B columns. Clin. Chim. Acta 205, 1–9. https://doi.org/10.1016/0009-8981(92)90348-t

Ghoddoussi, F., Galloway, M.P., Jambekar, A., Bame, M., Needleman, R., Brusilow, W.S.A., 2010. Methionine sulfoximine, an inhibitor of glutamine synthetase, lowers brain glutamine and glutamate in a mouse model of ALS. J. Neurol. Sci. 290, 41–47. https://doi.org/10.1016/j.jns.2009.11.013

Gianotti, L., Alexander, J.W., Gennari, R., Pyles, T., Babcock, G.F., 1995. Oral Glutamine Decreases Bacterial Translocation and Improves Survival in Experimental Gut-Origin Sepsis. Jpen-parenter Enter 19, 69–74. https://doi.org/10.1177/014860719501900169

Gill, S., Stevenson, J., Kristiana, I., Brown, A.J., 2011. Cholesterol-Dependent Degradation of Squalene Monooxygenase, a Control Point in Cholesterol Synthesis beyond HMG-CoA Reductase. Cell Metab. 13, 260–273. https://doi.org/10.1016/j.cmet.2011.01.015

Goldstein, J.L., Rawson, R.B., Brown, M.S., 2002. Mutant Mammalian Cells as Tools to Delineate the Sterol Regulatory Element-Binding Protein Pathway for Feedback Regulation of Lipid Synthesis. Arch Biochem Biophys 397, 139–148. https://doi.org/10.1006/abbi.2001.2615

González, A., Hall, M.N., Lin, S.-C., Hardie, D.G., 2020. AMPK and TOR: The Yin and Yang of Cellular Nutrient Sensing and Growth Control. Cell Metab 31, 472–492. https://doi.org/10.1016/j.cmet.2020.01.015

Gorman, G.S., Chinnery, P.F., DiMauro, S., Hirano, M., Koga, Y., McFarland, R., Suomalainen, A., Thorburn, D.R., Zeviani, M., Turnbull, D.M., 2016. Mitochondrial diseases. Nat Rev Dis Primers 2, 16080. https://doi.org/10.1038/nrdp.2016.80

Greenfield, J.R., Farooqi, I.S., Keogh, J.M., Henning, E., Habib, A.M., Blackwood, A., Reimann, F., Holst, J.J., Gribble, F.M., 2009. Oral glutamine increases circulating glucagon-like peptide 1, glucagon, and insulin concentrations in lean, obese, and type 2 diabetic subjects. Am J Clin Nutrition 89, 106–113. https://doi.org/10.3945/ajcn.2008.26362

Gruetter, R., Novotny, E.J., Boulware, S.D., Mason, G.F., Rothman, D.L., Shulman, G.I., Prichard, J.W., Shulman, R.G., 1994. Localized 13C NMR Spectroscopy in the Human Brain of Amino Acid Labeling from d-[1-13C]Glucose. J Neurochem 63, 1377–1385. https://doi.org/10.1046/j.1471-4159.1994.63041377.x

Häberle, J., Görg, B., Rutsch, F., Schmidt, E., Toutain, A., Benoist, J.-F., Gelot, A., Suc, A.-L., Höhne, W., Schliess, F., Häussinger, D., Koch, H.G., 2005. Congenital Glutamine Deficiency with Glutamine Synthetase Mutations. New Engl J Medicine 353, 1926–1933. https://doi.org/10.1056/nejmoa050456

Häberle, J., Görg, B., Toutain, A., Rutsch, F., Benoist, J.-F., Gelot, A., Suc, A.-L., Koch, H.G., Schliess, F., Häussinger, D., 2006. Inborn error of amino acid synthesis: Human glutamine synthetase deficiency. J Inherit Metab Dis 29, 352–358. https://doi.org/10.1007/s10545-006-0256-5

Hankard, R., Mauras, N., Hammond, D., Hammond, M., Darmaun, D., 1999. Is glutamine a 'conditionally essential' amino acid in Duchenne muscular dystrophy? Clin Nutr 18, 365–369. https://doi.org/10.1016/s0261-5614(99)80017-x

Hel, W.S. van der, Notenboom, R.G.E., Bos, I.W.M., Rijen, P.C. van, Veelen, C.W.M. van, Graan, P.N.E. de, 2005. Reduced glutamine synthetase in hippocampal areas with neuron loss in temporal lobe epilepsy. Neurology 64, 326–333. https://doi.org/10.1212/01.wnl.0000149636.44660.99

Henderson, R., O'Kane, M., McGilligan, V., Watterson, S., 2016. The genetics and screening of familial hypercholesterolaemia. J Biomed Sci 23, 39. https://doi.org/10.1186/s12929-016-0256-1

Hillary, R.F., FitzGerald, U., 2018. A lifetime of stress: ATF6 in development and homeostasis. J. Biomed. Sci. 25, 48. https://doi.org/10.1186/s12929-018-0453-1

Hoerner, C.R., Chen, V.J., Fan, A.C., 2018. The 'Achilles Heel' of Metabolism in Renal Cell Carcinoma: Glutaminase Inhibition as a Rational Treatment Strategy. Kidney Cancer Preprint, 1–17. https://doi.org/10.3233/kca-180043

Horn, C.L., Morales., A.L., Savard, C., Farrell, G.C., Ioannou, G.N., 2021. Role of Cholesterol-Associated Steatohepatitis in the Development of NASH. Hepatology Commun 6, 12–35. https://doi.org/10.1002/hep4.1801

Huang, L.-J., Chen, R.-H., 2023. Lipid saturation induces degradation of squalene epoxidase for sterol homeostasis and cell survival. Life Sci. Alliance 6, e202201612. https://doi.org/10.26508/lsa.202201612

Huber, M.D., Vesely, P.W., Datta, K., Gerace, L., 2013. Erlins restrict SREBP activation in the ER and regulate cellular cholesterol homeostasis. J. Cell Biol. 203, 427–436. https://doi.org/10.1083/jcb.201305076

Iacobazzi, V., Infantino, V., 2014. Citrate – new functions for an old metabolite. Biol. Chem. 395, 387–399. https://doi.org/10.1515/hsz-2013-0271

Ikonen, E., 2008. Cellular cholesterol trafficking and compartmentalization. Nat Rev Mol Cell Bio 9, 125–138. https://doi.org/10.1038/nrm2336

Inoue, J., Ito, Y., Shimada, S., Satoh, S., Sasaki, T., Hashidume, T., Kamoshida, Y., Shimizu, M., Sato, R., 2011. Glutamine stimulates the gene expression and processing of sterol regulatory element binding proteins, thereby increasing the expression of their target genes. FEBS J. 278, 2739–2750. https://doi.org/10.1111/j.1742-4658.2011.08204.x

Ioannou, G.N., Morrow, O.B., Connole, M.L., Lee, S.P., 2009. Association between dietary nutrient composition and the incidence of cirrhosis or liver cancer in the united states population. Hepatology 50, 175–184. https://doi.org/10.1002/hep.22941

Iqbal, J., Hussain, M.M., 2009. Intestinal lipid absorption. Am J Physiol-endoc M 296, E1183–E1194. https://doi.org/10.1152/ajpendo.90899.2008

Irisawa, M., Inoue, J., Ozawa, N., Mori, K., Sato, R., 2009. The Sterol-sensing Endoplasmic Reticulum (ER) Membrane Protein TRC8 Hampers ER to Golgi Transport of Sterol Regulatory Element-binding Protein-2 (SREBP-2)/SREBP Cleavage-activated Protein and Reduces SREBP-2 Cleavage*. J. Biol. Chem. 284, 28995–29004. https://doi.org/10.1074/jbc.m109.041376

Ishihara, N., Eura, Y., Mihara, K., 2004. Mitofusin 1 and 2 play distinct roles in mitochondrial fusion reactions via GTPase activity. J Cell Sci 117, 6535–6546. https://doi.org/10.1242/jcs.01565

Jeske, D.J., Dietschy, J.M., 1980. Regulation of rates of cholesterol synthesis in vivo in the liver and carcass of the rat measured using [3H]water. J Lipid Res 21, 364–376. https://doi.org/10.1016/s0022-2275(20)39816-3

Jiang, S.-Y., Tang, J.-J., Xiao, X., Qi, W., Wu, S., Jiang, C., Hong, J., Xu, J., Song, B.-L., Luo, J., 2019. Schnyder corneal dystrophy-associated UBIAD1 mutations cause corneal cholesterol accumulation by stabilizing HMG-CoA reductase. PLoS Genet. 15, e1008289. https://doi.org/10.1371/journal.pgen.1008289

Kanamori, K., Ross, B.D., Chung, J.C., Kuo, E.L., 1996. Severity of Hyperammonemic Encephalopathy Correlates with Brain Ammonia Level and Saturation of Glutamine Synthetase In Vivo. J Neurochem 67, 1584–1594. https://doi.org/10.1046/j.1471-4159.1996.67041584.x

Kao, C., Hsu, J., Bandi, V., Jahoor, F., 2013. Alterations in glutamine metabolism and its conversion to citrulline in sepsis. Am J Physiol-endoc M 304, E1359–E1364. https://doi.org/10.1152/ajpendo.00628.2012

Karinch, A.M., Pan, M., Lin, C.-M., Strange, R., Souba, W.W., 2001. Glutamine Metabolism in Sepsis and Infection. J Nutrition 131, 2535S-2538S. https://doi.org/10.1093/jn/131.9.2535s

Katt, W.P., Lukey, M.J., Cerione, R.A., 2017. A tale of two glutaminases: homologous enzymes with distinct roles in tumorigenesis. Future Med Chem 9, 223–243. https://doi.org/10.4155/fmc-2016-0190

Kim, G.W., Lee, D.H., Jeon, Y.H., Yoo, J., Kim, S.Y., Lee, S.W., Cho, H.Y., Kwon, S.H., 2021. Glutamine Synthetase as a Therapeutic Target for Cancer Treatment. Int. J. Mol. Sci. 22, 1701. https://doi.org/10.3390/ijms22041701

Kim, M., Gwak, J., Hwang, S., Yang, S., Jeong, S.M., 2019. Mitochondrial GPT2 plays a pivotal role in metabolic adaptation to the perturbation of mitochondrial glutamine metabolism. Oncogene 38, 4729–4738. https://doi.org/10.1038/s41388-019-0751-4

Kolovou, G., Mikhailidis, D., Anagnostopoulou, K., Daskalopoulou, S., Cokkinos, D., 2006. Tangier Disease Four Decades of Research: A Reflection of the Importance of HDL. Curr Med Chem 13, 771–782. https://doi.org/10.2174/092986706776055580

Kong, Y., Wu, M., Wan, X., Sun, M., Zhang, Y., Wu, Z., Li, C., Liang, X., Gao, L., Ma, C., Yue, X., 2023. Lipophagy-mediated cholesterol synthesis inhibition is required for the survival of hepatocellular carcinoma under glutamine deprivation. Redox Biology 63, 102732. https://doi.org/10.1016/j.redox.2023.102732

Kovacević, Z., Morris, H.P., 1972. The role of glutamine in the oxidative metabolism of malignant cells. Cancer Res 32, 326–33.

Krause, M. da S., Bittencourt, P.I.H. de, 2008. Type 1 diabetes: can exercise impair the autoimmune event? The L-arginine/glutamine coupling hypothesis. Cell Biochem. Funct. 26, 406–433. https://doi.org/10.1002/cbf.1470

Krebs, H.A., 1935. Metabolism of amino-acids. Biochem J 29, 1951–1969. https://doi.org/10.1042/bj0291951

Kuan, Y.-C., Takahashi, Y., Maruyama, T., Shimizu, M., Yamauchi, Y., Sato, R., 2020. Ring finger protein 5 activates sterol regulatory element–binding protein 2 (SREBP2) to promote cholesterol biosynthesis via inducing polyubiquitination of SREBP chaperone SCAP. J. Biol. Chem. 295, 3918–3928. https://doi.org/10.1074/jbc.ra119.011849

Lacey, J.M., Wilmore, D.W., 1990. Is Glutamine a Conditionally Essential Amino Acid? Nutr Rev 48, 297–309. https://doi.org/10.1111/j.1753-4887.1990.tb02967.x

Lange, Y., Swaisgood, M.H., Ramos, B.V., Steck, T.L., 1989. Plasma Membranes Contain Half the Phospholipid and 90% of the Cholesterol and Sphingomyelin in Cultured Human Fibroblasts*. J Biol Chem 264, 3786–3793. https://doi.org/10.1016/s0021-9258(19)84918-9

Larrea, D., Pera, M., Gonelli, A., Cabrera, R.Q., Akman, H.O., Guardia-Laguarta, C., Velasco, K.R., Area-Gomez, E., Bello, F. dal, Stefani, D.D., Horvath, R., Shy, M.E., Schon, E.A., Giacomello, M., 2019. MFN2 mutations in Charcot-Marie-Tooth disease alter mitochondria-associated ER membrane function but do not impair bioenergetics. Hum Mol Genet 28, ddz008-. https://doi.org/10.1093/hmg/ddz008

Larson, T.A., 2018. Sex Steroids, Adult Neurogenesis, and Inflammation in CNS Homeostasis, Degeneration, and Repair. Front Endocrinol 9, 205. https://doi.org/10.3389/fendo.2018.00205

Le, A., Lane, A.N., Hamaker, M., Bose, S., Gouw, A., Barbi, J., Tsukamoto, T., Rojas, C.J., Slusher, B.S., Zhang, H., Zimmerman, L.J., Liebler, D.C., Slebos, R.J.C.,

Lorkiewicz, P.K., Higashi, R.M., Fan, T.W.M., Dang, C.V., 2012. Glucose-Independent Glutamine Metabolism via TCA Cycling for Proliferation and Survival in B Cells. Cell Metab 15, 110–121. https://doi.org/10.1016/j.cmet.2011.12.009

Lee, S., Sterky, F.H., Mourier, A., Terzioglu, M., Cullheim, S., Olson, L., Larsson, N.-G., 2012. Mitofusin 2 is necessary for striatal axonal projections of midbrain dopamine neurons. Hum Mol Genet 21, 4827–4835. https://doi.org/10.1093/hmg/dds352

Legendre, F., MacLean, A., Appanna, V.P., Appanna, V.D., 2020. Biochemical pathways to **α**-ketoglutarate, a multi-faceted metabolite. World J. Microbiol. Biotechnol. 36, 123. https://doi.org/10.1007/s11274-020-02900-8

Leite, J.S.M., Raizel, R., Hypólito, T.M., Rosa, T. dos S., Cruzat, V.F., Tirapegui, J., 2016. l-glutamine and l-alanine supplementation increase glutamine-glutathione axis and muscle HSP-27 in rats trained using a progressive high-intensity resistance exercise. Appl Physiology Nutrition Metabolism 41, 842–849. https://doi.org/10.1139/apnm-2016-0049

Leone, R.D., Zhao, L., Englert, J.M., Sun, I.-M., Oh, M.-H., Sun, I.-H., Arwood, M.L., Bettencourt, I.A., Patel, C.H., Wen, J., Tam, A., Blosser, R.L., Prchalova, E., Alt, J., Rais, R., Slusher, B.S., Powell, J.D., 2019. Glutamine blockade induces divergent metabolic programs to overcome tumor immune evasion. Science 366, 1013–1021. https://doi.org/10.1126/science.aav2588

Li, X., Straub, J., Medeiros, T.C., Mehra, C., Brave, F. den, Peker, E., Atanassov, I., Stillger, K., Michaelis, J.B., Burbridge, E., Adrain, C., Münch, C., Riemer, J., Becker, T., Pernas, L.F., 2022. Mitochondria shed their outer membrane in response to infection-induced stress. Science 375, eabi4343. https://doi.org/10.1126/science.abi4343

Li, Y.-J., Cao, Y.-L., Feng, J.-X., Qi, Y., Meng, S., Yang, J.-F., Zhong, Y.-T., Kang, S., Chen, X., Lan, L., Luo, L., Yu, B., Chen, S., Chan, D.C., Hu, J., Gao, S., 2019. Structural insights of human mitofusin-2 into mitochondrial fusion and CMT2A onset. Nat Commun 10, 4914. https://doi.org/10.1038/s41467-019-12912-0

Liang, J.Q., Teoh, N., Xu, L., Pok, S., Li, X., Chu, E.S.H., Chiu, J., Dong, L., Arfianti, E., Haigh, W.G., Yeh, M.M., Ioannou, G.N., Sung, J.J.Y., Farrell, G., Yu, J., 2018. Dietary cholesterol promotes steatohepatitis related hepatocellular carcinoma through dysregulated metabolism and calcium signaling. Nat Commun 9, 4490. https://doi.org/10.1038/s41467-018-06931-6

Liemburg-Apers, Dania C., Schirris, T.J.J., Russel, F.G.M., Willems, P.H.G.M., Koopman, W.J.H., 2015. Mitoenergetic Dysfunction Triggers a Rapid Compensatory Increase in Steady-State Glucose Flux. Biophys. J. 109, 1372–1386. https://doi.org/10.1016/j.bpj.2015.08.002

Liemburg-Apers, Dania C., Willems, P.H.G.M., Koopman, W.J.H., Grefte, S., 2015. Interactions between mitochondrial reactive oxygen species and cellular glucose metabolism. Arch. Toxicol. 89, 1209–1226. https://doi.org/10.1007/s00204-015-1520-y

Liou, L., Kaptoge, S., 2020. Association of small, dense LDL-cholesterol concentration and lipoprotein particle characteristics with coronary heart disease: A systematic review and meta-analysis. Plos One 15, e0241993. https://doi.org/10.1371/journal.pone.0241993

LOBO, C., RUIZ-BELLIDO, M.A., ALEDO, J.C., MÁRQUEZ, J., CASTRO, I.N.D., ALONSO, F.J., 2000. Inhibition of glutaminase expression by antisense mRNA decreases growth and tumourigenicity of tumour cells. Biochem J 348, 257. https://doi.org/10.1042/0264-6021:3480257

Locasale, J.W., 2018. New concepts in feedback regulation of glucose metabolism. Curr. Opin. Syst. Biol. 8, 32–38. https://doi.org/10.1016/j.coisb.2017.11.005

Lomelino, C.L., Andring, J.T., McKenna, R., Kilberg, M.S., 2017. Asparagine synthetase: Function, structure, and role in disease. J Biol Chem 292, 19952–19958. https://doi.org/10.1074/jbc.r117.819060

Love, M.I., Huber, W., Anders, S., 2014. Moderated estimation of fold change and dispersion for RNA-seq data with DESeq2. Genome Biol 15, 550. https://doi.org/10.1186/s13059-014-0550-8

Lu, W., Pelicano, H., Huang, P., 2010. Cancer Metabolism: Is Glutamine Sweeter than Glucose? Cancer Cell 18, 199–200. https://doi.org/10.1016/j.ccr.2010.08.017

Luo, J., Yang, H., Song, B.-L., 2019. Mechanisms and regulation of cholesterol homeostasis. Nat Rev Mol Cell Bio 1–21. https://doi.org/10.1038/s41580-019-0190-7

Ma, X., Qian, H., Chen, A., Ni, H.-M., Ding, W.-X., 2021. Perspectives on Mitochondria–ER and Mitochondria–Lipid Droplet Contact in Hepatocytes and Hepatic Lipid Metabolism. Cells 10, 2273. https://doi.org/10.3390/cells10092273

Mancini, G., Pirruccio, K., Yang, X., Blücher, M., Rodeheffer, M., Horvath, T.L., 2019. Mitofusin 2 in Mature Adipocytes Controls Adiposity and Body Weight. Cell Reports 26, 2849-2858.e4. https://doi.org/10.1016/j.celrep.2019.02.039

Mann, J.P., Duan, X., Patel, S., Tábara, L.C., Scurria, F., Alvarez-Guaita, A., Haider, A., Luijten, I., Page, M., Protasoni, M., Lim, K., Virtue, S., O'Rahilly, S., Armstrong, M., Prudent, J., Semple, R.K., Savage, D.B., 2023. A mouse model of human mitofusin-2-related lipodystrophy exhibits adipose-specific mitochondrial stress and reduced leptin secretion. Elife 12, e82283. https://doi.org/10.7554/elife.82283

Mansour, A., Tehrani, M.R.M.-, Qorbani, M., Heshmat, R., Larijani, B., Hosseini, S., 2015. Effect of glutamine supplementation on cardiovascular risk factors in patients with type 2 diabetes. Nutrition 31, 119–126. https://doi.org/10.1016/j.nut.2014.05.014

Margerie, D., Lefebvre, P., Raverdy, V., Schwahn, U., Ruetten, H., Larsen, P., Duhamel, A., Labreuche, J., Thuillier, D., Derudas, B., Gheeraert, C., Dehondt, H., Dhalluin, Q., Alexandre, J., Caiazzo, R., Nesslany, P., Verkindt, H., Pattou, F., Staels, B., 2019. Hepatic transcriptomic signatures of statin treatment are associated with impaired glucose homeostasis in severely obese patients. Bmc Med Genomics 12, 80. https://doi.org/10.1186/s12920-019-0536-1

Martin, D.B., Vagelos, P.R., 1962. The Mechanism of Tricarboxylic Acid Cycle Regulation of Fatty Acid Synthesis. J. Biol. Chem. 237, 1787–1792. https://doi.org/10.1016/s0021-9258(19)73938-6

Martínez-Reyes, I., Chandel, N.S., 2020. Mitochondrial TCA cycle metabolites control physiology and disease. Nat Commun 11, 102. https://doi.org/10.1038/s41467-019-13668-3

Martins, I.J., Berger, T., Sharman, M.J., Verdile, G., Fuller, S.J., Martins, R.N., 2009. Cholesterol metabolism and transport in the pathogenesis of Alzheimer's disease. J Neurochem 111, 1275–1308. https://doi.org/10.1111/j.1471-4159.2009.06408.x

Maslansky, C.J., Williams, G.M., 1982. Primary cultures and the levels of cytochromeP450 in hepatocytes from mouse, rat, hamster, and rabbit liver. Vitr. - Plant 18, 683–693. https://doi.org/10.1007/bf02796423

McDonald, J.G., Thompson, B.M., McCrum, E.C., Russell, D.W., 2007. Extraction and Analysis of Sterols in Biological Matrices by High Performance Liquid

Chromatography Electrospray Ionization Mass Spectrometry. Methods Enzymol 432, 145–170. https://doi.org/10.1016/s0076-6879(07)32006-5

Meer, G. van, Voelker, D.R., Feigenson, G.W., 2008. Membrane lipids: where they are and how they behave. Nat Rev Mol Cell Bio 9, 112–124. https://doi.org/10.1038/nrm2330

Melchinger, P., Garcia, B.M., 2023. Mitochondria are midfield players in steroid synthesis. Int J Biochem Cell Biology 160, 106431. https://doi.org/10.1016/j.biocel.2023.106431

Meng, D., Yang, Q., Wang, H., Melick, C.H., Navlani, R., Frank, A.R., Jewell, J.L., 2020. Glutamine and asparagine activate mTORC1 independently of Rag GTPases. J. Biol. Chem. 295, 2890–2899. https://doi.org/10.1074/jbc.ac119.011578

Mick, E., Titov, D.V., Skinner, O.S., Sharma, R., Jourdain, A.A., Mootha, V.K., 2020. Distinct mitochondrial defects trigger the integrated stress response depending on the metabolic state of the cell. Elife 9, e49178. https://doi.org/10.7554/elife.49178

Min, H.-K., Kapoor, A., Fuchs, M., Mirshahi, F., Zhou, H., Maher, J., Kellum, J., Warnick, R., Contos, M.J., Sanyal, A.J., 2012. Increased Hepatic Synthesis and Dysregulation of Cholesterol Metabolism Is Associated with the Severity of Nonalcoholic Fatty Liver Disease. Cell Metab 15, 665–674. https://doi.org/10.1016/j.cmet.2012.04.004

Misko, A.L., Sasaki, Y., Tuck, E., Milbrandt, J., Baloh, R.H., 2012. Mitofusin2 Mutations Disrupt Axonal Mitochondrial Positioning and Promote Axon Degeneration. J Neurosci 32, 4145–4155. https://doi.org/10.1523/jneurosci.6338-11.2012

Monné, M., Vozza, A., Lasorsa, F.M., Porcelli, V., Palmieri, F., 2019. Mitochondrial Carriers for Aspartate, Glutamate and Other Amino Acids: A Review. Int J Mol Sci 20, 4456. https://doi.org/10.3390/ijms20184456

Motori, E., Atanassov, I., Kochan, S.M.V., Folz-Donahue, K., Sakthivelu, V., Giavalisco, P., Toni, N., Puyal, J., Larsson, N.-G., 2020. Neuronal metabolic rewiring promotes resilience to neurodegeneration caused by mitochondrial dysfunction. Sci Adv 6, eaba8271. https://doi.org/10.1126/sciadv.aba8271

Mourier, A., Motori, E., Brandt, T., Lagouge, M., Atanassov, I., Galinier, A., Rappl, G., Brodesser, S., Hultenby, K., Dieterich, C., Larsson, N.-G., 2015. Mitofusin 2 is

required to maintain mitochondrial coenzyme Q levels. J Cell Biol 208, 429–442. https://doi.org/10.1083/jcb.201411100

Mukhopadhyay, S., Goswami, D., Adiseshaiah, P.P., Burgan, W., Yi, M., Guerin, T.M., Kozlov, S.V., Nissley, D.V., McCormick, F., 2020. Undermining Glutaminolysis Bolsters Chemotherapy While NRF2 Promotes Chemoresistance in KRAS-Driven Pancreatic Cancers. Cancer Res 80, 1630–1643. https://doi.org/10.1158/0008-5472.can-19-1363

Nair, P., 2013. Brown and Goldstein: The Cholesterol Chronicles. Proc National Acad Sci 110, 14829–14832. https://doi.org/10.1073/pnas.1315180110

Nepogodiev, D., Martin, J., Biccard, B., Makupe, A., Bhangu, A., Surgery, N.I. for H.R.G.H.R.U. on G., Nepogodiev, D., Martin, J., Biccard, B., Makupe, A., Ademuyiwa, A., Adisa, A.O., Aguilera, M.-L., Chakrabortee, S., Fitzgerald, J.E., Ghosh, D., Glasbey, J.C., Harrison, E.M., Ingabire, J.C.A., Salem, H., Lapitan, M.C., Lawani, I., Lissauer, D., Magill, L., Moore, R., Osei-Bordom, D.C., Pinkney, T.D., Qureshi, A.U., Medina, A.R.-D. la, Rayne, S., Sundar, S., Tabiri, S., Verjee, A., Yepez, R., Garden, O.J., Lilford, R., Brocklehurst, P., Morton, D.G., Bhangu, A., 2019. Global burden of postoperative death. Lancet 393, 401. https://doi.org/10.1016/s0140-6736(18)33139-8

Nervi, F., Weis, H., Dietschy, J., 1975. The kinetic characteristics of inhibition of hepatic cholesterogenesis by lipoproteins of intestinal origin. J Biol Chem 250, 4145–4151. https://doi.org/10.1016/s0021-9258(19)41398-7

Newsholme, P., 2001. Why Is L-Glutamine Metabolism Important to Cells of the Immune System in Health, Postinjury, Surgery or Infection?2. J Nutrition 131, 2515S-2522S. https://doi.org/10.1093/jn/131.9.2515s

Newsholme, P., Procopio, J., Lima, M.M.R., Pithon-Curi, T.C., Curi, R., 2003. Glutamine and glutamate—their central role in cell metabolism and function. Cell Biochem Funct 21, 1–9. https://doi.org/10.1002/cbf.1003

Nissler, K., Petermann, H., Wenz, I., Brox, D., 1995. Fructose 2,6-bisphosphate metabolism in Ehrlich ascites tumour cells. J. Cancer Res. Clin. Oncol. 121, 739–745. https://doi.org/10.1007/bf01213320

Notkola, I.L., Sulkava, R., Pekkanen, J., Erkinjuntti, T., Ehnholm, C., Kivinen, P., Tuomilehto, J., Nissinen, A., 1998. Serum total cholesterol, apolipoprotein E epsilon 4 allele, and Alzheimer's disease. Neuroepidemiology 17, 14–20. https://doi.org/10.1159/000026149

Noureddin, M., Zelber-Sagi, S., Wilkens, L.R., Porcel, J., Boushey, C.J., Marchand, L.L., Rosen, H.R., Setiawan, V.W., 2020. Diet Associations With Nonalcoholic Fatty Liver Disease in an Ethnically Diverse Population: The Multiethnic Cohort. Hepatology 71, 1940–1952. https://doi.org/10.1002/hep.30967

Nowaczyk, M.J.M., Irons, M.B., 2012. Smith–Lemli–Opitz syndrome: Phenotype, natural history, and epidemiology. Am J Medical Genetics Part C Seminars Medical Genetics 160C, 250–262. https://doi.org/10.1002/ajmg.c.31343

Özbalci, C., Sachsenheimer, T., Brügger, B., 2013. Membrane Biogenesis, Methods and Protocols. Methods Mol Biology 1033, 3–20. https://doi.org/10.1007/978-1-62703-487-6_1

Pamiljans, V., Krishnaswamy, P.R., Dumville, G., Meister, A., 1962. Studies on the Mechanism of Glutamine Synthesis; Isolation and Properties of the Enzyme from Sheep Brain *. Biochemistry-us 1, 153–158. https://doi.org/10.1021/bi00907a023

Pavlova, N.N., Hui, S., Ghergurovich, J.M., Fan, J., Intlekofer, A.M., White, R.M., Rabinowitz, J.D., Thompson, C.B., Zhang, J., 2018. As Extracellular Glutamine Levels Decline, Asparagine Becomes an Essential Amino Acid. Cell Metab 27, 428-438.e5. https://doi.org/10.1016/j.cmet.2017.12.006

Peifer, M., Hertwig, F., Roels, F., Dreidax, D., Gartlgruber, M., Menon, R., Krämer, A., Roncaioli, J.L., Sand, F., Heuckmann, J.M., Ikram, F., Schmidt, R., Ackermann, S., Engesser, A., Kahlert, Y., Vogel, W., Altmüller, J., Nürnberg, P., Thierry-Mieg, J., Thierry-Mieg, D., Mariappan, A., Heynck, S., Mariotti, E., Henrich, K.-O., Gloeckner, C., Bosco, G., Leuschner, I., Schweiger, M.R., Savelyeva, L., Watkins, S.C., Shao, C., Bell, E., Höfer, T., Achter, V., Lang, U., Theissen, J., Volland, R., Saadati, M., Eggert, A., Wilde, B. de, Berthold, F., Peng, Z., Zhao, C., Shi, L., Ortmann, M., Büttner, R., Perner, S., Hero, B., Schramm, A., Schulte, J.H., Herrmann, C., O'Sullivan, R.J., Westermann, F., Thomas, R.K., Fischer, M., 2015. Telomerase activation by genomic rearrangements in high-risk neuroblastoma. Nature 526, 700–704. https://doi.org/10.1038/nature14980

Pernas, L., Scorrano, L., 2015. Mito-Morphosis: Mitochondrial Fusion, Fission, and Cristae Remodeling as Key Mediators of Cellular Function. Annu Rev Physiol 78, 1–27. https://doi.org/10.1146/annurev-physiol-021115-105011

Petrus, P., Lecoutre, S., Dollet, L., Wiel, C., Sulen, A., Gao, H., Tavira, B., Laurencikiene, J., Rooyackers, O., Checa, A., Douagi, I., Wheelock, C.E., Arner, P., McCarthy, M., Bergo, M.O., Edgar, L., Choudhury, R.P., Aouadi, M., Krook, A., Rydén, M., 2020. Glutamine Links Obesity to Inflammation in Human White

Adipose Tissue. Cell Metab 31, 375-390.e11. https://doi.org/10.1016/j.cmet.2019.11.019

Pham, A.H., Meng, S., Chu, Q.N., Chan, D.C., 2012. Loss of Mfn2 results in progressive, retrograde degeneration of dopaminergic neurons in the nigrostriatal circuit. Hum Mol Genet 21, 4817–4826. https://doi.org/10.1093/hmg/dds311

Pochini, L., Scalise, M., Galluccio, M., Indiveri, C., 2014. Membrane transporters for the special amino acid glutamine: structure/function relationships and relevance to human health. Front Chem 2, 61. https://doi.org/10.3389/fchem.2014.00061

Preiss, D., Seshasai, S.R.K., Welsh, P., Murphy, S.A., Ho, J.E., Waters, D.D., DeMicco, D.A., Barter, P., Cannon, C.P., Sabatine, M.S., Braunwald, E., Kastelein, J.J.P., Lemos, J.A. de, Blazing, M.A., Pedersen, T.R., Tikkanen, M.J., Sattar, N., Ray, K.K., 2011. Risk of Incident Diabetes With Intensive-Dose Compared With Moderate-Dose Statin Therapy: A Meta-analysis. Jama 305, 2556–2564. https://doi.org/10.1001/jama.2011.860

Qing, G., Li, B., Vu, A., Skuli, N., Walton, Z.E., Liu, X., Mayes, P.A., Wise, D.R., Thompson, C.B., Maris, J.M., Hogarty, M.D., Simon, M.C., 2012. ATF4 Regulates MYC-Mediated Neuroblastoma Cell Death upon Glutamine Deprivation. Cancer Cell 22, 631–644. https://doi.org/10.1016/j.ccr.2012.09.021

Quirós, P.M., Prado, M.A., Zamboni, N., D'Amico, D., Williams, R.W., Finley, D., Gygi, S.P., Auwerx, J., 2017. Multi-omics analysis identifies ATF4 as a key regulator of the mitochondrial stress response in mammals. J Cell Biol 216, 2027–2045. https://doi.org/10.1083/jcb.201702058

Rafikov, R., Sun, X., Rafikova, O., Meadows, M.L., Desai, A.A., Khalpey, Z., Yuan, J.X.-J., Fineman, J.R., Black, S.M., 2015. Complex I dysfunction underlies the glycolytic switch in pulmonary hypertensive smooth muscle cells. Redox Biol. 6, 278–286. https://doi.org/10.1016/j.redox.2015.07.016

Ramírez, S., Gómez-Valadés, A.G., Schneeberger, M., Varela, L., Haddad-Tóvolli, R., Altirriba, J., Noguera, E., Drougard, A., Flores-Martínez, Á., Imbernón, M., Chivite, I., Pozo, M., Vidal-Itriago, A., Garcia, A., Cervantes, S., Gasa, R., Nogueiras, R., Gama-Pérez, P., Garcia-Roves, P.M., Cano, D.A., Knauf, C., Servitja, J.-M., Horvath, T.L., Gomis, R., Zorzano, A., Claret, M., 2017. Mitochondrial Dynamics Mediated by Mitofusin 1 Is Required for POMC Neuron Glucose-Sensing and Insulin Release Control. Cell Metab 25, 1390-1399.e6. https://doi.org/10.1016/j.cmet.2017.05.010

Ray, T.K., Skipski, V.P., Barclay, M., Essner, E., Archibald, F.M., 1969. Lipid Composition of Rat Liver Plasma Membranes. J Biol Chem 244, 5528–5536. https://doi.org/10.1016/s0021-9258(18)63595-1

Refolo, L.M., Pappolla, M.A., Malester, B., LaFrancois, J., Bryant-Thomas, T., Wang, R., Tint, G.S., Sambamurti, K., Duff, K., 2000. Hypercholesterolemia Accelerates the Alzheimer's Amyloid Pathology in a Transgenic Mouse Model. Neurobiol Dis 7, 321–331. https://doi.org/10.1006/nbdi.2000.0304

Reitzer, L.J., Wice, B.M., Kennell, D., 1979. Evidence that glutamine, not sugar, is the major energy source for cultured HeLa cells. J Biol Chem 254, 2669–2676. https://doi.org/10.1016/s0021-9258(17)30124-2

Robinson, S.R., 2000. Neuronal expression of glutamine synthetase in Alzheimer's disease indicates a profound impairment of metabolic interactions with astrocytes. Neurochem Int 36, 471–482. https://doi.org/10.1016/s0197-0186(99)00150-3

Rocha, N., Bulger, D.A., Frontini, A., Titheradge, H., Gribsholt, S.B., Knox, R., Page, M., Harris, J., Payne, F., Adams, C., Sleigh, A., Crawford, J., Gjesing, A.P., Bork-Jensen, J., Pedersen, O., Barroso, I., Hansen, T., Cox, H., Reilly, M., Rossor, A., Brown, R.J., Taylor, S.I., McHale, D., Armstrong, M., Oral, E.A., Saudek, V., O'Rahilly, S., Maher, E.R., Richelsen, B., Savage, D.B., Semple, R.K., 2017. Human biallelic MFN2 mutations induce mitochondrial dysfunction, upper body adipose hyperplasia, and suppression of leptin expression. Elife 6, e23813. https://doi.org/10.7554/elife.23813

Rosa, C.V.D. da, Azevedo, S.C.S.F., Bazotte, R.B., Peralta, R.M., Buttow, N.C., Pedrosa, M.M.D., Godoi, V.A.F. de, Natali, M.R.M., 2015. Supplementation with L-Glutamine and L-Alanyl-L-Glutamine Changes Biochemical Parameters and Jejunum Morphophysiology in Type 1 Diabetic Wistar Rats. Plos One 10, e0143005. https://doi.org/10.1371/journal.pone.0143005

Rotello, R.J., Lieberman, R.C., Lepoff, R.B., Gerschenson, L.E., 1992. Characterization of uterine epithelium apoptotic cell death kinetics and regulation by progesterone and RU 486. Am J Pathology 140, 449–56.

Rothman, D.L., Novotny, E.J., Shulman, G.I., Howseman, A.M., Petroff, O.A., Mason, G., Nixon, T., Hanstock, C.C., Prichard, J.W., Shulman, R.G., 1992. 1H-[13C] NMR measurements of [4-13C]glutamate turnover in human brain. Proc National Acad Sci 89, 9603–9606. https://doi.org/10.1073/pnas.89.20.9603

Rouslin, W., MacGee, J., Gupte, S., Wesselman, A., Epps, D.E., 1982. Mitochondrial cholesterol content and membrane properties in porcine myocardial ischemia. Am J Physiol-heart C 242, H254–H259. https://doi.org/10.1152/ajpheart.1982.242.2.h254

Ryan, D.G., Yang, M., Prag, H.A., Blanco, G.R., Nikitopoulou, E., Segarra-Mondejar, M., Powell, C.A., Young, T., Burger, N., Miljkovic, J.L., Minczuk, M., Murphy, M.P., Kriegsheim, A. von, Frezza, C., 2021. Disruption of the TCA cycle reveals an ATF4-dependent integration of redox and amino acid metabolism. Elife 10, e72593. https://doi.org/10.7554/elife.72593

Sakai, J., Duncan, E.A., Rawson, R.B., Hua, X., Brown, M.S., Goldstein, J.L., 1996. Sterol-Regulated Release of SREBP-2 from Cell Membranes Requires Two Sequential Cleavages, One Within a Transmembrane Segment. Cell 85, 1037–1046. https://doi.org/10.1016/s0092-8674(00)81304-5

Samocha-Bonet, D., Wong, O., Synnott, E.-L., Piyaratna, N., Douglas, A., Gribble, F.M., Holst, J.J., Chisholm, D.J., Greenfield, J.R., 2011. Glutamine Reduces Postprandial Glycemia and Augments the Glucagon-Like Peptide-1 Response in Type 2 Diabetes Patients 1 1 1. J Nutrition 141, 1233–1238. https://doi.org/10.3945/jn.111.139824

Sandoval, H., Yao, C.-K., Chen, K., Jaiswal, M., Donti, T., Lin, Y.Q., Bayat, V., Xiong, B., Zhang, K., David, G., Charng, W.-L., Yamamoto, S., Duraine, L., Graham, B.H., Bellen, H.J., 2014. Mitochondrial fusion but not fission regulates larval growth and synaptic development through steroid hormone production. Elife 3, e03558. https://doi.org/10.7554/elife.03558

Sanli, T., Steinberg, G.R., Singh, G., Tsakiridis, T., 2014. AMP-activated protein kinase (AMPK) beyond metabolism. Cancer Biol Ther 15, 156–169. https://doi.org/10.4161/cbt.26726

Sappington, D.R., Siegel, E.R., Hiatt, G., Desai, A., Penney, R.B., Jamshidi-Parsian, A., Griffin, R.J., Boysen, G., 2016. Glutamine drives glutathione synthesis and contributes to radiation sensitivity of A549 and H460 lung cancer cell lines. Biochimica Et Biophysica Acta Bba - Gen Subj 1860, 836–843. https://doi.org/10.1016/j.bbagen.2016.01.021

Sattar, N., Preiss, D., Murray, H.M., Welsh, P., Buckley, B.M., Craen, A.J. de, Seshasai, S.R.K., McMurray, J.J., Freeman, D.J., Jukema, J.W., Macfarlane, P.W., Packard, C.J., Stott, D.J., Westendorp, R.G., Shepherd, J., Davis, B.R., Pressel, S.L., Marchioli, R., Marfisi, R.M., Maggioni, A.P., Tavazzi, L., Tognoni, G., Kjekshus, J., Pedersen, T.R., Cook, T.J., Gotto, A.M., Clearfield, M.B., Downs,

J.R., Nakamura, H., Ohashi, Y., Mizuno, K., Ray, K.K., Ford, I., 2010. Statins and risk of incident diabetes: a collaborative meta-analysis of randomised statin trials. Lancet 375, 735–742. https://doi.org/10.1016/s0140-6736(09)61965-6

Schonewille, M., Boer, J.F. de, Mele, L., Wolters, H., Bloks, V.W., Wolters, J.C., Kuivenhoven, J.A., Tietge, U.J.F., Brufau, G., Groen, A.K., 2016. Statins increase hepatic cholesterol synthesis and stimulate fecal cholesterol elimination in mice. J Lipid Res 57, 1455–1464. https://doi.org/10.1194/jlr.m067488

Scriver, C.R., Sly, W.S., Childs, B., Beaudet, A.L., Valle, D., Kinzler, K.W., Vogelstein, B., 2001. The Metabolic and Molecular Bases of Inherited Disease, 8th ed, Journal of Inherited Metabolic Disease. McGraw-Hill Professional. https://doi.org/10.1023/a:1017409002434

Shen, C., Houghton, P.J., 2013. The mTOR pathway negatively controls ATM by up-regulating miRNAs. Proc National Acad Sci 110, 11869–11874. https://doi.org/10.1073/pnas.1220898110

Shen, Y., Gu, H.-M., Qin, S., Zhang, D.-W., 2022. Surf4, cargo trafficking, lipid metabolism, and therapeutic implications. J. Mol. Cell Biol. 14, mjac063. https://doi.org/10.1093/jmcb/mjac063

Sherman, B.T., Hao, M., Qiu, J., Jiao, X., Baseler, M.W., Lane, H.C., Imamichi, T., Chang, W., 2022. DAVID: a web server for functional enrichment analysis and functional annotation of gene lists (2021 update). Nucleic Acids Res 50, W216–W221. https://doi.org/10.1093/nar/gkac194

Sherrill, B.C., Dietschy, J.M., 1978. Characterization of the sinusoidal transport process responsible for uptake of chylomicrons by the liver. J Biol Chem 253, 1859–1867. https://doi.org/10.1016/s0021-9258(19)62331-8

Shie, F.-S., Jin, L.-W., Cook, D.G., Leverenz, J.B., LeBoeuf, R.C., 2002. Diet-induced hypercholesterolemia enhances brain A beta accumulation in transgenic mice. Neuroreport 13, 455–9. https://doi.org/10.1097/00001756-200203250-00019

Sokolov, A., Radhakrishnan, A., 2010. Accessibility of Cholesterol in Endoplasmic Reticulum Membranes and Activation of SREBP-2 Switch Abruptly at a Common Cholesterol Threshold. J Biol Chem 285, 29480–29490. https://doi.org/10.1074/jbc.m110.148254

Solsona-Vilarrasa, E., Fucho, R., Torres, S., Nuñez, S., Nuño-Lámbarri, N., Enrich, C., García-Ruiz, C., Fernández-Checa, J.C., 2019. Cholesterol enrichment in liver mitochondria impairs oxidative phosphorylation and disrupts the assembly of

respiratory supercomplexes. Redox Biol 24, 101214. https://doi.org/10.1016/j.redox.2019.101214

Spady, D.K., Bilheimer, D.W., Dietschy, J.M., 1983. Rates of receptor-dependent and -independent low density lipoprotein uptake in the hamster. Proc National Acad Sci 80, 3499–3503. https://doi.org/10.1073/pnas.80.11.3499

Spady, D.K., Dietschy, J.M., 1983. Sterol synthesis in vivo in 18 tissues of the squirrel monkey, guinea pig, rabbit, hamster, and rat. J Lipid Res 24, 303–315. https://doi.org/10.1016/s0022-2275(20)37999-2

Spann, N.J., Glass, C.K., 2013. Sterols and oxysterols in immune cell function. Nat Immunol 14, 893–900. https://doi.org/10.1038/ni.2681

Sparks, D.L., Scheff, S.W., Hunsaker, J.C., Liu, H., Landers, T., Gross, D.R., 1994. Induction of Alzheimer-like β-Amyloid Immunoreactivity in the Brains of Rabbits with Dietary Cholesterol. Exp Neurol 126, 88–94. https://doi.org/10.1006/exnr.1994.1044

Spodenkiewicz, M., Diez-Fernandez, C., Rüfenacht, V., Gemperle-Britschgi, C., Häberle, J., 2016. Minireview on Glutamine Synthetase Deficiency, an Ultra-Rare Inborn Error of Amino Acid Biosynthesis. Biology 5, 40. https://doi.org/10.3390/biology5040040

Stine, Z.E., Dang, C.V., 2020. Glutamine Skipping the Q into Mitochondria. Trends Mol Med 26, 6–7. https://doi.org/10.1016/j.molmed.2019.11.004

Stuppia, G., Rizzo, F., Riboldi, G., Bo, R.D., Nizzardo, M., Simone, C., Comi, G.P., Bresolin, N., Corti, S., 2015. MFN2-related neuropathies: Clinical features, molecular pathogenesis and therapeutic perspectives. J Neurol Sci 356, 7–18. https://doi.org/10.1016/j.jns.2015.05.033

Sun, L.-P., Seemann, J., Goldstein, J.L., Brown, M.S., 2007. Sterol-regulated transport of SREBPs from endoplasmic reticulum to Golgi: Insig renders sorting signal in Scap inaccessible to COPII proteins. Proc. Natl. Acad. Sci. 104, 6519–6526. https://doi.org/10.1073/pnas.0700907104

Swerdlow, D.I., Preiss, D., Kuchenbaecker, K.B., Holmes, M.V., Engmann, J.E.L., Shah, T., Sofat, R., Stender, S., Johnson, P.C.D., Scott, R.A., Leusink, M., Verweij, N., Sharp, S.J., Guo, Y., Giambartolomei, C., Chung, C., Peasey, A., Amuzu, A., Li, K., Palmen, J., Howard, P., Cooper, J.A., Drenos, F., Li, Y.R., Lowe, G., Gallacher, J., Stewart, M.C.W., Tzoulaki, I., Buxbaum, S.G., A, D.L. van der, Forouhi, N.G., Onland-Moret, N.C., Schouw, Y.T. van der, Schnabel, R.B.,

Hubacek, J.A., Kubinova, R., Baceviciene, M., Tamosiunas, A., Pajak, A., Topor-Madry, R., Stepaniak, U., Malyutina, S., Baldassarre, D., Sennblad, B., Tremoli, E., Faire, U. de, Veglia, F., Ford, I., Jukema, J.W., Westendorp, R.G.J., Borst, G.J. de, Jong, P.A. de, Algra, A., Spiering, W., Zee, A.H.M. der, Klungel, O.H., Boer, A. de, Doevendans, P.A., Eaton, C.B., Robinson, J.G., Duggan, D., Consortium, D., Consortium, M., Consortium, I., Kjekshus, J., Downs, J.R., Gotto, A.M., Keech, A.C., Marchioli, R., Tognoni, G., Sever, P.S., Poulter, N.R., Waters, D.D., Pedersen, T.R., Amarenco, P., Nakamura, H., McMurray, J.J.V., Lewsey, J.D., Chasman, D.I., Ridker, P.M., Maggioni, A.P., Tavazzi, L., Ray, K.K., Seshasai, S.R.K., Manson, J.E., Price, J.F., Whincup, P.H., Morris, R.W., Lawlor, D.A., Smith, G.D., Ben-Shlomo, Y., Schreiner, P.J., Fornage, M., Siscovick, D.S., Cushman, M., Kumari, M., Wareham, N.J., Verschuren, W.M.M., Redline, S., Patel, S.R., Whittaker, J.C., Hamsten, A., Delaney, J.A., Dale, C., Gaunt, T.R., Wong, A., Kuh, D., Hardy, R., Kathiresan, S., Castillo, B.A., Harst, P. van der, Brunner, E.J., Tybjaerg-Hansen, A., Marmot, M.G., Krauss, R.M., Tsai, M., Coresh, J., Hoogeveen, R.C., Psaty, B.M., Lange, L.A., Hakonarson, H., Dudbridge, F., Humphries, S.E., Talmud, P.J., Kivimäki, M., Timpson, N.J., Langenberg, C., Asselbergs, F.W., Voevoda, M., Bobak, M., Pikhart, H., Wilson, J.G., Reiner, A.P., Keating, B.J., Hingorani, A.D., Sattar, N., 2015. HMG-coenzyme A reductase inhibition, type 2 diabetes, and bodyweight: evidence from genetic analysis and randomised trials. Lancet 385, 351–361. https://doi.org/10.1016/s0140-6736(14)61183-1

Tabas, I., 1997. Free Cholesterol-Induced Cytotoxicity A Possible Contributing Factor to Macrophage Foam Cell Necrosis in Advanced Atherosclerotic Lesions. Trends Cardiovas Med 7, 256–263. https://doi.org/10.1016/s1050-1738(97)00086-8

Tambay, V., Raymond, V.-A., Bilodeau, M., 2021. MYC Rules: Leading Glutamine Metabolism toward a Distinct Cancer Cell Phenotype. Cancers 13, 4484. https://doi.org/10.3390/cancers13174484

Tanigami, H., Rebel, A., Martin, L.J., Chen, T.-Y., Brusilow, S.W., Traystman, R.J., Koehler, R.C., 2005. Effect of glutamine synthetase inhibition on astrocyte swelling and altered astroglial protein expression during hyperammonemia in rats. Neuroscience 131, 437–449. https://doi.org/10.1016/j.neuroscience.2004.10.045

Taylor, W.M., Halperin, M.L., 1973. Regulation of Pyruvate Dehydrogenase in Muscle INHIBITION BY CITRATE. J. Biol. Chem. 248, 6080–6083. https://doi.org/10.1016/s0021-9258(19)43511-4

Tenniswood, M.P., Guenette, R.S., Lakins, J., Mooibroek, M., Wong, P., Welsh, J.E., 1992. Active cell death in hormone-dependent tissues. Cancer Metast Rev 11, 197–220. https://doi.org/10.1007/bf00048064

Thirumangalakudi, L., Prakasam, A., Zhang, R., Bimonte-Nelson, H., Sambamurti, K., Kindy, M.S., Bhat, N.R., 2008. High cholesterol-induced neuroinflammation and amyloid precursor protein processing correlate with loss of working memory in mice. J Neurochem 106, 475–485. https://doi.org/10.1111/j.1471-4159.2008.05415.x

Tiemeier, D.C., Milman, G., 1972. Chinese hamster liver glutamine synthetase. Purification, physical and biochemical properties. J Biological Chem 247, 2272–7.

Tomita, H., Hines, K.M., Herron, J.M., Li, A., Baggett, D.W., Xu, L., 2022. 7-Dehydrocholesterol-derived oxysterols cause neurogenic defects in Smith-Lemli-Opitz syndrome. Elife 11, e67141. https://doi.org/10.7554/elife.67141

Tompkins, S.C., Sheldon, R.D., Rauckhorst, A.J., Noterman, M.F., Solst, S.R., Buchanan, J.L., Mapuskar, K.A., Pewa, A.D., Gray, L.R., Oonthonpan, L., Sharma, A., Scerbo, D.A., Dupuy, A.J., Spitz, D.R., Taylor, E.B., 2019. Disrupting Mitochondrial Pyruvate Uptake Directs Glutamine into the TCA Cycle away from Glutathione Synthesis and Impairs Hepatocellular Tumorigenesis. Cell Reports 28, 2608-2619.e6. https://doi.org/10.1016/j.celrep.2019.07.098

Tong, X., Zhao, F., Thompson, C.B., 2009. The molecular determinants of de novo nucleotide biosynthesis in cancer cells. Curr Opin Genet Dev 19, 32–37. https://doi.org/10.1016/j.gde.2009.01.002

Trapnell, C., Roberts, A., Goff, L., Pertea, G., Kim, D., Kelley, D.R., Pimentel, H., Salzberg, S.L., Rinn, J.L., Pachter, L., 2012. Differential gene and transcript expression analysis of RNA-seq experiments with TopHat and Cufflinks. Nat Protoc 7, 562–578. https://doi.org/10.1038/nprot.2012.016

Tsai, Y.C., Leichner, G.S., Pearce, M.M.P., Wilson, G.L., Wojcikiewicz, R.J.H., Roitelman, J., Weissman, A.M., 2012. Differential regulation of HMG-CoA reductase and Insig-1 by enzymes of the ubiquitin-proteasome system. Mol. Biol. Cell 23, 4484–4494. https://doi.org/10.1091/mbc.e12-08-0631

Tuchman, M., Lichtenstein, G.R., Rajagopal, B.S., McCann, M.T., Furth, E.E., Bavaria, J., Kaplan, P.B., Gibson, J.B., Berry, G.T., 1997. Hepatic Glutamine Synthetase Deficiency in Fatal Hyperammonemia after Lung Transplantation. Ann Intern Med 127, 446. https://doi.org/10.7326/0003-4819-127-6-199709150-00005

Tur, J., Pereira-Lopes, S., Vico, T., Marín, E.A., Muñoz, J.P., Hernández-Alvarez, M., Cardona, P.-J., Zorzano, A., Lloberas, J., Celada, A., 2020. Mitofusin 2 in Macrophages Links Mitochondrial ROS Production, Cytokine Release, Phagocytosis, Autophagy, and Bactericidal Activity. Cell Rep. 32, 108079. https://doi.org/10.1016/j.celrep.2020.108079

UJIIE, M., DICKSTEIN, D.L., CARLOW, D.A., JEFFERIES, W.A., 2009. Blood–Brain Barrier Permeability Precedes Senile Plaque Formation in an Alzheimer Disease Model. Microcirculation 10, 463–470. https://doi.org/10.1080/mic.10.6.463.470

Vamecq, J., Dessein, A.-F., Fontaine, M., Briand, G., Porchet, N., Latruffe, N., Andreolotti, P., Cherkaoui-Malki, M., 2012. Mitochondrial Dysfunction and Lipid Homeostasis. Curr Drug Metab 13, 1388–1400. https://doi.org/10.2174/138920012803762792

Wall, C.T.J., Lefebvre, G., Metairon, S., Descombes, P., Wiederkehr, A., Santo-Domingo, J., 2022. Mitochondrial respiratory chain dysfunction alters ER sterol sensing and mevalonate pathway activity. J Biol Chem 298, 101652. https://doi.org/10.1016/j.jbc.2022.101652

Wang, L., Li, J., Guo, L., Li, P., Zhao, Z., Zhou, H., Di, L., 2018. Molecular link between glucose and glutamine consumption in cancer cells mediated by CtBP and SIRT4. Oncogenesis 7, 26. https://doi.org/10.1038/s41389-018-0036-8

Wang, L., Wang, S., Li, W., 2012. RSeQC: quality control of RNA-seq experiments. Bioinformatics 28, 2184–2185. https://doi.org/10.1093/bioinformatics/bts356

Wasinski, F., Gregnani, M.F., Ornellas, F.H., Bacurau, A.V.N., Câmara, N.O., Araujo, R.C., Bacurau, R.F., 2014. Lymphocyte Glucose and Glutamine Metabolism as Targets of the Anti-Inflammatory and Immunomodulatory Effects of Exercise. Mediat. Inflamm. 2014, 326803. https://doi.org/10.1155/2014/326803

Weiss, J.S., 2009. More on Schnyder Corneal Dystrophy. Ophthalmology 116, 2260. https://doi.org/10.1016/j.ophtha.2009.07.022

Wernerman, J., 2008. Clinical Use of Glutamine Supplementation. J Nutrition 138, 2040S-2044S. https://doi.org/10.1093/jn/138.10.2040s

Williams, N.C., O'Neill, L.A.J., 2018. A Role for the Krebs Cycle Intermediate Citrate in Metabolic Reprogramming in Innate Immunity and Inflammation. Front. Immunol. 9, 141. https://doi.org/10.3389/fimmu.2018.00141

Wolozin, B., Kellman, W., Ruosseau, P., Celesia, G.G., Siegel, G., 2000. Decreased Prevalence of Alzheimer Disease Associated With 3-Hydroxy-3-Methyglutaryl

Coenzyme A Reductase Inhibitors. Arch Neurol-chicago 57, 1439–1443. https://doi.org/10.1001/archneur.57.10.1439

Xin, Y., Li, J., Wu, W., Liu, X., 2021. Mitofusin-2: A New Mediator of Pathological Cell Proliferation. Frontiers Cell Dev Biology 9, 647631. https://doi.org/10.3389/fcell.2021.647631

Xu, D., Wang, Z., Zhang, Y., Jiang, W., Pan, Y., Song, B.-L., Chen, Y., 2015. PAQR3 modulates cholesterol homeostasis by anchoring Scap/SREBP complex to the Golgi apparatus. Nat. Commun. 6, 8100. https://doi.org/10.1038/ncomms9100

Yang, C., Ko, B., Hensley, C.T., Jiang, L., Wasti, A.T., Kim, J., Sudderth, J., Calvaruso, M.A., Lumata, L., Mitsche, M., Rutter, J., Merritt, M.E., DeBerardinis, R.J., 2014. Glutamine Oxidation Maintains the TCA Cycle and Cell Survival during Impaired Mitochondrial Pyruvate Transport. Mol Cell 56, 414–424. https://doi.org/10.1016/j.molcel.2014.09.025

Yao, C.-H., Wang, R., Wang, Y., Kung, C.-P., Weber, J.D., Patti, G.J., 2019. Mitochondrial fusion supports increased oxidative phosphorylation during cell proliferation. Elife 8, e41351. https://doi.org/10.7554/elife.41351

Ye, J., Rawson, R.B., Komuro, R., Chen, X., Davé, U.P., Prywes, R., Brown, M.S., Goldstein, J.L., 2000. ER Stress Induces Cleavage of Membrane-Bound ATF6 by the Same Proteases that Process SREBPs. Mol Cell 6, 1355–1364. https://doi.org/10.1016/s1097-2765(00)00133-7

Yoo, H., Stephanopoulos, G., Kelleher, J.K., 2004. Quantifying carbon sources for de novo lipogenesis in wild-type and IRS-1 knockout brown adipocytes. J. Lipid Res. 45, 1324–1332. https://doi.org/10.1194/jlr.m400031-jlr200

Yoo, H.C., Yu, Y.C., Sung, Y., Han, J.M., 2020. Glutamine reliance in cell metabolism. Exp Mol Medicine 52, 1496–1516. https://doi.org/10.1038/s12276-020-00504-8

Yu, W., Gong, J.-S., Ko, M., Garver, W.S., Yanagisawa, K., Michikawa, M., 2005. Altered Cholesterol Metabolism in Niemann-Pick Type C1 Mouse Brains Affects Mitochondrial Function*. J Biol Chem 280, 11731–11739. https://doi.org/10.1074/jbc.m412898200

Zaman, M., Shutt, T.E., 2022. The Role of Impaired Mitochondrial Dynamics in MFN2-Mediated Pathology. Frontiers Cell Dev Biology 10, 858286. https://doi.org/10.3389/fcell.2022.858286

Zanetti, G., Prinz, S., Daum, S., Meister, A., Schekman, R., Bacia, K., Briggs, J.A., 2013. The structure of the COPII transport-vesicle coat assembled on membranes. Elife 2, e00951. https://doi.org/10.7554/elife.00951

Zelcer, N., Sharpe, L.J., Loregger, A., Kristiana, I., Cook, E.C.L., Phan, L., Stevenson, J., Brown, A.J., 2014. The E3 Ubiquitin Ligase MARCH6 Degrades Squalene Monooxygenase and Affects 3-Hydroxy-3-Methyl-Glutaryl Coenzyme A Reductase and the Cholesterol Synthesis Pathway. Mol. Cell. Biol. 34, 1262–1270. https://doi.org/10.1128/mcb.01140-13

Zhang, C.-S., Hawley, S.A., Zong, Y., Li, M., Wang, Z., Gray, A., Ma, T., Cui, J., Feng, J.-W., Zhu, M., Wu, Y.-Q., Li, T.Y., Ye, Z., Lin, S.-Y., Yin, H., Piao, H.-L., Hardie, D.G., Lin, S.-C., 2017. Fructose-1,6-bisphosphate and aldolase mediate glucose sensing by AMPK. Nature 548, 112–116. https://doi.org/10.1038/nature23275

Zhang, J., Fan, J., Venneti, S., Cross, J.R., Takagi, T., Bhinder, B., Djaballah, H., Kanai, M., Cheng, E.H., Judkins, A.R., Pawel, B., Baggs, J., Cherry, S., Rabinowitz, J.D., Thompson, C.B., 2014. Asparagine Plays a Critical Role in Regulating Cellular Adaptation to Glutamine Depletion. Mol Cell 56, 205–218. https://doi.org/10.1016/j.molcel.2014.08.018

Zhang, J., Pavlova, N.N., Thompson, C.B., 2017. Cancer cell metabolism: the essential role of the nonessential amino acid, glutamine. Embo J 36, 1302–1315. https://doi.org/10.15252/embj.201696151

Zhang, X., Wang, C., Song, G., Gan, K., Kong, D., Nie, Q., Ren, L., 2013. Mitofusion-2-mediated alleviation of insulin resistance in rats through reduction in lipid intermediate accumulation in skeletal muscle. J Biomed Sci 20, 45. https://doi.org/10.1186/1423-0127-20-45

Zhang, Z., Li, T.-E., Chen, M., Xu, D., Zhu, Y., Hu, B.-Y., Lin, Z.-F., Pan, J.-J., Wang, X., Wu, C., Zheng, Y., Lu, L., Jia, H.-L., Gao, S., Dong, Q.-Z., Qin, L.-X., 2020. MFN1-dependent alteration of mitochondrial dynamics drives hepatocellular carcinoma metastasis by glucose metabolic reprogramming. Brit J Cancer 122, 209–220. https://doi.org/10.1038/s41416-019-0658-4

Zhao, L., Chen, Yaxi, Tang, R., Chen, Yao, Li, Q., Gong, J., Huang, A., Varghese, Z., Moorhead, J.F., Ruan, X.Z., 2011. Inflammatory stress exacerbates hepatic cholesterol accumulation via increasing cholesterol uptake and de novo synthesis. J Gastroen Hepatol 26, 875–883. https://doi.org/10.1111/j.1440-1746.2010.06560.x

Zhao, Q., Zhou, X., Kuiper, R., Curbo, S., Karlsson, A., 2022. Mitochondrial dysfunction is associated with lipid metabolism disorder and upregulation of angiotensin-converting enzyme 2. Plos One 17, e0270418. https://doi.org/10.1371/journal.pone.0270418

Zhao, S., Torres, A., Henry, R.A., Trefely, S., Wallace, M., Lee, J.V., Carrer, A., Sengupta, A., Campbell, S.L., Kuo, Y.-M., Frey, A.J., Meurs, N., Viola, J.M., Blair, I.A., Weljie, A.M., Metallo, C.M., Snyder, N.W., Andrews, A.J., Wellen, K.E., 2016. ATP-Citrate Lyase Controls a Glucose-to-Acetate Metabolic Switch. Cell Reports 17, 1037–1052. https://doi.org/10.1016/j.celrep.2016.09.069

Zhao, Y.-F., Wang, L., Lee, S., Sun, Q., Tuo, Y., Wang, Y., Pei, J., Chen, C., 2010. Cholesterol induces mitochondrial dysfunction and apoptosis in mouse pancreatic beta-cell line MIN6 cells. Endocrine 37, 76–82. https://doi.org/10.1007/s12020-009-9275-y

Zhou, Y., Dhaher, R., Parent, M., Hu, Q.-X., Hassel, B., Yee, S.-P., Hyder, F., Gruenbaum, S.E., Eid, T., Danbolt, N.C., 2019. Selective deletion of glutamine synthetase in the mouse cerebral cortex induces glial dysfunction and vascular impairment that precede epilepsy and neurodegeneration. Neurochem Int 123, 22–33. https://doi.org/10.1016/j.neuint.2018.07.009

Zhu, Y., Li, T., Silva, S.R. da, Lee, J.-J., Lu, C., Eoh, H., Jung, J.U., Gao, S.-J., 2017. A Critical Role of Glutamine and Asparagine **γ**-Nitrogen in Nucleotide Biosynthesis in Cancer Cells Hijacked by an Oncogenic Virus. Mbio 8, e01179-17. https://doi.org/10.1128/mbio.01179-17

Züchner, S., Jonghe, P.D., Jordanova, A., Claeys, K.G., Guergueltcheva, V., Cherninkova, S., Hamilton, S.R., Stavern, G.V., Krajewski, K.M., Stajich, J., Tournev, I., Verhoeven, K., Langerhorst, C.T., Visser, M. de, Baas, F., Bird, T., Timmerman, V., Shy, M., Vance, J.M., 2006. Axonal neuropathy with optic atrophy is caused by mutations in mitofusin 2. Ann Neurol 59, 276–281. https://doi.org/10.1002/ana.20797